ROLE OF THE ABAXIAL BUNDLE SHEATH CELLS IN PHLOEM LOADING IN MAIZE LEAVES

Inaugural-Dissertation

zur Erlangung des Doktorgrades
der Mathematisch-Naturwissenschaftlichen Fakultät
der Heinrich-Heine-Universität Düsseldorf

vorgelegt von

Margaret Bezrutczyk
aus New York, USA

Düsseldorf, October 2020

aus dem Institut für
der Heinrich-Heine-Universität Düsseldorf

Gedruckt mit der Genehmigung der
Mathematisch-Naturwissenschaftlichen Fakultät der
Heinrich-Heine-Universität Düsseldorf

Berichterstatter:

1. Prof. Dr. Wolf B. Frommer

2. Prof. Dr. Rüdiger Simon

Tag der mündlichen Prüfung: 16.12.2020

TABLE OF CONTENTS

PREAMBLE

Abstract

The yield of maize plants depends on efficient allocation of sucrose from leaves to seeds, which is mediated by the sap-conducting tissue known as phloem. The process of translocating photoassimilates into the phloem is known as phloem loading, and it is thought to occur by different mechanisms in different species. Phloem loading of sugar has been well characterized in *Arabidopsis thaliana* (hereafter 'Arabidopsis'), where it is mediated by a combination of SWEET sucrose effluxers and subsequent uptake by SUT1/SUC2 H^+/sucrose symporters. In maize, ZmSUT1 is a H^+/sucrose symporter that actively draws sucrose from the apoplasmic space into the sieve element-companion cell complex (SE-CC), but it had not yet been shown if SWEETs efflux sucrose into the apoplasmic space in maize. Using a combination of single-cell RNA sequencing (scRNA-seq) and classical histological techniques such as *in situ* hybridization, we determined that a subtype of maize bundle sheath (BS) cell in the rank-2 intermediate veins shows high and specific expression of sugar and amino acid transporters, including sucrose transporters *SWEET13a*, *b*, and *c*. Therefore, we hypothesized that sucrose is transported from the mesophyll to the abaxial BS cells, where it is then exported to the apoplasm by SWEET13a, b, and c and subsequently taken up into the SE-CC by SUT1 for long distance transport. To determine if SWEET13a, b, and c were necessary for phloem loading, we generated triple knockout mutants using a multiplexed CRISPR-Cas9 approach, and discovered that the *sweet13a,b,c* plants were stunted, chlorotic, and accumulated more starch and soluble sugars in the leaves than wild-type: a phenotype consistent with a failure of phloem loading. Taken together, these experiments indicate that SWEET13a, b, and c are abaxial-bundle sheath localized transporters which export sucrose from the BS to the apoplasmic space adjacent to the phloem. SWEETs and other sugar transporters are also differentially regulated during pathogen and drought stress, and below I review what is known about the contribution of SWEETs and other sugar transport proteins to plant susceptibility and resistance to several agronomically important pathogens.

I. Introduction

Maize is the most productive crop in terms of biomass per acreage, and critical for subsistence farming in many regions of the world including Sub-Saharan Africa and Central America. Maize is used for animal feed, fermented for ethanol production, or processed into starch for countless industrial applications (Capeheart et al., 2020), and it is primarily carbohydrates, either in the form of cellulose or starch and sugar in the kernel's endosperm, that are used for these purposes. Carbohydrate partitioning refers to the process by which plants allocate sugars which are generated in source tissues and distribute them to sink tissues (such as seeds). Therefore, understanding carbohydrate partitioning in maize is critical for improving yield (Julius et al., 2017). Sucrose is produced in the mesophyll cells of the leaf and diffuses from the mesophyll through plasmodesmata (PD) to the bundle sheath towards the phloem for long distance transport. The sap-conducting elements of the phloem are called sieve elements (SE), and are connected to companion cells (CC) by PD. The route which sugars take to reach the sieve elements, and the methods by which they are translocated or concentrated, comprise the phloem loading strategy for a given species.

There are at least three postulated phloem loading strategies: A high percentage of woody plants are thought to use a symplasmic mechanism, or 'diffusion', facilitated by a higher concentration of sucrose in the mesophyll (MS) than phloem tissues, and abundant plasmodesmata between all cells from the site of synthesis in the mesophyll to the SE-CC (Eom et al., 2012; Turgeon, 2010). It has been proposed that other species, including some curcubits, employ a polymer-trap mechanism in which sucrose is transported along its concentration gradient into intermediary SE-CC cells where it is converted to raffinose and unable to diffuse back from the SE-CC, effectively concentrating sugar in the SE-CC. Polymer-trapping is an 'active' process that uses energy for the conversion to raffinose (Haritatos et al., 1996; Zhang and Turgeon, 2009), but because raffinose is much smaller than other molecules that are known to diffuse through PD, such as transcription factors (Kragler et al., 1998), it is not clear if size exclusion is the mechanism for preventing backward diffusion through PD. Finally, many species use an apoplasmic phloem loading step, in which an active H^+/sucrose symporter transports sucrose against its concentration gradient from the apoplasm to the SE-CC. It is also likely that many species employ more

than one method of phloem loading, especially under different environmental stresses (Liesche, 2017).

II. Evidence for apoplasmic phloem loading

Early support for the existence of apoplasmic phloem loading came from experiments indicating that sugars were concentrated in the SE-CC relative to other leaf cells of *Beta vulgaris* and maize. In 1973, Geiger submerged *Beta vulgaris* (henceforth, 'beet') leaves in increasing concentrations of mannitol and observed incipient plasmolysis upon freezing, depending on the degree of cryoprotection the mannitol provided (Geiger et al., 1973). A higher concentration of sugars was calculated in the SE-CC (30 bars) than in the surrounding mesophyll and phloem parenchyma cells (13 bars). The authors speculated this concentrating step could be achieved by transporting the sucrose to the apoplasm followed by concentration in the SE-CC. Evert found a similar difference in sucrose concentration in maize in the mesophyll (11 bar) and phloem parenchyma vs SE-CC (18 bar) (Evert et al., 1978), though it was still not clear if this accumulation of sugar in the phloem was preceded by an apoplasmic step or some other modification to symplasmic movement of sugars from the mesophyll via plasmodesmata (Giaquinta, 1983).

The arrangement of plasmodesmatal connections between cell types provided further evidence for an apoplasmic phloem loading step. In maize, there are abundant PD between mesophyll cells, mesophyll and bundle sheath cells, and bundle sheath and phloem parenchyma, but very few between the SE-CC and surrounding cell types. It is especially notable that the PD between MS and BS are up to 12x more frequent in C4 species such as maize, than in related C3 plants such as rice, presumably because many intermediate products of photosynthesis must be shuttled between MS and BS for C4 photosynthesis (Danila et al., 2019). It appears that there are PD between the vascular parenchyma (either phloem or xylem parenchyma) and thick-walled sieve tubes (TST) (Evert et al., 1977), but the TST are thought to be involved in retrieval of sucrose leaked from the companion cells and thin walled sieve tubes, and do not contribute to long distance sucrose transport out of the leaf (Botha, 2013).

To assess whether membrane-bound proteins were involved in the apoplasmic phloem loading step, non-membrane permeable sulfhydryl-group modifier PCMBS was applied to beet leaves. The authors reasoned that any sulfhydryl groups affected by PCMBS application must be facing the apoplasm, because unlike membrane permeable sulfhydryl-group modifiers, PCMBS did not have a measurable effect on cellular photosynthesis or respiration, and therefore most likely did not affect intracellular sulfhydryl-groups. PCMBS application blocked sucrose uptake into the SE-CC, and the authors concluded that this disrupted proteins necessary for sucrose transport across the membrane, which therefore must be necessary for uptake (Giaquinta, 1976). However, PCMBS also affects water transport through aquaporins (Kuwahara et al., 1997; Macey, 1984) which is likely important for phloem loading, as water is drawn from the xylem to generate the pressure needed for bulk sap flow (Knoblauch et al., 2016; Münch, 1930); therefore it is possible that PCMBS-induced blockage of phloem loading was the result of disrupted aquaporin function. The fact that beet leaf sap is alkaline relative to the apoplasmic fluid, and that the onset of ATPase activity in the sieve element plasma membrane occurs at the sink-source transition, provided further evidence for involvement of a hydrogen ion-driven mechanism (Giaquinta, 1977). Giaquinta concluded that an active transport mechanism must exist in some species, involving a H^+/sucrose symporter to concentrate sugar in the SE-CC (Giaquinta, 1983). In 1992, a *Spinacia oleracea* sucrose transporter (SoSUT) was cloned (Riesmeier et al., 1992), and it was soon determined that SUTs, including Arabidopsis SUC1 and SUC2 (Sauer and Stolz, 1994) and *Solanum tuberosum* SUT1 (Riesmeier et al., 1993), were the long-speculated H^+/sucrose symporters driving the concentration of sucrose in the phloem of apoplasmic phloem loading species. In Arabidopsis, AtSUC2 was found to be a H^+/sucrose symporter localized to the plasma membrane of cells in the phloem of the leaf. *atsuc2* plants were somewhat stunted, showed low fecundity, and accumulated more starch in the leaves compared to wild-type (Gottwald et al., 2000; Srivastava et al., 2008, 2009). The *atsuc2* phenotype, functional characterization of AtSUC2 as an H^+/sucrose symporter, and localization of the AtSUC2 protein in the plasma membrane of the companion cells were consistent with the hypothesis that AtSUC2 was necessary for actively drawing sucrose from the apoplasm into the SE-CC (Gottwald et al., 2000; Turgeon, 2010; Stadler and Sauer, 1996; Truernit and Sauer, 1995).

III. SWEETs are a novel class of sugar transporter

If sucrose is concentrated in the SE-CC by a membrane-bound protein actively drawing sucrose into SE-CC, then it was clear that there must be some mechanism for export of sucrose into the apoplasm. Given that they are passive sugar transporters, SWEETs were potential candidates for sucrose efflux into the apoplasmic space prior to phloem loading. The family of SWEET sugar transporters in Arabidopsis was discovered by screening for glucose-transporting membrane proteins in cultured human embryonic kidney (HEK) cells (Chen et al., 2010). In total, 17 AtSWEETs were found, which could be grouped into four clades based on sequence homology (Eom et al., 2015). Clades I, II, and IV primarily transport hexoses, clade III transports sucrose. Additionally, it has been shown that AtSWEEET13 and 14 transport both sucrose and gibberellin (Kanno et al., 2016). SWEETs are critical for many developmental processes in Arabidopsis and maize. In Arabidopsis, *SWEET11*, *12*, and *15* are necessary for seed filling (Chen et al., 2015). Sucrose is secreted from Arabidopsis nectaries by AtSWEET9 and subsequently cleaved by sucrose synthase into hexose-rich nectar (Lin et al., 2014). Pollen grain development requires contribution from AtSWEET8 for normal cell wall development (Sun et al., 2013).

AtSWEET11 and *12* were found to be highly expressed in Arabidopsis leaf tissue, and encode proteins which are pH-independent, low affinity sucrose transporters. Double homozygous *atsweet11,12* mutants were smaller than wild-type under high light conditions and accumulated starch and soluble sugar in the leaves, a phenotype that bears resemblance to *atsuc2* and is consistent with a reduction in sucrose export from the leaf. Colorimetric detection of GUS activity in translational reporter fusion-transformed Arabidopsis plants demonstrated that these transporters were specifically localized to cell files along the veins, which likely correspond to the phloem parenchyma (Chen et al., 2012). Therefore, the canonical apoplasmic phloem loading pathway was established in Arabidopsis: AtSWEET11 and 12 efflux sucrose into the apoplasmic space, where it is taken up actively by H^+/sucrose symporter AtSUC2.

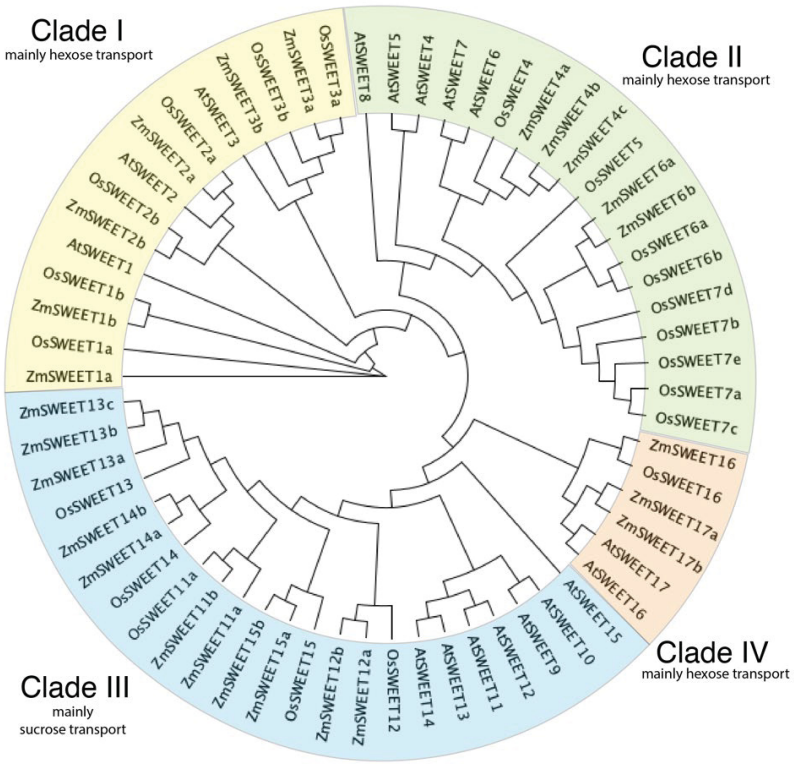

Figure 1. Cladogram of SWEET sugar transporters in *Zea mays*, *Arabidopsis thaliana*, and *Oryza sativa* Japonica group. Amino acid sequences were retrieved from Ensembl from AGPv4 B73 reference genome (maize), IRGSP-1.0 (rice), and TAIR10 (Arabidopsis), and aligned with MEGAX using MUSCLE (Gap Open -2.90, Gap Extend 0, Hydrophobicity Multiplier 1.2, UPGMA for all iterations). The maximum likelihood tree was created from these alignments using IQTREE webserver (Trifinopoulos et al., 2016) using the BLOSUM62 substitution model and 1000 bootstraps

IV. Rice may use a symplasmic phloem loading mechanism

Evidence suggests that rice may use a symplasmic, rather than apoplasmic mechanism. Neither OsSUT1 nor OsSWEET13, which are the closest orthologs in rice to AtSUC2 and AtSWEET11 and 12, are necessary for rice phloem loading (Eom et al., 2016, 2019). OsSUT1 is localized to the veins of rice leaves, blades, and internodes, as well as the phloem at the transition from maternal to filial tissue in rice grains and pollen (Hirose et al., 2010). OsSUT1 is the only SUT in rice which complements the phenotype of *atsuc2* mutants when expressed under the *AtSUC2* promoter (*pAtSUC2:OsSUT1*) indicating that it is the closest functional ortholog to *AtSUC2*. Therefore, it was thought that it would function similarly to AtSUC2, as the driver for sucrose transport to the SE-CC. Surprisingly, *ossut1* mutants were indistinguishable from wild-type in terms of growth and

leaf soluble sugar and starch content, suggesting that it is not an important component of the phloem loading pathway in rice (Eom et al., 2016). Knockout mutants of *OsSWEET13*, the closest ortholog to *AtSWEET11* and *12*, are indistinguishable from wild-type under normal conditions, but show an increased leaf angle and accumulation of sugars and starch under low light conditions (Eom et al., 2019). However, plants with homozygous mutations of *OsSUT2*, which is a tonoplast-localized SUT, showed a severe growth-defective phenotype (Eom et al., 2011). It is speculated that rice may use a symplasmic mechanism, in which cytosolic levels of sucrose in mesophyll must be higher than in companion cells to generate a gradient. SUT2 is a proton-symporter localized to the tonoplast, which may actively concentrate sucrose in the cytosol, creating such a gradient.

V. SWEETs in maize are critical for many biological functions

In maize, there are 24 SWEETs, divided into four clades I-IV, as in Arabidopsis. Clade I contains SWEETs 1a, 1b, 2, 3a, 3b; Clade II contains SWEET4a, b, and c, and 6a and b; Clade III contains SWEET11a, 11b, 12a, 12b, 13a-c, 14a, 14b, 15a, and 15b; Clade IV contains SWEET16a, 16b, and 17 (Eom et al., 2015) (Figure 1). Several of these transporters have been implicated in critical processes in maize growth and carbon allocation. *SWEET4c* is highly expressed in the basal endosperm transfer layer (BETL) at the base of the developing seed. SWEET4c imports hexoses derived by apoplasmic hydrolysis of sucrose by a secreted invertase into the BETL (Sosso et al., 2015). Glucose imported into the seed triggers a signaling cascade that leads to upregulation of sugar transporters and development of extensive invaginations in the BETL, which facilitates rapid seed filling (Sosso et al., 2015). SWEET1b, also known as CST1, is a glucose transporter localized to the plasma membrane of subsidiary cells in the maize leaf. It acts as a positive regulator of stomatal opening by sequestering glucose in the subsidiary cells, possibly by preventing glucose-induced hexokinase-mediated stomatal closure in guard cells (Wang et al., 2019). Characterization of the remaining 22 SWEETS is outstanding.

VI. Maize leaf development and vein ontogeny

Vascular architecture differs between monocots and dicots, for instance, while Arabidopsis has conjoint, collateral open and closed bundles, maize has a conjoint, collateral and closed-type vasculature. Like other C4 monocots, maize has a unique vein class known as rank-2 intermediate veins (Sedelnikova et al., 2018), which is not present in dicots or C3 monocots. Leaf initiation begins when polar auxin transport streams mediated by ZmSoPIN1, ZmPIN1, ZmPIN2 converge in the shoot apical meristem and form auxin maxima (Carraro et al., 2006; O'Connor et al., 2014) (Figure 2a). During initiation of leaf primordia development, layers L1 and L2 divide periclinally to form the developing leaf, with cells continually dividing from the base (Poethig and Sussex, 1985). Epidermis is derived from L1, and internal structures including vascular tissue, mesophyll, and bundle sheath derive from L2. L2 begins as an invagination of L1, which wraps around the outside of the folded L2 like an envelope as the leaf expands. The auxin stream convergence that initiates the leaf formation discharges basipetally through the center of the expanding leaf primordium, which delineates the position of the nascent leaf midrib (Figure 2a) (Kumar and Kellogg, 2019). Two other auxin maxima form adjacent to the midvein on either side, forming the lateral major veins. These major veins are initiated when the leaf still consists of only 3 cell layer types: L1 (proto-epidermis) on the top and bottom layer, an upper and lower L2 layer, and the procambial cells in the middle (Figure 2b, c). There are three categories of veins in maize: Major veins, and rank-1 and rank-2 intermediate veins (Sharman, 1942). Rank-1 and rank-2 intermediate veins (also known as intermediate and minor veins, respectively) are generated by the initiation of auxin maxima adjacent to major veins, and develop basipetally (Evert et al., 1996).

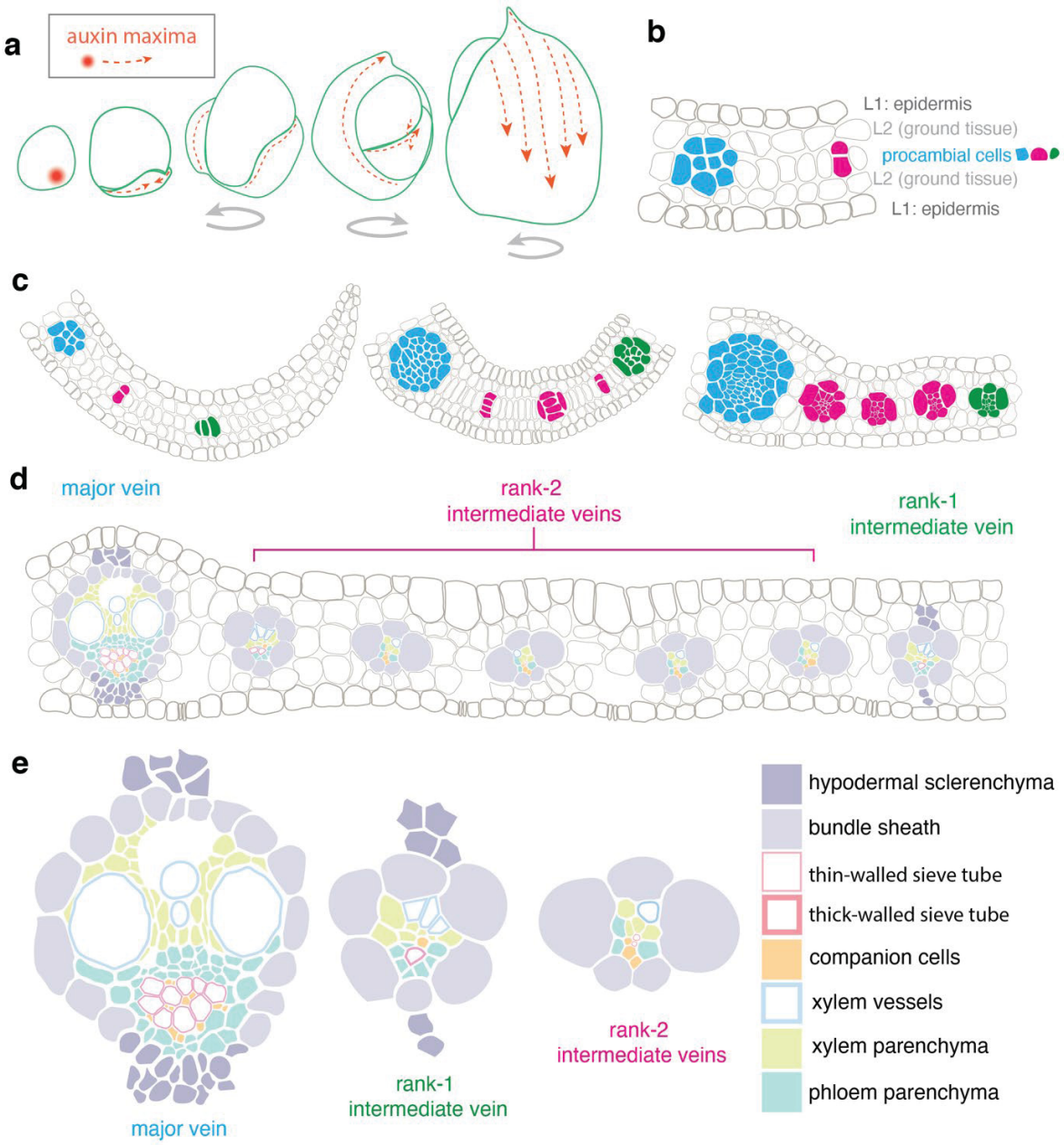

Figure 2. Development of the vasculature of the maize leaf. **a.** Auxin maxima define the position of the leaf primordia, and basipetal flow of auxin defines the position of leaf midrib and lateral veins. **b.** Three different layers comprise the leaf when the procambium cell complexes begin to divide. **c.** Cell patterning at P2-P5 stages of leaf development **d.** Rank-2 intermediate veins are the most abundant vein type, followed by rank-1 intermediate veins, which are easily distinguished by the presence of hypodermal sclerenchyma; major veins are the least abundant. **e.** Three vein types in maize: Major, rank-1 intermediate, and rank-2 intermediate, and the cell types present in each vein. **c-d** adapted from (Sedelnikova et al., 2018).

Dorsoventrality is patterned in the shoot apical meristem during the initiation of leaf primordia by a network of transcription factors which suppress abaxial identity on the adaxial side, and vice versa. For example, expression of *ROLLED LEAF1 (Rld1*) is spatially confined to the adaxial leaf by abaxial miRNA166-mediated transcript cleavage, and this post transcriptional repression is necessary for the development of normal abaxial leaf identity (Juarez et al., 2004; Timmermans et al., 1998). This pattern is maintained throughout development by specific localization of numerous transcription factors, including the abaxial expression of *KANADI* (Candela et al., 2008). Many cellular structures of the leaf display differential dorsoventral patterning: the structure and density of stomata are different on the abaxial and adaxial sides of the leaf (Driscoll et al., 2005), and the vascular patterning is dorsoventrally defined, with xylem and phloem on the adaxial and abaxial sides, respectively. There is evidence that in barley, the bundle sheath cells are differentiated along the dorsoventral axis. Barley abaxial BS ("L-type") have larger chloroplasts than adaxial BS ("S-type"), which have smaller chloroplasts and numerous PD connecting them to the mestome sheath. Based on their abundant PD with mestome sheath cells adjacent to the vasculature, it has been proposed that barley S-type BS are specialized for photoassimilate transport (Williams et al., 1989). It was not known if maize BS cells are differentiated, though they do show substantial size differences, with the two abaxial BS much smaller than the lateral and adaxial BS on average (Bosabalidis et al., 1994).

VII. Rank-2 intermediate veins are a C4 adaptation and the site of phloem loading

Rank-2 intermediate veins are the most numerous vein type in maize, and though they are similar in size to rank-1 intermediate veins, they are distinguishable by their lack of hypodermal sclerenchyma (Sedelnikova et al., 2018) (Figure 2d, e). Major veins are responsible for long distance transport, while rank-2 intermediate veins are critical for phloem loading (Fritz et al., 1983, 1989; Russell and Evert, 1985; Sedelnikova et al., 2018). Rank-2 intermediate veins outnumber rank-1 intermediate veins by approximately 7:1 and major veins by 10:1, and they are considered the primary site of phloem loading (Esau, 1943; Evert et al., 1977) (Figure 2d). Early support for rank-2 intermediate veins as the primary site of phloem loading in maize came from $^{14}CO_2$ labelling studies. In 1989, Fritz

exposed the tip of leaf sections to light and $^{14}CO_2$, and sampled at incremental distances along the path of sucrose transport medial to the light exposure site. In the 'loading' zone where light exposure occurred, the phloem of rank-2 veins was heavily labelled, but not major and rank-1 intermediate veins. With increasing distance from the light-exposed portion, rank-1 and major veins showed a high density of radiolabeled carbon, and lower density in rank-2 intermediate veins. This is consistent with the hypothesis that the labelled carbon was first taken up by rank-2 veins and transported laterally to rank-1 and major veins for long-distance transport (Fritz et al., 1989). Sucrose generally flows via phloem sap from the leaf tip towards the base, but in maize leaves which have been light-starved and supplied with exogenous sucrose solutions, the flow of sucrose was reversed (Heyser et al., 1977). Based on the movement of water-soluble dye, it was found that water moves through the xylem of major veins acropetally, and exits the vasculature radially in the rank-2 and rank-1 intermediate veins (Canny and McCully, 1986). Specifically, it was found that water-soluble ions such as K^+ are transported via the bundle sheath cells to the mesophyll along the transpiration stream (Keunecke et al., 2001).

C3 and C4 plants both have major and rank-1 intermediate veins, but rank-2 intermediate veins are limited to C4 monocots and may be an adaptation to achieve a higher vein density relative to C3 plants. The primary innovation of C4 photosynthesis is the sequestration of carbon reduction by the enzyme RuBisCO to a low-oxygen environment. In maize, this environment is the suberized bundle sheath cell, in which CO_2 is released from the 4-carbon (C4) molecule malate directly at the site of RuBisCO activity; this significantly reduces RuBisCO's otherwise wasteful tendency to perform oxygenation instead of carboxylation, especially in hot, dry environments. The other primary element of photosynthesis is carbon fixation: in maize, this takes place in mesophyll cells, which are exposed to the air in substomatal cavities (Sedelnikova et al., 2018). To facilitate this division of labor, each MS cell is in direct contact with a BS cell. This high vein density results in a ratio of MS to BS closer to 1:1 than that of C3 species, and may also have the added effect of increasing the efficiency of sucrose export from the leaf. Interestingly, veins in the husk leaf are widely spaced, with several MS cells in between veins of the maize cob leaves, and these interim MS cells which are not in direct contact with BS cells utilize C3 photosynthesis, suggesting

that high vein density and the capacity to engage in C4 photosynthesis are correlated. (Langdale et al., 1988; Pengelly et al., 2011).

VIII. Evidence for apoplasmic phloem loading in maize

In order to assess potential phloem loading pathways in the maize leaf, plasmodesmograms were generated based on examination of transmission electron microscopy images of the maize leaf vasculature. It was found that plasmodesmata connect MS to MS, MS to BS, BS cells to vascular parenchyma, but not BS or vascular parenchyma to CC or thin-walled sieve tubes, indicating that the SE-CC complex is symplasmically isolated from the rest of the leaf (Evert et al., 1977, 1978). It is important to note that the presence of plasmodesmata does not indicate whether molecules can actually pass through, as partial or complete occlusion can render plasmodesmata impassible. A theoretical model of symplasmic connectivity is shown in Figure 3. Plasmolysis studies, similar to those performed on beet leaves as described in section II, indicate that the SE-CC has an osmotic potential of 18 bars, while mesophyll and phloem parenchyma cells had only 11 bars, suggesting that solutes are concentrated in the SE-CC (Evert et al., 1978). Sucrose is the only soluble sugar found in xylem exudates of cut maize leaves, suggesting that unlike fructose and glucose, sucrose alone is normally found in the apoplasmic space. This result suggested that sucrose is the main form of photoassimilate exported into the apoplasmic space for phloem loading (Heyser et al., 1978). Together, the results of these experiments indicated that maize employed an active phloem loading mechanism to transport sucrose into the SE-CC.

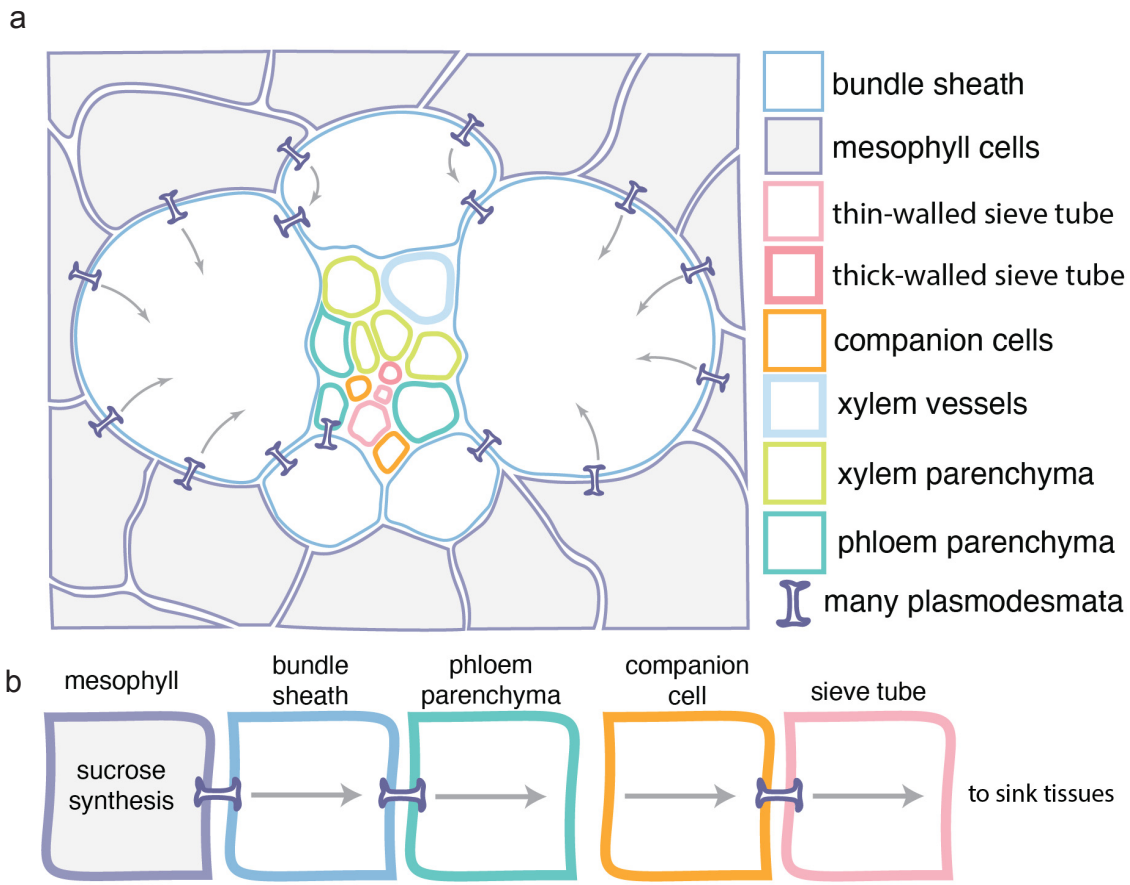

Figure 3. Symplasmic continuity between cell types in the maize leaf. **a.** Illustration of a rank-2 intermediate vein in cross section. **b.** A simplified schematic of cell types involved in sucrose phloem loading, based on what has been shown in Arabidopsis: sucrose is synthesized in the mesophyll and diffuses along its concentration gradient via plasmodesmata through bundle sheath and phloem parenchyma cells. The companion cell-sieve element complex is symplasmically isolated from the rest of the leaf, and an apoplasmic phloem loading step appears to be necessary in both Arabidopsis and maize.

Genetic evidence for active phloem loading in maize was first provided by mutants of *ZmSUT1*, the closest homolog in maize to *AtSUC2*. Like its Arabidopsis homolog AtSUC2, ZmSUT1 is localized to the plasma membrane and transports sucrose in a pH-dependent manner. *zmsut1* mutants have a severely stunted growth phenotype, thin, chlorotic leaves, and are defective at sucrose export from source leaves, as evidenced by higher levels of starch and soluble sugars at dawn in *zmsut1* leaves than in wild-type leaves. Results from *in situ* hybridization as well as transcriptional and translational fluorescent marker lines indicate that *ZmSUT1* mRNA and ZmSUT1 protein are both found in companion cells, but also xylem parenchyma, phloem parenchyma, and bundle sheath cells (Baker et al., 2016;

Slewinski et al., 2009). Based on its localization in xylem parenchyma, which is connected to thick-walled sieve tubes by abundant plasmodesmata, ZmSUT1 is likely involved in sucrose retrieval in addition to its role in CC sucrose uptake. The functional characterization of the ZmSUT1 protein as a H^+/sucrose symporter and the phenotype of *zmsut1* indicated sucrose is actively loaded into the phloem from the apoplasm. However, the identity of a transporter that exports sucrose to the apoplasmic space was unknown.

IX. Maize SWEET13a, b, and c are candidates for missing phloem loading transporter

The closest homologs of Arabidopsis SWEET11 and 12 are ZmSWEET13a, b, and c. We searched for *SWEET13a*, *b*, and *c* transcripts in publicly available bulk-RNAseq data, and found that they were among the most highly expressed transporters in the maize leaf (Chang et al., 2012; Denton et al., 2017; Li et al., 2010; Tausta et al., 2014). To assess the function of SWEET13a, b, and c, we performed transport assays in yeast and *Xenopus laevis* oocytes which indicated that all three paralogs can transport sucrose (Bezrutczyk et al., 2018a). A transporter which exports sucrose to the apoplasmic space would have to be localized to the plasma membrane, and to assess the subcellular localization of SWEET13a, b, and c, I transiently transformed *N. benthamiana* leaf cells with a translational C-terminal GFP fusion reporter construct, and demonstrated that all three SWEET13 homologs are localized to the plasma membrane. Together, these results indicate that SWEET13a, b, and c are plasma membrane localized sucrose transporters with transcripts highly expressed in source leaf tissue, consistent with their putative role as sugar transporters exporting sucrose to the apoplasmic space prior to SUT1 uptake into SE-CC (Baker et al., 2016; Slewinski et al., 2009).

The bundle sheath cells of barley appear to be functionally differentiated, with the 'S-type' medial and adaxial BS cells possibly specialized for sugar transport into the vasculature (Williams et al., 1989). To determine whether bundle sheath cells of maize are differentiated, and to assess the transcriptional profiles of the cells of the maize leaf involved in phloem loading, I performed single cell RNA sequencing (scRNA-seq) on protoplasts released from the maize leaf. Thanks to rapidly expanding use of single cell sequencing technology, we are at the beginning of a revolution of understanding the

relationship of genomics, epigenetics, and transcriptomics of plant tissues at single cell resolution. There now exist numerous published transcriptome atlases of the cells in the Arabidopsis root meristem, as well as the Arabidopsis leaf (Denyer et al., 2019; Kim et al., 2020; Rosenberg et al., 2018; Ryu et al., 2019; Shulse et al., 2019; Wang et al., 2020).

X. scRNA-seq reveals bundle sheath cell sub-populations specialized for phloem loading

Using the 10x Genomics Chromium microfluidics system, protoplasted leaf cells were partitioned, and cDNA libraries of each cell generated and sequenced. However, only mesophyll and bundle sheath were recovered in this experiment. Mesophyll protoplasts are readily released, but a suberin-lignin sheath surrounds the bundle sheath cells and vascular cells within, preventing efficient release of BS or vascular cell protoplasts (Kanai and Edwards, 1973). Many protocol modifications, including increasing enzymatic concentrations and temperature, failed to improve the diversity of cell types released as protoplasts. Additionally, because filtration steps risk damaging the protoplasts, it was difficult to completely remove debris, such as xylem vessels, from the cell suspension. Debris caused the microfluidic device to clog during cell partitioning on one occasion, and cDNA synthesis failed on two occasions. Because of these challenges, a complete atlas could not be constructed. However, two datasets were generated with 3763 and 3242 cells, based on which I determined that a subtype of maize bundle sheath cell shows enrichment of transcripts of *SWEET13a*, *b*, and *c*, as well as amino acid transporters such as *UmamiT21a.* This suggests that these BS cells may be specialized for nutrient transport (Bezrutczyk et al., 2020). Notably, all BS cells in the dataset, including the transport-specialized BS cells, show high expression of canonical C4 photosynthesis genes. Several transcription factors such as *DOF3* (*DNA-binding with one finger*) and *bZIP4 (BASIC LEUCINE ZIPPER4)* were also expressed in the transport-specific BS cells. Using RNA *in situ* hybridization, and translational GUS fusion reporter lines, I showed that the transport-specialized sub-population of BS cells are the abaxial bundle sheath cells, which are directly adjacent to the phloem. This phenomenon appears to be limited to rank-2 intermediate veins, which are the most abundant, smallest, and as described in VII, shown to be the main site of phloem loading. In a parallel study, scRNA-seq of the Arabidopsis

leaf was performed, with all known Arabidopsis leaf cell types represented (Kim et al., 2020). The cells of the phloem parenchyma cluster were enriched for mRNAs encoding many transport proteins, including sucrose transporters *AtSWEET11* and *AtSWEET12*, amino acid transporter *AtUmamiT21,* and nitrate transporters *AtNPF5.8* and *AtNPF5.*9, which are homologous to genes encoding transporters which are enriched in the maize abaxial bundle sheath cluster. Therefore, rank-2 intermediate veins of maize appear to have co-opted the nutrient transport functions which were canonically thought to be the purview of phloem parenchyma, based on Arabidopsis single-cell transcriptional profiles (Chen et al., 2012; Kim et al., 2020).

To determine if SWEET13a, b, and c were necessary for phloem loading, we generated triple knockout mutants using a multiplexed CRISPR-Cas9 approach, and discovered that the plants were stunted, chlorotic, and accumulated starch and soluble sugars in the bundle sheath at a much higher rate than wild-type: a phenotype consistent with a failure of phloem loading (Bezrutczyk et al., 2018a). Together, these results indicate that SWEET13a, b, and c are abaxial-bundle sheath expressed transporters which are necessary for sucrose export to the apoplasmic space adjacent to the phloem.

XI. Dynamic regulation of SWEETs upon pathogen challenge

In addition to the role that SWEET transporters play in plant development under optimal conditions, these transporters are dynamically regulated when the plant is stressed, presumably to allocate sugars to tissues in which they are needed or alternatively, to feed pathogens (Bezrutczyk et al., 2018b). Carbon partitioning may be severely disrupted during pathogen infection, as the pathogen may elicit the expression of sugar transporters to generate a new ‘sink’. Bacteria, fungi, viruses all alter sugar partitioning. For example, *SWEET4a* and *SWEET4b*, which are expressed in the developing seed under normal conditions, are upregulated at the site of *Ustilago maydis* infection (Sosso et al., 2019), presumably to feed the pathogen. In rice, the relationship between *OsSWEET* induction and *Xanthomonas oryzae* pv. *oryzae* (*Xoo*) has been well established. *Xoo* invades the rice xylem and secretes a TAL effector which binds to known sites in the promoter of *SWEET11*, *13*, or *14*, depending on the strain (Chen et al., 2010; Chu et al., 2006; Yang et

al., 2006). This results in an upregulation of the transporter. Rice varieties with naturally-occurring polymorphisms in these TAL effector binding sites, as well as elite varieties in which CRISPR-Cas9-mediated mutations have been induced, are resistant to *Xoo* infection (Eom et al., 2019; Oliva et al., 2019; Zaka et al., 2018).

XII. Pathogen feeding vs. sugar signaling hypothesis

To explain why pathogens cause an upregulation of sugar transporters, there are at least two hypotheses, which are not mutually exclusive. First, a pathogen may consume the plant-generated sugars to fuel its own metabolic processes and reproduction. Alternatively, changes in sugar concentrations can be detected by the plant and act as signals to generate robust defense mechanisms: hexose sensing in the secretory pathway can lead to the upregulation of defense genes (Gebauer et al., 2017; Herbers et al., 1996; Horsfall and Dimond, 1957). Sugar transporters themselves may act as sugar sensors (Bezrutczyk et al., 2018b). Necrotrophic and biotrophic fungal pathogens elicit different responses in plants. Necrotrophic pathogens tend to destroy cells, and the plant may upregulate transporters which draw sugars leaked from damaged cells away from the apoplasmic space, thereby limiting the pathogen's ability to feed on sugars released from decaying cells. Biotrophic pathogens, on the other hand, may elicit a salicylic acid-mediated hypersensitive response, in which the plant releases a burst of reactive oxygen species at the site of infection and creates an island of dead tissue around the pathogen, effectively stranding it (Glazebrook, 2005). Biotrophic pathogens may feed from appressoria positioned next to a cell in the apoplasm (Sosso et al., 2019), or by haustoria which feed from a sealed compartment, the extrahaustorial space (Moore et al., 2015). Our understanding of how transporters are involved in pathogen feeding and defense will be greatly aided by specific localization of transporters relative to the site of pathogen feeding. Ultimately, the use of genetically encoded sensors which show ratiometric responses to sugars in the plant cell, apoplasmic space, and inside the pathogen, will allow us to monitor the transfer of sugars from host to pathogen.

CONCLUSION

Sugar transport from the source to sink tissues involves the critical step of phloem loading, and it has been shown that in Arabidopsis, this is accomplished by SWEET sugar transporters in phloem parenchyma exporting sucrose into the apoplasmic space, where it is actively taken up by SUC2 into the sieve element-companion cell complex for long distance transport. To understand the role of individual cell types involved in phloem loading in maize, I performed single cell RNAseq on protoplasts released from the maize leaf. Only mesophyll and bundle sheath cells were recovered in this experiment, with a small group of cells that may have represented companion cells discarded due to low mRNA counts. I determined that a subset of BS is specialized, and express transcriptional networks related to transport, as evidenced by enrichment of *SWEET13a*, *b*, and *c* sucrose transporter mRNAs, as well as other sugar and amino acid transporter mRNAs. Localization of *SWEET13a, b,* and *c* mRNA via *in situ* hybridization, and SWEET13a protein via GUS staining, indicated that the specialized BS cells are the abaxial bundle sheath (^{ab}BS) cells of the rank-2 intermediate veins. Many of the transporters which are enriched in the ^{ab}BS cells in maize are homologous to transporters which are enriched in the phloem parenchyma cells of Arabidopsis, indicating that maize rank-2 intermediate vein ^{ab}BS cells and Arabidopsis phloem parenchyma cells may share a transcriptional network. Several of the transport proteins encoded by mRNAs that are enriched in the ^{ab}BS cells are upregulated during the source-sink transition of the maize leaf, suggesting that they may be part of a co-regulated phloem loading transcriptional module. To determine if SWEET13a, b, and c are important for phloem loading, CRISPR-Cas9-mediated knock-out mutants were generated, and *sweet13abc* plants were stunted compared to wild-type. The leaves of *sweet13abc* also showed an accumulation of starch and soluble sugars at dawn, unlike wild-type plants. The mutant plants' stunted growth morphology and carbohydrate accumulation in leaves are both consistent with impaired phloem loading. Together, these results suggest that in the rank-2 intermediate veins, which are the main site of phloem loading, sucrose is exported from the abaxial BS to the apoplasm by SWEET13a, b, and c and subsequently taken up into the SE-CC by SUT1 for long distance transport. This represents a novel pathway for phloem loading via ^{ab}BS cells instead of

phloem parenchyma. SWEETs and other sugar transporters also play a role in pathogen defense, and modification of sugar transporter expression has been shown to be useful for engineering solutions to this agricultural challenge.

SYNOPSIS OF PUBLICATIONS AND MANUSCRIPTS

Margaret Bezrutczyk, Nora R. Zöllner, Colin P. S. Kruse, Thomas Hartwig, Tobias Lautwein, Karl Köhrer, Wolf B. Frommer and Ji-Yun Kim, **Phloem loading via the abaxial bundle sheath cells in maize leaves.**

doi: https://doi.org/10.1101/2020.09.06.284943

Submitter's contributions: Conceived and designed experiments with W.B.F and J.K.. Performed experiments: grew plants, optimized protoplasting protocol with J.K., analyzed single cell sequencing and bulk sequencing data with C.P.S.K, designed probes and performed in situ hybridizations with N.Z., designed GUS constructs, performed GUS staining, performed RT-qPCR, co-wrote manuscript with W.B.F. and J.K. Transformation of B104 with SWEET13a:GUS construct was performed at VIB-Ghent Transformation Facility, 10x Genomics Chromium cell partitioning and cDNA library preparation was performed at HHU Genome Center (T.L, K.K). Bulk RNA library preparation was performed by T.H.

Supplementary results included

Bezrutczyk, M., Hartwig, T., Horschman, M., Char, S.N., Yang, J., Yang, B., Frommer, W.B. and Sosso, D. (2018), **Impaired phloem loading in zmsweet13a,b,c sucrose transporter triple knock-out mutants in Zea mays.** New Phytol, 218: 594-603. doi:10.1111/nph.15021

Accepted for publication: April 2018.

Submitter's contributions: Conceived and designed experiments with W.B.F and D.S.. Performed experiments: genotyped and phenotyped plants with assistance from M.H., performed RT-qPCR, transformed and imaged transgenic tobacco plants for subcellular localization, performed photosynthesis measurements, contributed to writing manuscript with W.B.F. and D.S. Prepared revisions with W.B.F. and D.S. D.S. performed sucrose transport assays. T.H., S.N.C, J.Y. performed GWAS analysis. B.Y. transformed Hi-II plants with CRISPR-Cas9 construct targeting *SWEET13a*, *b*, and *c*.

Bezrutczyk, M., Yang, J., Eom, J.-S., Prior, M., Sosso, D., Hartwig, T., Szurek, B., Oliva, R., Vera-Cruz, C., White, F.F., Yang, B. and Frommer, W.B. (2018), **Sugar flux and signaling in plant–microbe interactions**. Plant J, 93: 675-685. doi:10.1111/tpj.13775

Accepted for publication: November 2017.

Submitter's contributions: Wrote manuscript with W.B.F.

PHLOEM LOADING VIA THE ABAXIAL BUNDLE SHEATH CELLS IN MAIZE LEAVES

Margaret Bezrutczyk, Nora R. Zöllner, Colin P. S. Kruse, Thomas Hartwig, Tobias Lautwein, Karl Köhrer, Wolf B. Frommer and Ji-Yun Kim

Phloem loading via the abaxial bundle sheath cells in maize leaves

Margaret Bezrutczyk[1], Nora R. Zöllner[1], Colin P. S. Kruse[2], Thomas Hartwig[1], Tobias Lautwein[3], Karl Köhrer[3], Wolf B. Frommer[1,4,*] and Ji-Yun Kim[1]

AFFILIATIONS

[1] Institute for Molecular Physiology, Heinrich-Heine-University Düsseldorf, Düsseldorf 40225, Germany

[2] Los Alamos National Laboratory, Los Alamos, New Mexico, USA, 87545

[3] Biological and Medical Research Center (BMFZ), Genomics and Transcriptomics Laboratory (GTL), Medical Faculty, Heinrich Heine University Düsseldorf, Düsseldorf, Germany

[4] Institute of Transformative Bio-Molecules (WPI-ITbM), Nagoya University, Chikusa, Nagoya 464-8601, Japan

* Correspondence: frommew@hhu.de

ABSTRACT

Leaves are asymmetric, with differential functionalization of abaxial and adaxial tissues. The bundle sheath (BS) surrounding the vasculature of the C3 crop barley is dorsoventrally differentiated into three domains: adaxial structural, lateral S-type, and abaxial L-type. S-type cells seem to transfer assimilates towards the phloem. Here we used single-cell RNA sequencing to investigate BS differentiation in C4 maize. Abaxial BS (^{ab}BS) cells of rank-2 intermediate veins specifically expressed three SWEET sucrose uniporters (*SWEET13a, b,* and *c*) and UmamiT amino acid efflux transporters. *SWEET13a, b, c* were also identified in the phloem parenchyma (PP). Thus maize acquired a unique mechanism for phloem loading in which ^{ab}BS cells provide the main pathway for apoplasmic sucrose transfer towards the phloem. This pathway predominates in veins responsible for phloem loading (rank-2 intermediate), while rank-1 intermediate and major veins export sucrose from the phloem parenchyma (PP) adjacent to the sieve element companion cell (SE/CC) complex, as in Arabidopsis. We surmise that ^{ab}BS identity is subject to dorsoventral patterning and has components of PP identity. These observations provide first insights into the unique transport-specific properties of ^{ab}BS cells and support for a modification to the canonical phloem loading pathway of maize, which may be generalizable to other C4 monocots.

KEYWORDS

Single cell sequencing, *Zea mays* L., SWEET, SUT, sucrose, transporter, UmamiT, amino acid transporter

INTRODUCTION

Leaves are typically asymmetric: there are often differences in the relative stomatal and trichome densities and cuticle properties between the abaxial and adaxial leaf surfaces. While maize leaves are amphistomatic, asymmetry remains apparent, with bulliform cells only on the adaxial side and a conjoint, collateral and closed-type vasculature, with adaxial xylem and abaxial phloem. Dorsoventral patterning in maize leaf is initiated in the shoot apical meristem at the earliest stages of leaf primordia development by expression of *RGD2* (*Ragged seedling2*) (Henderson et al., 2006) and adaxial expression of *RLD1* (*Rolled leaf1*), which is conferred by miRNA166-mediated *RLD1* transcript cleavage on the abaxial side (Juarez et al., 2004b, 2004a). This pattern is maintained throughout development by specific localization of numerous transcription factors, including the abaxial expression of *KANADI* (Candela et al., 2008). Bundle sheath cells (BSCs) of maize are not known to be functionally differentiated. In barley leaves, the BSCs are anatomically distinct: abaxial side "L-type" BSC have large chloroplasts, while "S-type" BSCs, with small chloroplasts, surround the rest of the mestome sheath. It was proposed that the S-type cells may be specialized for photoassimilate transport, based on the rapid disappearance of starch after the light period and the abundant plasmodesmatal connections between S-type cells, mestome sheath, and phloem (Williams et al., 1989). In maize, the two abaxial BSCs (^{ab}BSCs) are typically smaller compared to the medial BSCs. *In situ* hybridization and immunolocalization had shown that Rubisco, the glutamine synthetase isoform GS1-4 (*GLN3*), and malic enzyme localized specifically to BS, with transcripts and proteins equally represented in all BSCs (Langdale et al., 1988a; Martin et al., 2006). Here we used single cell RNA sequencing (scRNA-seq) to test whether the BS of the C4 plant maize is uniform or also shows a dorsoventral differentiation of its cells, as found in barley. The analysis identified mesophyll- and bundle sheath-specific transcripts and found that the BS could be subclustered into two groups, one specifically expressing a variety of genes including SWEET13 sucrose transporters, UmamiT and AAP amino acid transporters, as well as several transcription factors. *In situ* hybridization and analysis of translational GUS fusions demonstrated that the subclustering was due to dorsoventral patterning, as evidenced by the finding that the three SWEET13 paralogs were specifically expressed in ^{ab}BS. These findings not only show that the maize leaf BS is functionally differentiated, but also identify a unique pathway for apoplasmic phloem loading in a C4 plant. In addition, the three SWEET13s were also present in cells that most likely represent the phloem parenchyma, similar to the profiles of their Arabidopsis orthologs AtSWEET11, 12, and 13. Maize ^{ab}BS thus appears to use a combination of dorsoventral patterning and PP identity to drive sucrose into the apoplasm of the phloem.

RESULTS

mRNA patterns of specific cell types in maize leaves

To determine whether maize leaves contain multiple BSC types, we performed single-cell sequencing on protoplasts isolated from maize leaves. We first established a protocol for protoplast release. To minimize the possibility of a developmental gradient across cells, fully differentiated tissue was harvested from the distal portion of leaf 2 of late V2 stage plants (first and second leaf collar exposed) (Li et al., 2010) (Fig. 1a). Standard leaf protoplasting protocols leave intact bundle sheath 'strands,' consisting of BSCs and the vasculature (Kanai and Edwards, 1973; Langdale et al., 1989). In a parallel study, we were able to optimize protoplasting of Arabidopsis leaves to increase the yield of vascular cell types (Kim et al., 2020). We compared published protocols and varied parameters such as incubation time, enzyme concentration, enzyme blend, and preincubation in L-cysteine (Ortiz-Ramírez et al., 2018). Efficiency of the release of putative vascular cells was monitored using qRT-PCR with cell-type specific markers, under the assumption that the *SWEET13* paralogs, analogous to their Arabidopsis orthologs, would be specific to phloem parenchyma. Although none of the protocols were able to yield efficient release of putative vascular cells, we obtained apparent release of both BSCs and vascular cells with Protocol 4 (Supplementary Fig. 1).

An estimated 7,000 protoplasts were pipetted into a 10x Chromium microfluidic chip, and single cell cDNA libraries were generated and sequenced. Gel bead-specific barcodes were used to identify mRNAs present in specific cells. After filtering the dataset to select for healthy cells, 4,035 cells with an average of 4,874 mRNA molecules per cell were analyzed. Unsupervised clustering was performed using Seurat (Butler et al., 2018) to determine the relationship between mRNA expression profiles in PCA space, ultimately represented in a two-dimensional UMAP plot (Fig. 1b). Cell identities were assigned to the clusters based on established marker genes for different cell types (Supplementary Table 1). We obtained six clusters, five of which formed a large supercluster that all had mesophyll identities, and one separate cluster corresponding to bundle sheath identity (Fig. 1c). The distribution of marker genes was consistent with the roles of mesophyll and BS cells in C4 photosynthesis (Supplementary Fig. 2, Supplementary Table 2). The ratio of mesophyll to BSC was ~75:1, indicating a low efficiency of BSC retrieval. To our surprise, no vascular cells were recovered. The BS cluster was further divided into two subclusters, the "upper" and "lower" subclusters, which later were assigned as abaxial (^{ab}BS) and adaxial (^{ad}BS) bundle sheath cells (Fig. 1d, Fig. 2) (see below).

Mesophyll and bundle sheath clusters show canonical expression of C4 photosynthesis genes

Unsupervised clustering resulted in five clusters of mesophyll cells based on the presence of canonical C4 marker genes. At first sight the presence of five clusters was surprising. Cluster MS1 included most mesophyll cells and likely represents the core mesophyll. MS1 was enriched in photosynthetic processes. MS2 was enriched for the GO terms triose phosphate transport (GO:0035436; GO:0015717), nucleic acid metabolic process, immune system process (GO:0002376) and RNA metabolic process (GO:0016070) (Supplementary Table 1, 3). MS3 and MS4 contained high levels of rRNA transcripts. rRNA was not removed before sample preparation nor were cells with higher rRNA transcript levels, as rRNA levels can vary between cells. Whether these rRNA-enriched clusters represent biologically relevant cell populations in the leaf or are due to artifacts was not further evaluated. An additional subcluster, MS5, had an apparent mesophyll identity, but was clearly separated from the other mesophyll clusters. The main determinants for this separate clustering were iron/metal-related processes (Supplementary Text). Due to the focus on BSCs, localization and biological relevance of MS5 was not characterized further. Our clustering data are supported by the presence of transcripts for the glutamine synthetase *GLN4* (corresponding to *gln1-3* and protein GS1-3) in the MS1-4 cells, consistent with previous *in situ* and immunolocalization data that detected glutamine synthetase specifically in the mesophyll (Supplementary Fig. 3) (Martin et al., 2006).

It may be interesting to explore further whether the subclustering of mesophyll cells represents developmental trajectories or physiological differences. We did not identify an obvious pattern that could be attributed to, for example, dorsoventral patterning due to developmental gradients or due to changes in light properties as it passes through the leaf. Similar observations regarding the presence of multiple mesophyll clusters were made for scRNA-seq analyses of Arabidopsis leaves, however, it was not possible to assign palisade and spongy parenchyma to any of the mesophyll clusters (Kim et al., 2020).

Both subsets of bundle sheath cells express canonical C4 photosynthesis genes

In maize, photosynthesis is partitioned between the mesophyll and bundle sheath cells (Li et al., 2010; Chang et al., 2012; Friso et al., 2010), allowing us to differentiate between these cell populations based on their mRNA profiles. Maize leaves utilize an NADP-ME-dependent C4 pathway, and mesophyll cells and bundle sheath cells must exchange intermediate species via plasmodesmata, with specific enzymes highly upregulated in one cell type or the other. To identify the clusters, we selected several key marker genes that are known to be differentially expressed in either mesophyll or bundle sheath.

Most of the genes involved in primary carbon metabolism, which showed significant differential expression in the 2010 proteomics survey of MS and BS chloroplasts (Friso et al., 2010), were expressed in the expected cell types in our dataset (Supplementary Fig. 2, Supplementary Table 1, 2), except for the predicted chloroplast envelope transporter *TPT* and the Calvin cycle enzyme *PGK2*, which were both expressed nearly equally in both MS and BS clusters. For example, transcripts of pyruvate orthophosphate dikinase 2 (*PDK2*) were almost exclusively found in BSCs, while *PDK1* transcript levels were high in mesophyll (Supplementary Fig. 2, Supplementary Table 1, 2), in agreement with both proteomics data (Friso et al., 2010) and their corresponding contributions to C4 photosynthesis (Chastain et al., 2017). All cells in the BSC subcluster showed high and specific expression of the canonical C4 photosynthesis-related genes that function in the BSCs, including *RBCS*, *ME1*, and *PCK1* (Supplementary Fig. 2, Supplementary Table 2). The Rubisco small chain mRNAs (*RBCS1*, *RBCS2*) were equally distributed in both abaxial and adaxial BS subclusters (Fig. 1). The bundle sheath-specific glutamine synthetase *GLN3* (corresponding to gene *gln1-4* and protein GS1-4) was found in both BS subclusters, consistent with *in situ* and immunolocalization data that showed no evidence for a specific pattern for GS1-4 in the BS (Supplementary Fig. 3) (Martin et al., 2006).

Abaxial BS cluster is enriched for genes encoding transport proteins

The two BS cell subclusters (Fig. 1d) could either represent developmental trajectories along the leaf axis, BS cells from the three different vein classes (major vein or rank-l or rank-2 intermediate veins), different physiological states, or dorsoventral patterning. While the majority of mRNAs corresponded to BS identity, only 5 genes appeared specific to ^{ad}BS (the "lower subcluster") and 39 to ^{ab}BS (the "upper" subcluster) (Table 1). Surprisingly, among the genes with the highest difference between the two BS subclusters were the three *SWEET13a*, *b*, and *c* paralogs. SWEETs are uniporters, and maize SWEET13a, b and c function as sucrose transporters.

Similar to their orthologs AtSWEET11 and 12 from Arabidopsis, in maize leaves SWEET13a, b, and c are critical for phloem loading of sucrose (Bezrutczyk et al., 2018), though it remained unknown if the maize SWEET13s were co-expressed in the same cells and in which cell types they function. All three *SWEET13* paralogs were present in BSCs in maize, while the Arabidopsis orthologs *AtSWEET11*, *12* and *13* are specifically expressed in PP (Kim et al., 2020). This observation is consistent with the qRT-PCR results performed during the optimization of the protoplast protocol, which detected *SWEET13* transcripts, but no vascular cells were recovered by scRNA-seq. The "upper" BS subcluster, ^{ab}BS, showed a striking enrichment for transport proteins, with 9 of 39 ^{ab}BS-specific genes involved in transport (Table 1). Importantly, this included not only

SWEET13a, *b*, and *c*, but also an STP hexose transporter (STP3), the amino acid efflux transporter *UmamiTT21a* (Supplementary Fig. 4), two members of the H^+/amino acid symporter family, *AAP56* and *AAP45* (Deng, 2014), a member of the nitrate peptide transport family, and the H^+-ATPase AHA3 (Table 1). Notably, in Arabidopsis, transcripts for the closest Arabidopsis homolog of Zm*UmamiT21a*, *AtUmamiT21*, were enriched in PP (Fig. 3) and co-expressed with *AtSWEET11* and *12* in Arabidopsis. On the basis of the presence of SWEETs, UmamiT21 and other ^{ab}BS-enriched candidates, one may speculate that the transcription factors that in Arabidopsis are involved in PP identity have been recruited in maize to ^{ab}BS to drive the unique set of genes expressed in ^{ab}BS. *DOF3* (*DNA binding with one finger3*) is a transcription factor implicated in the control of SWEET gene expression in rice (Wu et al., 2018) which shows ^{ab}BS-specific expression in this dataset; two other transcription factors, *bZIP4* (*ABA-insensitive 5-like protein*) and *MYB25* (just below p-value cutoff), were enriched in ^{ab}BS. While ^{ab}BS-enriched, *bZIP* and *MYB25* were not BS-specific, but only sparsely expressed in mesophyll cells (Supplementary Figure 3).

Other BSC-specific genes such as *RBCS1* showed equal transcript distribution across all BS cells, excluding the possibility of an artefact, e.g., a gradient of cells differing in UMI counts. This included *UmamiT20a*, which was BS-enriched but equally expressed across both BS subclusters. The lack of specificity of many genes for subsets of BSC is consistent with published data from *in situ* hybridization and immunolocalization of *RBCS1* and glutamine synthetase, both of which did not show dorsoventral patterning (Langdale et al., 1988a; Martin et al., 2006; Langdale et al., 1988b).

To test the hypothesis that the two BS subclusters may represent spatially discrete BSC populations, *in situ* hybridization was used to localize the mRNAs of the *SWEET13a, b,* and *c* genes (Fig. 2b-f, Supplementary Fig. 5). Notably, transcripts of all three *SWEET13* genes were specifically detected in the two abaxial bundle sheath cells (^{ab}BSCs) adjacent to the phloem. Additionally, *SWEET13a, b,* and *c* transcripts localized to the PP (Fig. 2c, Supplementary Fig. 5) similar to *AtSWEET11*, *12,* and *13* (Kim et al., 2020; Chen et al., 2012). Using three independent sets of probes, transcripts of all three SWEET13s were almost exclusively found in the ^{ab}BS of rank-2 intermediate veins, which are a special adaptation of C4 monocots (Langdale et al., 1988a) and serve as the main sites of phloem loading (Fritz et al., 1989, 1983). *SWEET13a* was detected in both ^{ab}BS and PP in about 23% of the rank-2 intermediate veins. Thus, in the veins that are the main loading sites, sucrose efflux towards the SE/CC for phloem loading must occur predominantly from the ^{ab}BS into the apoplasm towards the phloem, and only to a smaller extent by direct release at the SE/CC from PP. Rank-1 intermediate veins seemed to have a more balanced distribution of *SWEET13a* between

[ab]BS and PP. In major veins, SWEET13 transcripts were also present in the medial vascular parenchyma, and the main path appeared to be through release from PP.

Since protein abundance does not always correlate with mRNA levels (Walley et al., 2016), we evaluated the cell specificity of the SWEET13a protein. Maize lines were generated that stably expressed translational GUS reporter fusions (*SWEET13a-GUS*) comprising 6 kb upstream of the ATG and all exons and introns. Six transgenic lines from three independent transformation events showed consistent localization of the SWEET13a-GUS fusion protein in the [ab]BS and phloem parenchyma of rank-1 and -2 intermediate veins, and in the PP of the major veins (Fig. 4; Supplementary Fig. 5). In summary, *in situ* hybridization and immunolocalization showed that *SWEET13a, b, and c* transcripts and SWEET13a protein were not only found in the PP of maize, but also in a subset of BSCs, specifically the [ab]BS. This is different from the cellular expression of their orthologs in the dicot Arabidopsis, suggesting that an additional sucrose phloem loading pathway evolved in C4 monocots (Langdale et al., 1988a).

SWEET13a- c and *SUT1* sucrose transporters are expressed in complementary cell types

Sucrose released from cells by SWEETs is taken up actively into the SE/CC by SUT1 H^+/sucrose symporters (Riesmeier et al., 1994; Bürkle et al., 1998; Gottwald et al., 2000; Slewinski et al., 2009). To directly compare SWEET13 and SUT localization, *in situ* hybridization was performed in parallel using the same method from leaves at the same stages of development. *SUT1* RNA was typically found in one or two cells in the phloem, which most likely represent companion cells, where it is responsible for phloem loading. In rank-1 and major veins, *SUT1* mRNA was also detected in the medial vascular parenchyma, where it likely contributes to sucrose retrieval (Heyser et al., 1977). In our experiments, *SUT1* transcripts were not detected in bundle sheath cells, consistent with *SUT1* expression below the detection limit in of our BSC single cell dataset (Fig. 2g-h; Supplementary Fig. 5).

Abaxial BS transcripts are co-regulated during the sink-source transition

In Arabidopsis, many PP-specific genes were found to also be co-regulated (Kim et al., 2020). We therefore tested whether several of the transporter genes identified in [ab]BS might also be co-regulated. *SUT1* H^+/sucrose symporter genes are typically lowly expressed in young net-importing leaves and induced during the sink to source transition (Bürkle et al., 1998; Riesmeier et al., 1993). RNA was extracted from different segments of leaf 3 of V2 plants, in which the tip had transitioned to source while the base was still in the sink state (Tausta et al., 2014) (Fig. 5a) for qRT-PCR. *SWEET13a,* and *UmamiT21, AAP45*, and *SUT1* had transcript levels that were 115-, 34-, 23-, and

10-fold higher, respectively, than in the tip of leaf 3 (source) compared to the base (sink) (Fig. 5a, b). SWEET13a protein levels were also higher in source regions of the leaf (Fig. 5c). SWEET13a was not detected in stem sections near the base of the plant, which contain whorls of developing leaves, nor in root tip (Fig. 5d-f). In leaves, SWEET13a protein was not detectable in tissue other than the tip of leaf 3, consistent with its role in phloem loading in source leaves The co-regulation of ^{ab}BS-enriched genes during the developmental transition of leaves not only links them to transfer of nutrients to the phloem, but also indicates that they are all controlled by the same regulatory system.

DISCUSSION

While single cell sequencing was successfully used to identify the transcriptomes of vascular cells in Arabidopsis (Kim et al., 2020), the suberin-lignin barrier surrounding the bundle sheath of maize leaves prevented access to vascular cell transcriptomes in maize. With an optimized protocol, BSC were released and could be identified based on a broad range of known marker genes. BSC separated into two subclusters. mRNA for BSC markers such as *RBCS* and GS1-4 were present at equal levels in both subclusters, whereas others were specifically enriched in one of the two subclusters. Because only moderately and highly expressed mRNAs are captured with droplet-based scRNA-seq protocols such as 10x Chromium, we cannot exclude that transcripts that appear to be specific are present at lower levels in the other cell types. A major surprise was the finding that mRNA for all three *SWEET13* paralogs was present in BSCs, in clear contrast to the distribution of their orthologs in Arabidopsis (Chen et al., 2012). Since barley BSCs seem clearly differentiated, with S-type cells suspected to represent a preferential site of sucrose transfer into the phloem (Williams et al., 1989), we tested whether *SWEET13a*, *b*, and *c* mRNA would be present in adaxial and lateral BSCs. To our surprise, *in situ* hybridization and the analysis of translational GUS fusions showed that all three SWEET13s were preferentially expressed in the ^{ab}BS cells of rank-2 intermediate veins, which are considered the main sites of phloem loading in maize. In maize, these two abaxial BSCs are smaller compared to the medial BSCs (Bosabalidis et al., 1994). In rank-2 intermediate veins of maize, it appears that the ^{ab}BS cells may have recruited sucrose-transporting *SWEETs* to export sucrose toward the abaxially localized phloem (Fig. 6). This presents a unique pathway, in which BSCs likely export photosynthetically derived sucrose to the apoplasm of the phloem on the abaxial side of the leaf. Rank-2 veins are thought to be an emergent phenomenon of C4 grasses (Sedelnikova et al., 2018). Rank-2 veins increase the ratio of BS to MS cells, the vein density, and the capacity for nutrient transport. They appear to be the main path for sucrose phloem loading. It is thus conceivable that the unique phloem loading pathway coevolved with the evolution of the rank-2 intermediate veins.

Given the findings of Williams *et al* (Williams et al., 1989), which indicate that barley uses adaxial and medial BSCs for phloem loading, our results suggest that the two species use distinct sets of BSCs for transferring sucrose from the BS to the phloem. This may be generalizable to other C3 and C4 species, and it will be interesting to explore whether *SWEETs* are also present in medial BSCs of barley. ^{ab}BS and ^{ad}BS transcript profiles are highly similar, possibly explaining why this differentiation of BSCs had previously not been identified.

In rank-1 intermediate and major veins, *SWEET13a, b* and *c* transcripts were also detected in cells in the vasculature that most likely correspond to phloem parenchyma, thus similar to the canonical pathway in Arabidopsis (Chen et al., 2012; Cayla et al., 2019). Phylogenetic and functional analyses had shown that the PP transporters AtSWEET11 and 12 from Arabidopsis are orthologous to the three SWEET13 isoforms (Bezrutczyk et al., 2018). Subsequent to SWEET-mediated efflux, sucrose is taken up actively by SUT1/SUC2 H^+/sucrose symporters in both maize and Arabidopsis (Gottwald et al., 2000; Slewinski et al., 2009). This is supported by *in situ* hybridization of *SUT1* in maize leaves (Supplementary Fig. 5). PP localization of *SUT1* is consistent with previously published results (Baker et al., 2016). We could not confirm previous data that indicated that SUT1 may also be expressed substantially in BSCs (Supplementary Fig. 5). Localization of *SUT1* in vascular parenchyma (VP) is consistent with a role in sucrose retrieval on the side of the phloem that faces the xylem. Our data are compatible with the presence of two distinct sites for phloem efflux in maize leaves, one from ^{ab}BS and a more standard path from PP (Fig. 6). This unique pathway may be a specific adaptation of maize leaves in the context of C4 photosynthesis, to provide higher rates of sucrose flux towards the phloem. No doubt, *SWEET13a, b* and *c* are key players for phloem loading, though at present we cannot assess the relative contribution of this new efflux step. This model could be tested by inhibiting SWEET activity specifically either in BSC or PP. However, since transcription factors driving expression of genes specifically in maize ^{ab}BS or PP are not currently known, this hypothesis could be tested by generation of lines in which *SWEET13* mRNA levels have been repressed through BSC-specific RNAi.

Notably, transcripts for other transporter genes were also enriched in ^{ab}BS. This includes UmamiT21a, a member of the UmamiT amino acid transporter family. One of the key findings from the analysis of PP in Arabidopsis by scRNA-seq was that multiple members of this family were specifically expressed in PP (Fig. 3, Table 1)(Kim et al., 2020). Since they appear to play roles analogous to that of SWEETs in cellular efflux of amino acids in Arabidopsis, it appears that ^{ab}BS, besides having clear BSC identity, has acquired components or subnetworks of the PP identity. The co-regulation of at least some of the ^{ab}BS-enriched genes further strengthens this hypothesis. Interestingly, we also observed a weak enrichment of the abaxial KANADI transcription factor (Fig. 2a). KANADI plays a key role in determining abaxial identity in leaves (Candela et al., 2008). We therefore hypothesize that one or several transcriptional regulators that are involved in the regulation of the efflux of sucrose and amino acids from PP have been brought under control of both a polarity cue and the BS identity cues in order to increase nutrient flux towards the maize phloem. It will be fascinating to identify the transcription factors that are involved in controlling the PP and BSC identities and to dissect the SWEET promoters to determine

which *cis*-elements are involved in the acquisition of the ^{ab}BS cell fate. Several transcriptional regulators have been identified as candidates for the induction of ^{ab}BS cell fate; however, the limitations of sequencing depth in 10x Genomics Chromium droplet-based scRNA-seq preclude a comprehensive profiling of all transcriptional regulators. Methods that provide higher sensitivity may help to address this aspect. Importantly, the ^{ab}BS genes identified provide unique insight into the specialized nature of this cell type.

Comparison of this phenomenon in other grasses, those that use both C3 and C4 photosynthesis, as well as a careful analysis of the evolution of rank-2 intermediate veins may provide insights into how widely distributed this mechanism is and may provide hints regarding the evolution of this regulatory rearrangement. Finally, new methods will be required to gain access to the vascular cells of maize, which are not accessible through the current methods. In summary, scRNA-seq enabled the identification of cells with a unique combination of properties on the adaxial side of the bundle sheath, cells that play key roles in C4 photosynthesis. The identification of this new property may be relevant to bioengineering of staple crops, for example, C4 rice.

Materials Availability

Plasmids generated in this study have been deposited to Addgene under the code Plasmid #159535.

Data and Code Availability

The raw data that support the findings of this study are available from the corresponding author upon reasonable request. All sequencing data will be deposited in the Gene Expression Omnibus GEO (www.ncbi.nlm.nih.gov/geo/) and the accession number will be updated here.

METHOD DETAILS

Plant growth.

Zea mays L. B73 seeds were germinated on filter paper with deionized, distilled water in darkness at 22-25 °C and transferred to soil upon coleoptile emergence. Plants were subsequently grown at 28-30 °C in a greenhouse supplemented by sodium lamps (400 μmol m^{-2} s^{-1}) from 8:00-20:00. Protoplasts for scRNA-seq were generated from the last 6 cm of the distal portion of V2 leaf 2. For each pool of protoplasts tested, leaf segments from six concurrently grown plants were used. *In situ* hybridization was performed on sections taken from the distal portion of leaf 2 of V2 plants, distal portion of leaf 5 of V4 plants, and distal portion of the flag leaf from VT plants, with similar results. All images shown are from V4 leaf 5. For GUS staining, tissue segments were taken 10 cm from

the tip of the third leaf below the flag leaf of T0 plants at growth stage VT (mature leaf tip), 4 cm from the tip of leaf 3 of T1 V2 plants (seedling leaf tip), 12 cm from the tip of T1 V2 plants (seedling leaf base), a stem section 1 cm above soil surface of T1 V2 plant (seedling stem), or the seminal root tip from T1 V2 plant (seedling root).

Genes analyzed here.

Gene IDs are provided as Supplementary Table 4.

Probe preparation for *in situ* hybridization.

RNA was extracted from leaves of V2 B73 seedlings by phenol-chloroform extraction as previously described (Bezrutczyk et al., 2018). cDNA synthesis was performed using QuantiTect Reverse Transcription Kit (Qiagen, Hilden, Germany). cDNA was amplified for each gene (Supplementary Table 5) using Takara PrimeSTAR GXL polymerase then subcloned into pJET1.2 using CloneJet PCR cloning kit (ThermoFisher, Meerbusch, Germany). For *SWEET13a, b,* and *c*, three unique regions in the 5'- and 3'-UTRs and in the coding region with lengths of ~100 bp were selected as probe templates. The three probes specific for one of the genes were combined for detection of the respective target gene. For *SUT1*, two regions in the 5'- and 3'-UTRs, unique to *SUT1* but common to all six isoforms, were selected as probe templates. All cDNA sequence alignments were performed using Geneious R11 (https://www.geneious.com) (Supplementary Fig. 6). Probe template regions were amplified with SP6 sequences flanking the forward primers for the sense probe, and reverse primers for antisense probes (Supplementary Table 5). The MEGAscript SP6 Transcription kit (ThermoFisher) was used with a 1:2 ratio of DIG-labelled UTP:UTP to generate DIG-labelled probes. Probes were precipitated after DNAse reaction by addition of 2 mg/mL glycogen, 0.1 volume 10% acetic acid, 0.1 volume NaOAc, and 2.5 volumes ethanol and centrifuged at 4 °C at 20,000 x *g* for 30 min. Pellets were washed with 70% ethanol in DEPC-treated water, allowed to dry, and resuspended in 25 µL RNAse-free 10 mM Tris-EDTA pH 8 and 25 µL formamide.

***In situ* hybridization.**

In situ hybridization was adapted from Jackson and Simon lab protocols (Jackson, 1992; Stahl and Simon, 2010). Leaf tip sections 1 cm in length were dissected from V2 or V5 plants into 4% paraformaldehyde, vacuum-infiltrated for 10 min and fixed overnight at 4 °C. Dehydration by ethanol series and paraplast embedding were performed as described (Malcomber and Kellogg, 2004). Sections (10 µm) were cut with a Leica RM 2155 microtome and mounted on ProbeOn Plus slides (Fisher). After deparaffinization with Histoclear and rehydration by a decreasing ethanol

series, tissue was permeabilized in a 2 µg/mL proteinase K solution, washed with 0.2% glycine and 1x PBS (1.3 M NaCl, 0.07 M Na_2HPO_4, 0.03 M NaH_2PO_4) for 2 min, and re-fixed with 4% paraformaldehyde for 10 min. Slides were washed with PBS and acetylated with 0.1 M triethanolamine and acetic anhydride for 10 min, then washed and dehydrated with an increasing ethanol series. Probes for each construct were mixed (e.g. all three antisense probes for *SWEET13a*), diluted 1:50 with formamide, denatured at 95 °C for 3 min, and further diluted 1:4 with hybridization buffer (300 mM NaCl, 10mM NaH_2PO_4, 10mM Na_2HPO_4, 10mM Tris-Cl pH 6.8, 5 mM EDTA, 50% formamide, 12.5% dextran sulfate, 1.25mg/mL tRNA). Probe incubation in slide pairs was performed at 55 °C overnight. Slides were rinsed three times with 0.2x SSC pH 7 (600 mM NaCl, 60 mM sodium citrate) at 55 °C for one hour, and washed with block reagent solution (Roche), washed with BSA blocking solution (10 mg/mL BSA, 0.1 M Tris-Cl, 150 mL NaCl, 0.3% Triton X-100) for 45 min, and incubated with anti-DIG antibody (Roche) for 2 hours at 22 °C. Slides were rinsed four times with BSA block solution for 15 min each, in Buffer C (100 mM Tris pH 9.5, 50 mM $MgCl_2$, 100 mM NaCl) for 15 minutes, and incubated with 50 µL NBT and 37.5 µL BCIP in 5 mL buffer C for 24-48 hours. Slides were washed with water, dehydrated with an increasing ethanol series, and mounted with Eukitt Quick-hardening mounting medium. Images were taken with an Olympus CKX53 cell culture microscope with EP50 camera. *In situ* hybridization experiments for each gene (probe combination) were performed as (at minimum) three independent experiments.

Generation of ZmSWEET13-GUS constructs.

ZmSWEET13a (Supplementary Table 4), including 5751 bp upstream of the start codon and 684 bp downstream of the stop codon, was isolated from B73 gDNA (Supplementary Table 5) and inserted into pJET using the CloneJET PCR cloning kit. The final construct consists of GUSplus inserted directly upstream of the *ZmSWEET13a* stop codon, preceded by a 9-alanine linker, in the Golden Gate vector pGGBb-AG, the *in silico* cloning of which was performed using Geneious R11 (Supplementary Fig. 6). The assembly of all fragments with the vector pGGBb-AG was performed using the Takara InFusion HD cloning kit, and validated by Sanger sequencing.

Maize transformation.

Agrobacterium tumefaciens strain EHA105 was transformed with the ZmSWEET13a:GUS vector at the Crop Genome Engineering Facility at VIB Ghent (https://www.psb.ugent.be/cgef). Transformed EHA105 carrying the respective plasmids was used to transform the inbred maize line

B104 via Agrobacterium-mediated transformation of 600 immature embryos according to previously described methods (Coussens et al., 2012). In brief, callus formation was induced using auxins and transgenic cells selected over several weeks using phosphinotricin (PPT) selection. Plantlets were then regenerated on hormone-free medium, and presence of the transgene confirmed using TraitCheck (Romer Labs; Butzbach, Germany) and PCR analysis. Three independent transformation events were derived from different starting immature embryos, yielding six plants in total: three plants from event A (pSWEET13a:SWEET13a:GUSplus[a]), two from event B (pSWEET13a:SWEET13a:GUSplus[b]), and one from event C (pSWEET13a:SWEET13a:GUSplus[c]).

GUS histochemistry.

Tissue segments were taken 10 cm from the tip of the third leaf below the flag leaf of T0 plants at growth stage VT (mature leaf tip), 4 cm from the tip of leaf 3 of T1 V2 plants (seedling leaf tip), 12 cm from the tip of T1 V2 plants (seedling leaf base), on the stem 1 cm above the soil surface of T1 V2 plant (seedling stem), or from the seminal root tip of T1 V2 plant (seedling root) at 13:00 o'clock. Tissue segments were dissected into cold acetone and vacuum-infiltrated for two min, vacuum infiltrated with GUS wash buffer (20 mM EDTA, 40 mM $C_6N_6FeK_3$, 40 mM $C_6FeK_4N_6$, 20% methanol, 57.6 mM Na_2HPO_4, 42 mM NaH_2PO_4, 0.1% Triton X-100), and incubated with GUS wash buffer including 0.2% X-Gluc at 37°C for 1-48 hours. Sections were dehydrated in 20%, 30%, 50% ethanol for 30 min, fixed in FAA (50% ethanol, 3.7% formaldehyde, 5% acetic acid) for 30 min, and further dehydrated in 75% and 100% ethanol. Embedding was performed by incubating sections at 60 °C in tert-butyl ethanol:paraplast dilutions at 3:1, 1:1, and 1:3 ratios. Melted paraplast (100%) was changed twice daily for three days. Paraplast-embedded tissue was poured into blocks, and 10-µm sections were cut with a Leica RM 2155 microtome. Sections were mounted on SUPERFROST PLUS Gold Slides (Thermo Scientific), deparaffinized with Histoclear, and mounted with Eukitt Quick-hardening mounting medium.

Single cell sequencing: protoplast preparation.

Tissue was sampled from the distal portion of leaf 2 (from 1 cm to 7 cm, as measured from the tip) from V2 plants. This region was selected because it is thought to be non-expanding, non-differentiating source tissue based on results from the RNAseq-defined developmental transcriptome of the maize leaf (Li et al., 2010). Leaf segments were harvested at 9:00 am, and tape was applied to adaxial epidermis to stabilize the tissue, which was scored every 5 mm from the midvein to leaf edge with a razor manifold consisting of scalpel blades taped together to ensure minimum distance between scores. Tape sections were placed abaxial-side down in pretreatment

solution (2 mM L-cysteine, 164 mM sorbitol) and vacuum-infiltrated for 10 min with 2 min of active pumping. Tape sections were incubated with gentle agitation (30 rpm, IKA Rocker 3D orbital shaker) for an additional 20 min in pre-treatment solution, then transferred to enzyme solution (cellulase "Onozuka" RS 1.25%, cellulase "Onozuka" R-10 1.25%, pectolyase Y-23 0.4%, macerozyme R-10 0.42%, sorbitol 0.4 M, MES 20 mM, KCL 20 mM, $CaCl_2$ 10 mM, BSA 0.1%, ß-mercaptoethanol 0.06%) for 3.5 h with gentle agitation (30 rpm on orbital shaker). Protoplasts were filtered through a Corning 70-µm nylon mesh strainer and centrifuged in a round bottom tube for 1.5 min at 100 x *g*. Enzyme solution was gently removed and replaced with cold wash solution (sorbitol 0.4M, MES 20mM, KCl 20mM, $CaCl_2$ 10mM, BSA 0.1%). Protoplasts were carefully resuspended in wash solution and centrifuged for 30 seconds at 100 x *g*, then strained through a 70-µm Scienceware Flowmi Cell Strainer to remove large debris. Washing solution steps were repeated four additional times to remove chloroplasts and small debris. Cell viability and concentration were quantified under an Olympus CKX53 cell culture microscope: 1 µL 0.4% Trypan blue was added to 9 µL of resuspended protoplasts in wash solution and pipetted into the chamber of a C-Chip Neubauer Improved Disposable Haemocytometer (NanoEntek; Seoul, South Korea); healthy (unstained) cells were counted. Protoplasts were resuspended to a concentration of 1,200 cells /µL. A variety of approaches to degrade the suberin-lignin-containing bundle sheath cell walls with the addition of other enzymes failed to produce healthy cells: Laccase (Sigma) and manganese peroxidase (Sigma), as well as enzymes provided by Novozymes (Copenhagen, Denmark), namely a cutinase, a fungal carbohydrase blend produced in *Aspergillus aculeatus*, a fungal beta-glucanase blend produced in *Humicola insolens*, a pectinase preparation produced in *Aspergillus*, a xylanase blend, and a multi-enzyme complex containing carbohydrases, including arabanase, cellulase, beta-glucanase, hemicellulose and xylanase, were each added to the existing protocol to a final concentration of 1-2% active enzyme weight/vol. Visual inspection of protoplasts during isolation revealed that addition of these enzymes caused protoplasts to rupture.

Protoplast protocol optimization

Several variations of the above protocol were tested prior to the final protoplast preparation, and the presence of diverse cell types was verified by qRT-PCR using primers specific to *MDH6*, *ME1*, *SWEET13a*, *SWEET13b*, and *SWEET13c* (Supplementary Table 5). Briefly, RNA was extracted from protoplasts using the RNEasy Mini Kit, and first strand cDNA was synthesized using Quantitect reverse transcription kit (Qiagen, Hilden, Germany). Quantitative reverse transcription PCR (qRT-PCR) was performed using Roche LightCycler 480 SYBR Green I Master polymerase on a Stratagene Mx3000P, and relative expression of transporter genes was calculated relative to

18S and Actin using the $2^{-\Delta CT}$ method. Modifications to the standard protoplast isolation protocol of 2 h in enzyme solution (see previous section) (Protocol 1) included doubling the concentration of enzymes in solution (Protocol 2), isolating BS strands released after 2 h followed by continued incubation of filtered BS strands in fresh enzyme solution to deplete mesophyll cells (Protocol 3), and incubating the leaf tissue in pretreatment solution (Protocol 4) (2 mM L-cysteine and164 mM sorbitol). The protocol which yielded the highest ratio of BS:MS marker genes (*ME1*: *MDH6*) included a pretreatment incubation step and 1x enzyme solution (Supplementary Fig. 1).

Cell partitioning, library prep, and sequencing.

To aim for partitioning of 7,000 cells, with the expectation that 3,500 cells would be sequenced, 6 µL of the protoplast suspension with an estimated 1,200 cells/µL was applied to the 10x Genomics Chromium microfluidic chip (Chemistry V3.0). Thereafter the standard manufacturer's protocol was followed. Twelve cycles were used for cDNA amplification, and the completed cDNA library was quantified using an Agilent AATI Fragment Analyzer. Sequencing was performed at Novogene (Sacramento, CA, USA) on a single lane with the Hi-Seq platform and the standard PE150 sequencing parameters.

Generation of single-cell expression matrices

Cellranger count (10x Genomics) was used to process fastq files provided by Novogene, with read 1 trimmed to 26 bp (r1-length=26), as the first 26 bp of a 10x library R1 comprise the cell barcode and UMI index, and the remaining comprises poly-A tail with no further information. A formatted reference genome was generated using Cellranger mkref using the maize B73 RefGen 4 (Jiao et al., 2017) whole genome sequence and annotation (fasta and gff3 downloaded from Ensembl B73 RefGen V4), to which reads were aligned using STAR (Dobin et al., 2013). For analysis of single cell sequencing data, see "Quantification and Statistical Analysis" section below.

Phylogeny of UmamiT transporters

BLAST results from the seed sequence AtUmamiT12 (At2g37460) to maize (AGP v4 (Jiao et al., 2017) and barley (IBSC v2 (Mascher et al., 2017)) were combined with BioMart (Smedley et al., 2009) results and filtered for the WAT1-related protein domain (panther ID PTHR31218). Genes passing this filter were selected as UmamiT family candidate genes. Two trees were generated: one using an alignment of all known splice variants, and one with only the representative transcript, with similar results. Alignment was performed in MEGA7 (Kumar et al., 2016) using MUSCLE with the following parameters: gap open penalty -2.9, gap extend penalty 0, hydrophobicity

multiplier 1.2, max iterations 8, clustering method UPGMA for iteration 1, 2; UPGMB for all subsequent iterations, and lambda 24. The maximum likelihood tree was created from these alignments using IQTREE webserver (Trifinopoulos et al., 2016) using the BLOSUM62 substitution model and 1000 bootstraps.

QUANTIFICATION AND STATISTICAL ANALYSIS

Sample selection for scRNA-Seq, qRT-PCR, and RNAseq

Plants chosen for protoplast release, qPCR, and RNAseq were randomly selected from among a larger number of individuals which had been grown concurrently and were at the same growth stage. True biological replicates (i.e., independently grown plants) were used as replicates for statistical analyses. The number of plants per sample and number of replicates is given in the Figure legends or in specific methods sections. To ensure reproducibility, the plants used in successive experiments were grown in the same greenhouse under controlled conditions. Samples for a given experiment were taken at the same developmental stage, at the same time of day.

Dimensionality reduction and cell clustering

The Seurat R package (v3.1)(Butler et al., 2018) was used for dimensionality reduction analysis and dataset filtering. To remove cells with low mRNA count (nFeature_RNA) and doublets, as well as damaged cells with high chloroplast (pt) or mitochondria (mt) genome-derived transcripts, cells were filtered (percent.pt <4 & percent.mt <0.75 & nFeature_RNA >1800 & nFeature_RNA <7000). Normalization, scaling, and variable feature detection were performed using SCTransform (Hafemeister and Satija, 2019). Cells were clustered using FindNeighbors to create a K-nearest neighbors graph using the first 50 principle components. FindClusters was used to iteratively group cells using a resolution of 0.2 or 23. These clusters were used as input for non-linear dimensional reduction using Uniform Manifold Approximation and Projection (UMAP)(McInnes et al., 2018).

Differential gene expression analysis across clusters

Genes differentially expressed across clusters or subclusters were identified by comparing average normalized mRNA counts in cells of a given cluster to that of cells in all other clusters using the Seurat function FindMarkers. Genes with an FDR corrected P-value <0.05 and an average logFC >0.5 were considered marker genes.

Identification of cluster identities

Canonical C4 photosynthesis-related genes were used as markers to define MSC and BSC clusters (Denton et al., 2017) (Supplementary Table 1). The cluster identified as BSC was subdivided into two subclusters when FindClusters was applied with a resolution of 23, and differential gene expression analysis was performed on these two subclusters with FindMarkers (for subclusters: logFC >0.5, FDR ≤0.01).

qRT-PCR of transporter genes in seedling leaf

Leaf segments were harvested from the distal and proximal end (tip and base) of leaf 3 of early V2 plants at 13:00. Tissue was ground in liquid nitrogen and RNA extracted as previously described (Bezrutczyk et al., 2018). First strand cDNA was synthesized using Quantitect reverse transcription kit (Qiagen). qRT-PCR to determine relative mRNA levels was performed using a Stratagene Mx3000P with primers for *18S, Actin, SWEET13a, 13b, 13c, SUT1, UmamiT21a*, and *STP3* (Supplementary Table 5). Relative expression of transporter genes was calculated relative to *18S* and *Actin* using the $2^{-\Delta CT}$ method for quantification, with similar results. Values shown in Figure 5b are the average of three technical (qRT-PCR) replicates of three pools of two plants; error bars represent SEM. Students two-tailed paired t-test values are shown. Two independent repeats confirmed the data.

Gene Ontology term analysis for mesophyll clusters

Marker genes for each of the five mesophyll clusters (LogFC >0.5; FDR-adjusted p-value <0.05) were used as input for Gene Ontology (Ashburner et al., 2000; The Gene Ontology Consortium, 2018) analysis via the online portal GO Gene Ontology database (doi: 10.5281/zenodo.3727280; released 2020-03-23). GO terms with FDR-corrected p-values <0.05 can be found in Supplementary Table 3.

Protoplast and bulk leaf tissue RNAseq

Protoplasts were generated according to the previously described method. Whole leaf tissue from sibling plants was ground in liquid nitrogen at the time leaf tissue was harvested for protoplast isolation. RNA from two pools of protoplasts made from four leaves each (P1 and P2), and two pools of four whole leaf segments each (L1 and L2) was extracted using the RNEasy Mini Kit (Qiagen), and four cDNA libraries were generated using the NEBNext Ultra DNA Library Prep Kit for Illumina (New England Biolabs, MA, USA) with modifications to select for 250-500 bp fragments. Sequencing of the four libraries was performed at Novogene (Sacramento, CA, USA) on a single lane with the Hi-Seq platform and the standard PE150 sequencing parameters. Reads were analyzed using a custom implementation of the Wyseq RNAseq analysis pipeline

(https://github.com/astauff/WySeq). Briefly, reads were trimmed using TrimGalore (v 0.6.5) and aligned to the AGPv4 B73 reference genome using STAR (v 2.5.1b). Counts were generated using Subread featureCounts (v 2.0.1), and differential expression was analyzed using the R-packages EdgeR (v3.30.3) and limma (v 3.44.3) using trimmed mean M-value (TMM) normalization factors. Reads corresponding to BSC-specific genes and MS-specific genes were normalized separately to compensate for the expected difference in cell populations represented in protoplasts and whole leaf tissue. Genes were filtered to remove those with a coefficient of variation >75th percentile within replicate groups prior to correlation analysis. Pearson correlation (Supplementary Fig. 7) and differentially expressed genes specific to BS and MS-cells (logFC > 1 or < -1) are presented (Supplementary Table 6). None of the genes in the ^{ab}BS subclusters were induced by protoplast isolation. Rather, several showed reduced mRNA levels in the protoplast sample.

REFERENCES

Ashburner, M. et al. (2000). Gene ontology: tool for the unification of biology. The Gene Ontology Consortium. Nat. Genet. **25**: 25–29.

Baker, R.F., Leach, K.A., Boyer, N.R., Swyers, M.J., Benitez-Alfonso, Y., Skopelitis, T., Luo, A., Sylvester, A., Jackson, D., and Braun, D.M. (2016). Sucrose transporter ZmSut1 expression and localization uncover new insights into sucrose phloem loading. Plant Physiol. **172**: 1876–1898.

Bezrutczyk, M., Hartwig, T., Horschman, M., Char, S.N., Yang, J., Yang, B., Frommer, W.B., and Sosso, D. (2018). Impaired phloem loading in *zmsweet13a,b,c* sucrose transporter triple knock-out mutants in *Zea mays*. New Phytol. **218**: 594–603.

Bosabalidis, A.M., Evert, R.F., and Russin, W.A. (1994). Ontogeny of the vascular bundles and contiguous tissues in the maize leaf blade. Am. J. Bot. **81**: 745–752.

Bürkle, L., Hibberd, J.M., Quick, W.P., Kühn, C., Hirner, B., and Frommer, W.B. (1998). The H^+-sucrose cotransporter NtSUT1 is essential for sugar export from tobacco leaves. Plant Physiol. **118**: 59–68.

Butler, A., Hoffman, P., Smibert, P., Papalexi, E., and Satija, R. (2018). Integrating single-cell transcriptomic data across different conditions, technologies, and species. Nat. Biotechnol. **36**: 411–420.

Candela, H., Johnston, R., Gerhold, A., Foster, T., and Hake, S. (2008). The *milkweed pod1* gene encodes a KANADI protein that is required for abaxial/adaxial patterning in maize leaves. Plant Cell **20**: 2073.

Cayla, T., Le Hir, R., and Dinant, S. (2019). Live-cell imaging of fluorescently tagged phloem proteins with confocal microscopy. Methods Mol. Biol. Clifton NJ **2014**: 95–108.

Chang, Y.-M., Liu, W.-Y., Shih, A.C.-C., Shen, M.-N., Lu, C.-H., Lu, M.-Y.J., Yang, H.-W., Wang, T.-Y., Chen, S.C.-C., Chen, S.M., Li, W.-H., and Ku, M.S.B. (2012). Characterizing regulatory and functional differentiation between maize mesophyll and bundle sheath cells by transcriptomic analysis. Plant Physiol. **160**: 165.

Chastain, C.J., Baird, L.M., Walker, M.T., Bergman, C.C., Novbatova, G.T., Mamani-Quispe, C.S., and Burnell, J.N. (2017). Maize leaf PPDK regulatory protein isoform-2 is specific to bundle sheath chloroplasts and paradoxically lacks a Pi-dependent PPDK activation activity. J. Exp. Bot. **69**: 1171–1181.

Chen, L.Q., Qu, X.Q., Hou, B.H., Sosso, D., Osorio, S., Fernie, A.R., and Frommer, W.B. (2012). Sucrose efflux mediated by SWEET proteins as a key step for phloem transport. Science **335**: 207–11.

Coussens, G., Aesaert, S., Verelst, W., Demeulenaere, M., De Buck, S., Njuguna, E., Inzé, D., and Van Lijsebettens, M. (2012). *Brachypodium distachyon* promoters as efficient building blocks for transgenic research in maize. J. Exp. Bot. **63**: 4263–4273.

Deng, L. (2014). A Genome-Wide Analysis of the AAAP Gene Family in Maize. J. Proteomics Bioinform. **07**.

Denton, A.K., Maß, J., Külahoglu, C., Lercher, M.J., Bräutigam, A., and Weber, A.P.M. (2017). Freeze-quenched maize mesophyll and bundle sheath separation uncovers bias in previous tissue-specific RNA-Seq data. J. Exp. Bot. **68**: 147–160.

Dobin, A., Davis, C.A., Schlesinger, F., Drenkow, J., Zaleski, C., Jha, S., Batut, P., Chaisson, M., and Gingeras, T.R. (2013). STAR: ultrafast universal RNA-seq aligner. Bioinformatics **29**: 15–21.

Friso, G., Majeran, W., Huang, M., Sun, Q., and van Wijk, K.J. (2010). Reconstruction of metabolic pathways, protein expression, and homeostasis machineries across maize bundle sheath and mesophyll chloroplasts: large-scale quantitative proteomics using the first maize genome assembly. Plant Physiol. **152**: 1219.

Fritz, E., Evert, R.F., and Heyser, W. (1983). Microautoradiographic studies of phloem loading and transport in the leaf of *Zea mays* L. Planta **159**: 193–206.

Fritz, E., Evert, R.F., and Nasse, H. (1989). Loading and transport of assimilates in different maize leaf bundles. Planta **178**: 1–9.

The Gene Ontology Consortium (2018). The Gene Ontology Resource: 20 years and still GOing strong. Nucleic Acids Res. **47**: D330–D338.

Gottwald, J.R., Krysan, P.J., Young, J.C., Evert, R.F., and Sussman, M.R. (2000). Genetic evidence for the *in planta* role of phloem-specific plasma membrane sucrose transporters. Proc. Natl. Acad. Sci. **97**: 13979.

Hafemeister, C. and Satija, R. (2019). Normalization and variance stabilization of single-cell RNA-seq data using regularized negative binomial regression. Genome Biol. **20**: 296.

Henderson, D.C., Zhang, X., Brooks III, L., and Scanlon, M.J. (2006). RAGGED SEEDLING2 is required for expression of KANADI2 and REVOLUTA homologues in the maize shoot apex. genesis **44**: 372–382.

Heyser, W., Heyser, R., Eschrich, W., and Fritz, E. (1977). The influence of externally supplied sucrose on phloem transport in the maize leaf strip. Planta **137**: 145–151.

Jackson, D. (1992). *In situ* hybridization in plants. In Molecular Plant Pathology. A practical approach, S.J. Gurr, M.J. McPherson, and D.J. Bowles, eds (Oxford University Press: Oxford), pp. 163–174.

Jiao, Y. et al. (2017). Improved maize reference genome with single-molecule technologies. Nature **546**: 524–527.

Juarez, M.T., Kui, J.S., Thomas, J., Heller, B.A., and Timmermans, M.C.P. (2004a). microRNA-mediated repression of rolled leaf1 specifies maize leaf polarity. Nature **428**: 84–88.

Juarez, M.T., Twigg, R.W., and Timmermans, M.C.P. (2004b). Specification of adaxial cell fate during maize leaf development. Development **131**: 4533.

Kanai, R. and Edwards, G.E. (1973). Separation of mesophyll protoplasts and bundle sheath cells from maize leaves for photosynthetic studies. Plant Physiol. **51**: 1133–1137.

Kim, J.Y., Symeonidi, E., Tin, P.Y., Denyer, T., Weidauer, D., Miras, M., Wudick, M., Lercher, M., Timmermans, M.C.P., and Frommer, W.B. (2020). Unique properties of leaf phloem cells revealed by single cell transcriptomics. Nat. Plants **submitted**.

Kumar, S., Stecher, G., and Tamura, K. (2016). MEGA7: Molecular Evolutionary Genetics Analysis version 7.0 for bigger datasets. Mol. Biol. Evol. **33**: 1870–1874.

Langdale, J.A., Lane, B., Freeling, M., and Nelson, T. (1989). Cell lineage analysis of maize bundle sheath and mesophyll cells. Dev. Biol. **133**: 128–139.

Langdale, J.A., Rothermel, B.A., and Nelson, T. (1988a). Cellular pattern of photosynthetic gene expression in developing maize leaves. Genes Dev. **2**: 106–115.

Langdale, J.A., Zelitch, I., Miller, E., and Nelson, T. (1988b). Cell position and light influence C4 versus C3 patterns of photosynthetic gene expression in maize. EMBO J. **7**: 3643–3651.

Li, P. et al. (2010). The developmental dynamics of the maize leaf transcriptome. Nat Genet **42**: 1060–7.

Malcomber, S.T. and Kellogg, E.A. (2004). Heterogeneous expression patterns and separate roles of the *SEPALLATA* gene *LEAFY HULL STERILE1* in grasses. Plant Cell **16**: 1692.

Martin, A. et al. (2006). Two cytosolic glutamine synthetase isoforms of maize are specifically involved in the control of grain production. Plant Cell **18**: 3252–3274.

Mascher, M. et al. (2017). A chromosome conformation capture ordered sequence of the barley genome. Nature **544**: 427–433.

McInnes, L., Healy, J., and Melville, J. (2018). UMAP: uniform manifold approximation and projection for dimension reduction. arXiv **eprint arXiv:1802.03426**.

Ortiz-Ramírez, C., Arevalo, E.D., Xu, X., Jackson, D.P., and Birnbaum, K.D. (2018). An efficient cell sorting protocol for maize protoplasts. Curr. Protoc. Plant Biol. **3**: e20072–e20072.

Riesmeier, J.W., Hirner, B., and Frommer, W.B. (1993). Potato sucrose transporter expression in minor veins indicates a role in phloem loading. Plant Cell **5**: 1591–1598.

Riesmeier, J.W., Willmitzer, L., and Frommer, W.B. (1994). Evidence for an essential role of the sucrose transporter in phloem loading and assimilate partitioning. EMBO J. **13**: 1–7.

Sedelnikova, O.V., Hughes, T.E., and Langdale, J.A. (2018). Understanding the genetic basis of C4 Kranz anatomy with a view to engineering C3 crops. Annu. Rev. Genet. **52**: 249–270.

Slewinski, T.L., Meeley, R., and Braun, D.M. (2009). Sucrose transporter1 functions in phloem loading in maize leaves. J. Exp. Bot. **60**: 881–892.

Smedley, D., Haider, S., Ballester, B., Holland, R., London, D., Thorisson, G., and Kasprzyk, A. (2009). BioMart – biological queries made easy. BMC Genomics **10**: 22.

Stahl, Y. and Simon, R. (2010). mRNA detection by whole mount *in situ* hybridization (WISH) or sectioned tissue *in situ* hybridization (SISH) in Arabidopsis. Methods Mol. Biol. Clifton NJ **655**: 239–251.

Tausta, S.L., Li, P., Si, Y., Gandotra, N., Liu, P., Sun, Q., Brutnell, T.P., and Nelson, T. (2014). Developmental dynamics of Kranz cell transcriptional specificity in maize leaf reveals early onset of C4-related processes. J. Exp. Bot. **65**: 3543–3555.

Trifinopoulos, J., Nguyen, L.-T., von Haeseler, A., and Minh, B.Q. (2016). W-IQ-TREE: a fast online phylogenetic tool for maximum likelihood analysis. Nucleic Acids Res. **44**: W232–W235.

Walley, J.W., Sartor, R.C., Shen, Z., Schmitz, R.J., Wu, K.J., Urich, M.A., Nery, J.R., Smith, L.G., Schnable, J.C., Ecker, J.R., and Briggs, S.P. (2016). Integration of omic networks in a developmental atlas of maize. Science **353**: 814–818.

Williams, M.L., Farrar, J.F., and Pollock, C.J. (1989). Cell specialization within the parenchymatous bundle sheath of barley. Plant Cell Environ. **12**: 909–918.

Wu, Y., Lee, S.-K., Yoo, Y., Wei, J., Kwon, S.-Y., Lee, S.-W., Jeon, J.-S., and An, G. (2018). Rice Transcription Factor OsDOF11 Modulates Sugar Transport by Promoting Expression of Sucrose Transporter and SWEET Genes. Mol. Plant **11**: 833–845.

ACKNOWLEDGMENTS

We would like to thank Reinout Laureyns (VIB-UGhent) for advice regarding in situ hybridization, Kajetan Linkert (HHU) regarding GUS histochemistry, Max Blank and Tatjana Buchmann (WF lab) for cDNA library preparation, and Thomas Kleist (HHU) for advice on phylogenetic analyses. This research was supported by Deutsche Forschungsgemeinschaft (DFG, German Research Foundation) under Germany´s Excellence Strategy – EXC-2048/1 – project ID 390686111 and SFB 1208 – Project-ID 267205415, as well as the Alexander von Humboldt Professorship to WBF.

AUTHOR CONTRIBUTIONS

Conceptualization, M.B., J.K., W.B.F.; Methodology, M.B., C.P.S.K, T.H., T.L.; Investigation, M.B, N.Z, T.L, C.P.S.K.; Resources, K.K, W.B.F.; Writing, M.B., W.B.F.; Supervision, J.K., W.B.F.

DECLARATION OF INTERESTS

The authors do not declare any competing interests.

MAIN FIGURES

SUPPLEMENTARY DATA

Table 1.

[ab]BS cluster	logFC	FDR	description
Zm00001d023677	4.990	2.3E-08	**SWEET13a**
Zm00001d041067	3.959	3.2E-08	**SWEET13c**
Zm00001d016625	3.675	3.3E-07	Os02g0519800 protein
Zm00001d023673	2.156	2.2E-06	**SWEET13b**
Zm00001d035717	2.140	3.3E-07	**UmamiT21a**
Zm00001d033551	1.412	3.3E-07	Phosphoglycerate mutase-like family protein
Zm00001d033980	1.252	4.5E-03	*Ustilago maydis* induced12
Zm00001d019062	1.180	2.9E-04	**Membrane H^+ATPase3**
Zm00001d035243	1.123	1.4E-03	**AAP45**
Zm00001d038753	1.114	7.7E-05	Ubiquitin domain-containing protein
Zm00001d017966	1.098	5.0E-04	Dihydropyrimidine dehydrogenase (NADP(+)) chloroplastic
Zm00001d012231	1.055	9.2E-04	**AAP56**
Zm00001d018867	0.992	1.1E-05	Syntaxin 132
Zm00001d000299	0.920	1.1E-05	Endosomal targeting BRO1-like domain-containing protein
Zm00001d002489	0.809	4.5E-03	PLATZ transcription factor family protein
Zm00001d035651	0.806	5.0E-04	DNA binding with one finger3
Zm00001d027268	0.753	6.5E-04	**STP3 (sugar transport protein 3)**
Zm00001d005344	0.737	1.4E-03	Histidine-containing phosphotransfer protein 2
Zm00001d013296	0.737	4.5E-03	ATP sulfurylase 1
Zm00001d030103	0.735	8.1E-03	Probable xyloglucan endotransglucosylase/hydrolase protein
Zm00001d052038	0.723	3.8E-03	Putative HLH DNA-binding domain superfamily protein
Zm00001d012559	0.692	2.1E-03	Stomatal closure-related actin-binding protein 1
Zm00001d015025	0.684	4.5E-03	AMP binding protein
Zm00001d038768	0.636	5.0E-03	Reticulon-like protein B4
Zm00001d044768	0.633	3.8E-03	**Protein NRT1/ PTR FAMILY 5.8**
Zm00001d033981	0.633	4.8E-03	ATP sulfurylase 1
Zm00001d015618	0.619	8.1E-03	Probable cinnamyl alcohol dehydrogenase
Zm00001d041710	0.597	5.0E-03	Glutathione synthetase chloroplastic
Zm00001d036401	0.596	5.0E-03	Endoplasmin homolog
Zm00001d018758	0.584	8.1E-03	Succinate dehydrogenase1
Zm00001d019670	0.578	8.5E-03	Kinesin-like protein KIN-4A
Zm00001d022042	0.574	9.4E-04	Eukaryotic translation initiation factor 5A
Zm00001d049597	0.567	4.9E-03	External alternative NAD(P)H-ubiquinone oxidoreductase B4
Zm00001d016662	0.536	3.8E-03	
Zm00001d018178	0.535	4.7E-03	bZIP4 (ABSCISIC ACID-INSENSITIVE 5-like protein 5)
Zm00001d032249	0.532	2.1E-03	KANADI 1
Zm00001d002625	0.531	3.4E-03	Probable methyltransferase PMT15
Zm00001d021773	0.517	9.9E-03	
Zm00001d039270	0.512	3.5E-03	Glutaredoxin family protein

Table 1.
Genes of interest differentially expressed between clusters [ab]BS and [ad]BS. 9 out of 39 genes specific to the [ab]BS cluster are specific to transmembrane transport (bold). Criteria for inclusion were average log fold change > 0.5 for all cells in subcluster and FDR-adjusted p-value < .01. The [ab]BSC specificity was validated for three genes, *SWEET13a*, *b* and *c*. Whether genes with lower FDR-adjusted p-values also show high specificity will require experimental validation.

Figure 1.

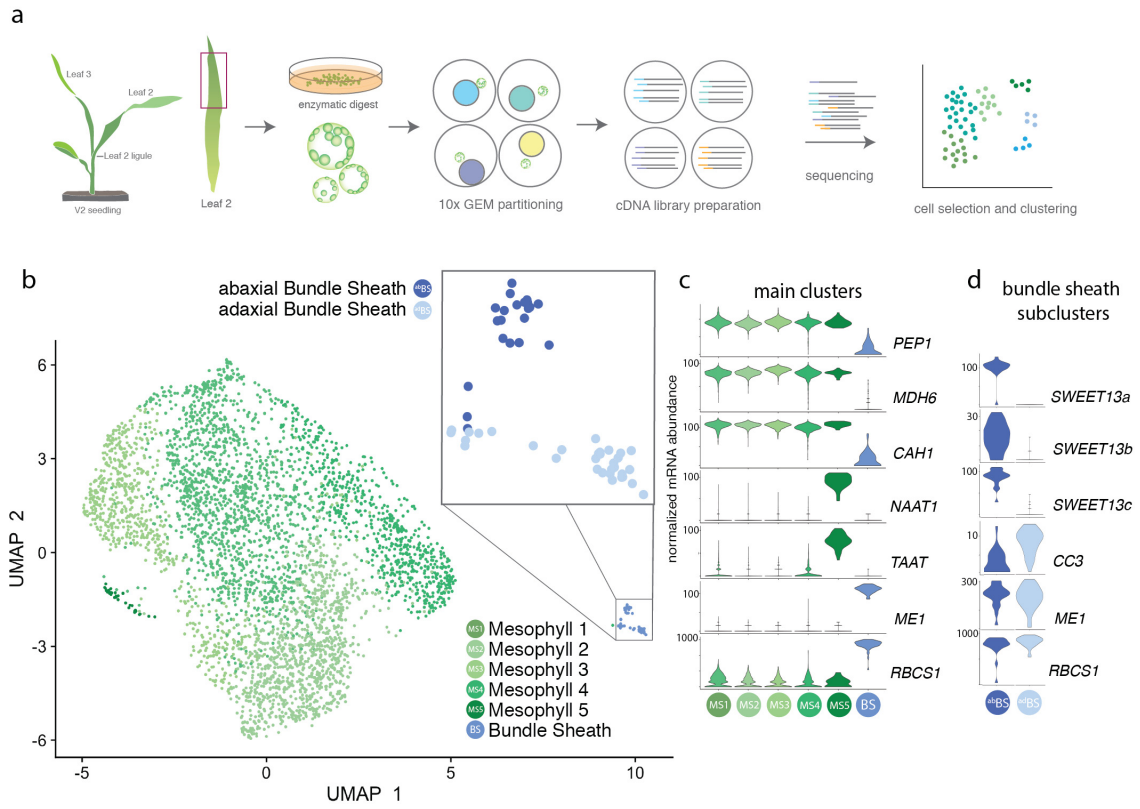

Figure 1. Mesophyll and bundle sheath clusters show canonical expression of C4 photosynthesis genes

a. Illustration of protoplasting, 10x Chromium Gel Bead-in-Emulsion (GEM) partitioning and cDNA synthesis, RNA sequencing, and data analysis. **b.** UMAP plot showing 2D representation of cell relationships in multidimensional space; bundle sheath cells separate into 2 subclusters at higher resolution (inset). The "upper" and "lower" cluster were later determined to correspond to abaxial and adaxial BSC (Fig. 2), and are therefore named ^{ab}BS and ^{ad}BS **c.** Violin plots showing distribution of normalized mRNA counts of marker genes for cells in each cluster. Genes were canonical C4 markers (*PEP1, MDH6, CA, ME1, RBCS*) or genes that identify unique clusters (*NAAT1, TAAT*). **d.** Violin plots showing normalized mRNA levels of genes differentially expressed between ^{ab}BS and BS^{ad} subclusters (*SWEET13a, b, and c*, *CC3*) and of example genes highly expressed in both clusters (*ME1*, *RBCS1*). Gene IDs are provided in Supplementary Table 4.

Figure 2.

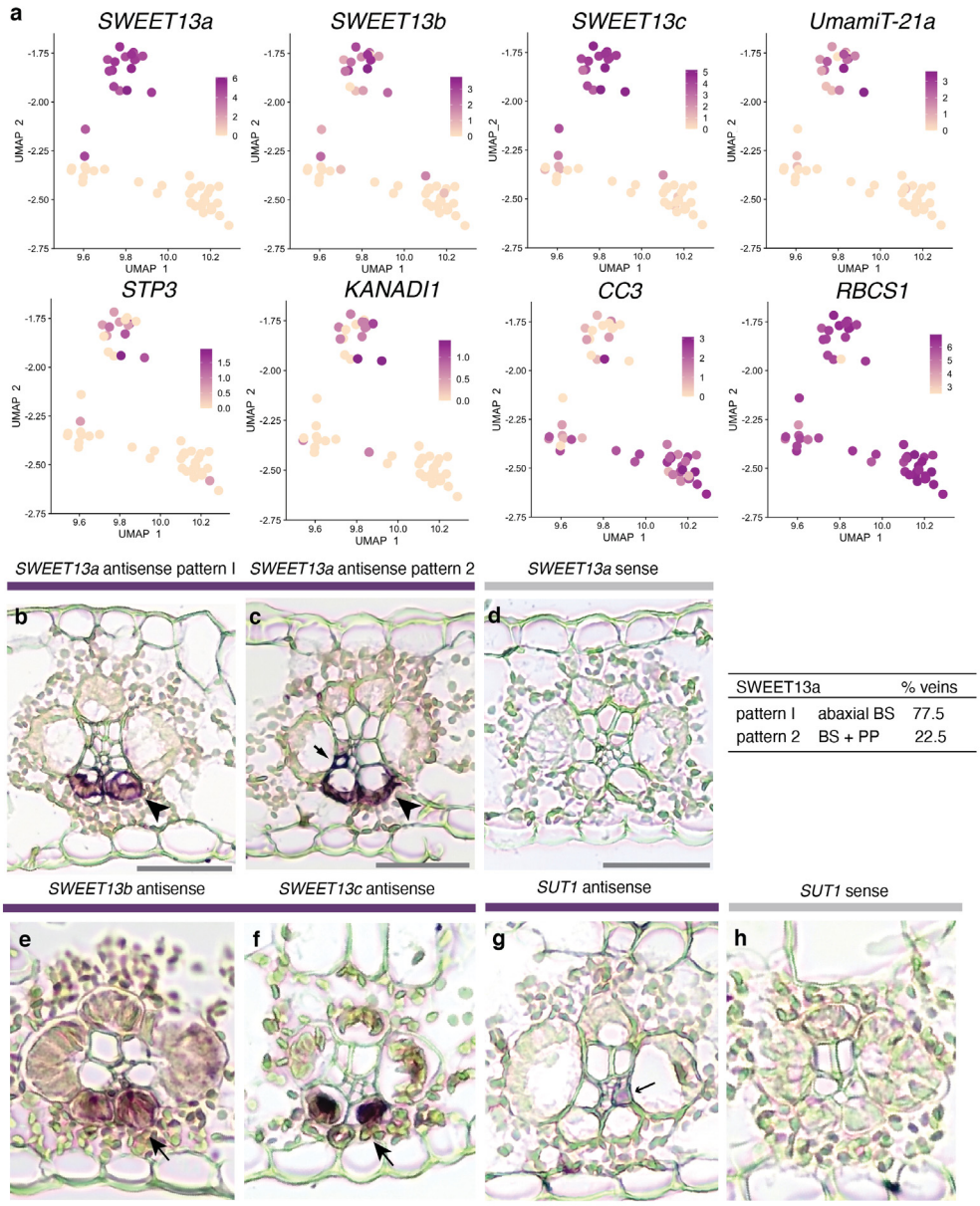

Figure 2. Abaxial BS cluster is enriched for genes encoding transport proteins
a. Feature plots show normalized levels of mRNAs for genes differentially expressed between the two clusters of bundle sheath cells plotted in UMAP space. **b - f.** *In situ* hybridization of *SWEET13a*, *SWEET13b*, and *SWEET13c.* Rank-2 intermediate veins from sections hybridized with antisense probes for *SWEET13a*, *SWEET13b*, and *SWEET13c* showed mRNA localization of three SWEET13 genes was largely limited to abaxial bundle sheath cells. **b - c.** *SWEET13a* mRNA localization was predominantly in ^{ab}BS cells in the majority of veins (77.5%) and to PP in a subset of veins (22.5%) (n = 824). **d.** No staining was visible after hybridization with *SWEET13a* sense probe. **e – f.** *SWEET13b* and *SWEET13c* probes showed signal predominantly in ^{ab}BS cells. **g.** *SUT1* mRNA is localized to a vascular cell which is likely a companion cell in rank-2 intermediate veins (arrow). **h.** No staining visible after hybridization with *SUT1* sense probe. See Supplementary Figure 5 for intermediate rank-1 and major veins. All error bars are 100µm.

Figure 3.

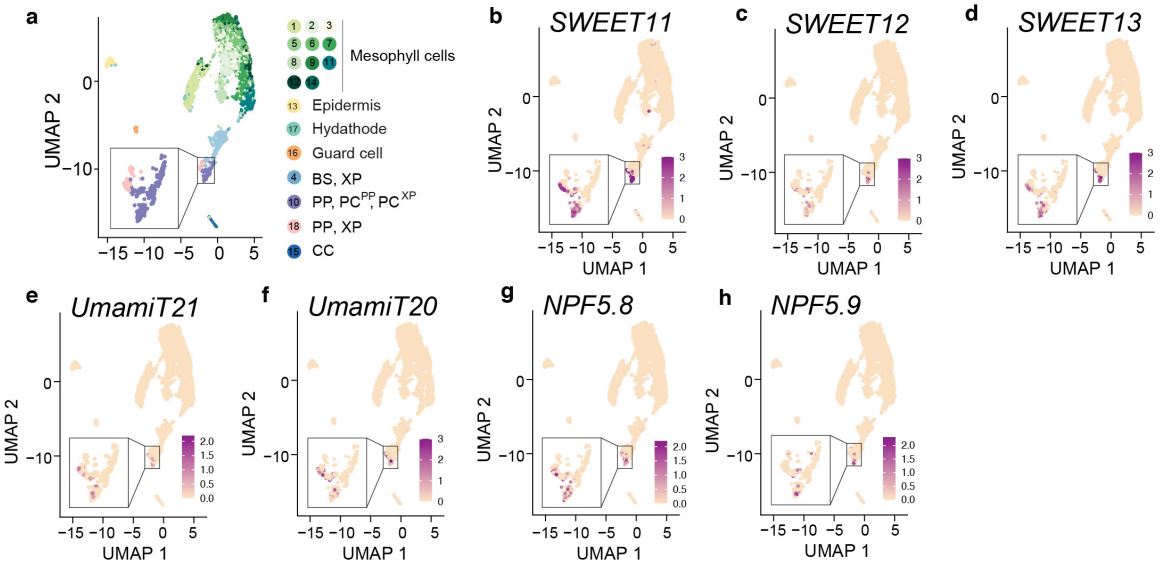

Figure 3. Arabidopsis homologs of maize [ab]BS-specific genes are expressed in Arabidopsis phloem parenchyma

Maize transporters showing [ab]BS mRNA enrichment are homologous to many Arabidopsis transporters with Arabidopsis phloem parenchyma mRNA enrichment. **a.** UMAP plot showing 2D representation of cell relationships in multidimensional space for single-cell sequencing of Arabidopsis leaf. Clusters are indicated by colors to the right of the UMAP plot. Feature plots show normalized levels of mRNA transcripts for Arabidopsis transport proteins homologous to abBS transport proteins. **b-d.** *AtSWEET11* (AT3G48740), *12* (AT5G23660), and *13* (AT5G50800) are orthologs to *ZmSWEET13a*, *b*, and *c*. **e.** *AtUmamiT21* (AT5G64700) is homologous to *ZmUmamiT21a*. **f.** *AtUmamiT20* (AT4G08290) is homologous to *ZmUmamiT21a* (Supplementary Fig. 4). g-h. *AtNPF5.8* (AT5G14940)_*and AtNPF5.9* (AT3G01350) are homologous to *ZmNRT1*.

Figure 4.

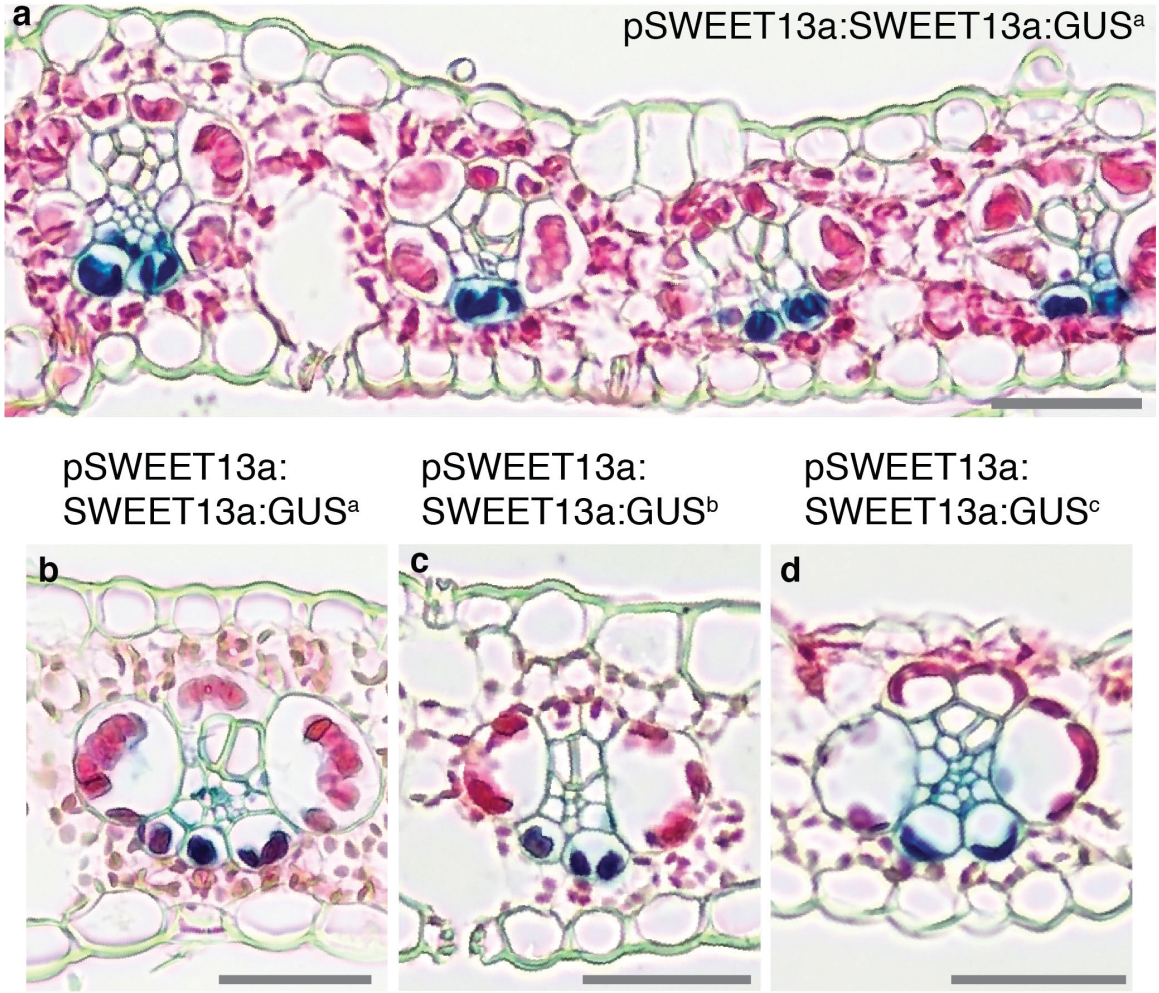

Figure 4. SWEET13a protein is localized to abaxial BSC of rank-2 veins
GUS histochemistry in leaves of maize lines transformed with the translational fusion construct pSWEET13a:SWEET13a-GUS. **a.** Chloro-bromoindigo precipitate (blue) is detected specifically in abaxial bundle sheath cells of maize plants transformed with pSWEET13a:SWEET13a:GUSplus. **b - d**. Three independent transformation events (a, b, and c: pSWEET13a:SWEET13a:GUS[a, b,] and [c]) showed similar expression patterns in rank-2 intermediate veins, rank-1 intermediate veins, and major veins (for rank-1 and major veins see Supplementary Fig. 5). **b.** Line "a," **c.** Line "b," **d.** Line "c." Sections are counterstained with Eosin-Y; scale bars are 100 μm.

Figure 5.

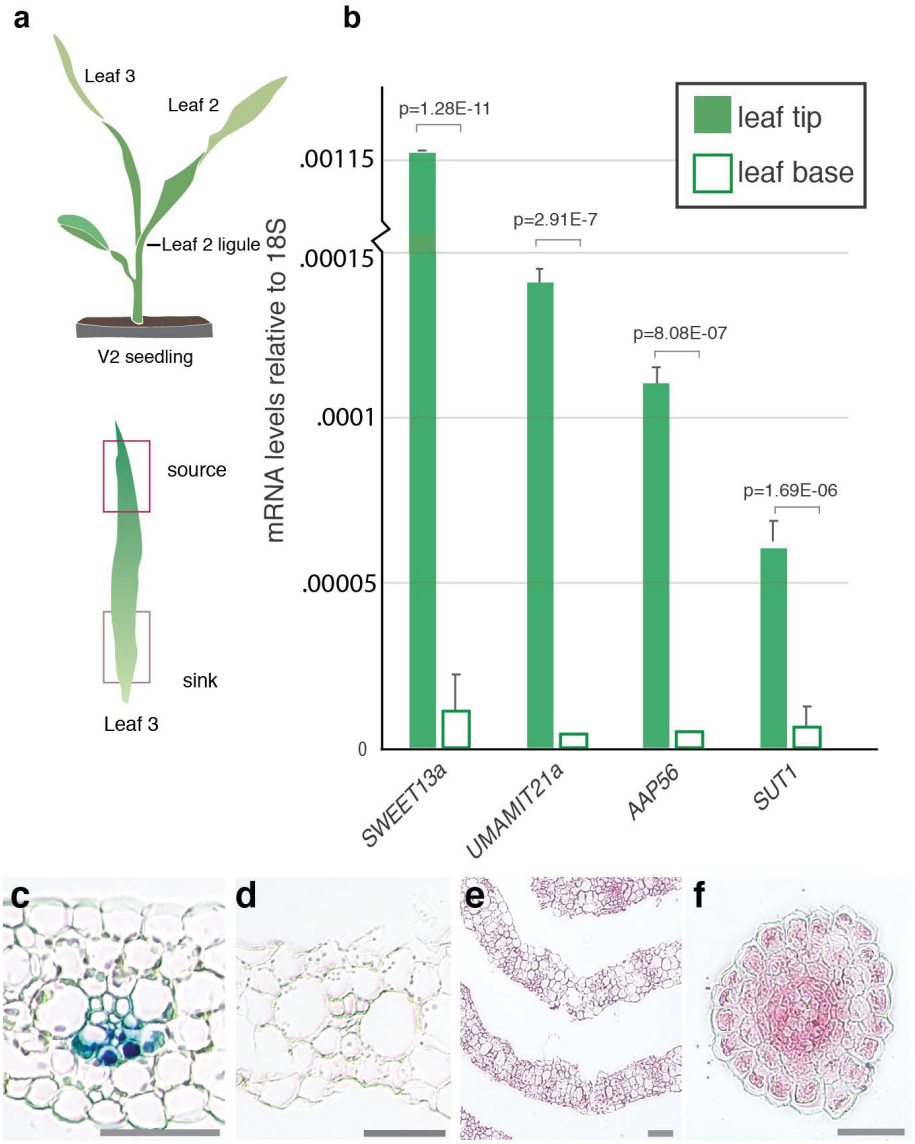

Figure 5. Abaxial BS transcripts are co-regulated during the sink-source transition

a. Tissue selected for qRT-PCR: V2-stage seedling with source and sink tissue highlighted; base of leaf 3 is still in the whorl and is net-sink tissue (Li et al., 2010). **b.** 18S-normalized mRNA levels of ^{ab}BS-specific transport proteins (*SWEET13a*, *UmamiT21a*, *AAP45*) and *SUT1* in source (tip) and sink (base) tissue. Values are average of three technical (qRT-PCR) replicates of three pools of two plants; error bars represent SEM. *Students two-tailed paired t-test values shown. Independent repeats confirmed the data.
c. pSWEET13a:SWEET13a:GUSplus transformed B73 seedling segments after 12-48 h incubation in GUS staining solution. V2 leaf 3 tip (12 h), **d.** leaf 3 sheath (48 h), **e.** stem cross section 1 cm above soil (48 h), **f.** cross section across root tip (48 h), Of these, only the tip of leaf 3 (source) showed chloro-bromoindigo precipitate indicative of SWEET13a expression. Scale bars: 100 µm.

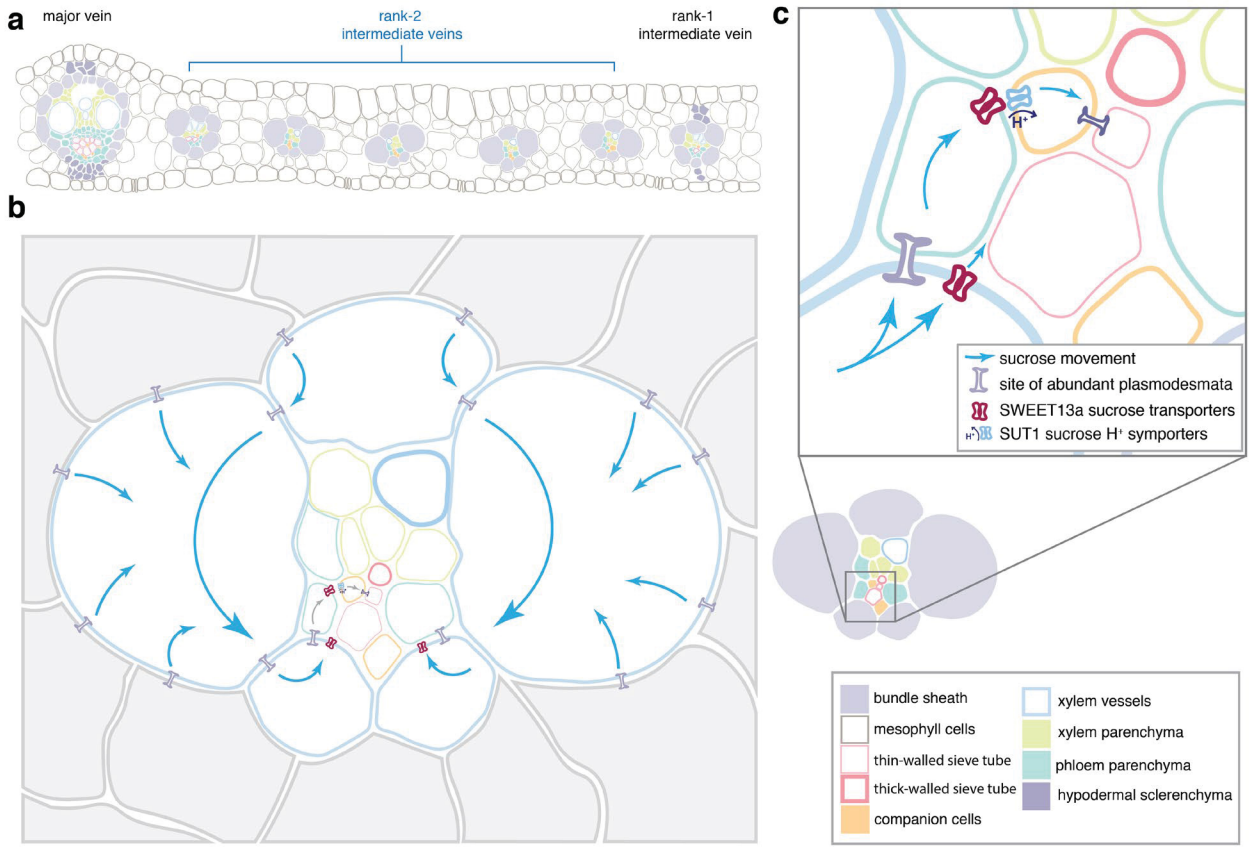

Figure 6. Phloem loading occurs via the ^{ab}BS in maize
a. Example of arrangement and relative numbers of major veins, rank-1 intermediate veins, and rank-2 intermediate veins in a mature maize leaf. Note that rank-1 intermediate veins are distinguished from rank-2 by the presence of hypodermal sclerenchyma. **b.** A rank-2 intermediate vein surrounded by bundle sheath (blue outline) and mesophyll (grey) cells. Sucrose movement down its concentration gradient is indicated by blue arrows. **b.** Inset panel shows detail of sucrose movement from bundle sheath cells into apoplasm via SWEET13 transporters, or to phloem parenchyma (teal) via plasmodesmata, where it is then effluxed to the apoplasmic space by SWEETs. Sucrose in the apoplasm is taken up by SUT1 into the companion cells-sieve element (orange, pink) complex for long distance transport.

SUPPLEMENTARY DATA

Supplementary text

A subset of mesophyll cells appears to be specialized in iron metabolism

Subcluster MS5 (visible in the lower left corner of Figure 1b) shared mesophyll identity but appeared be specialized in metal accumulation and transport, as indicated by high and specific expression of four nicotianamine synthase genes, *NAS1, 2,* 9, and *10*, which are involved in iron chelation; one iron phytosiderophore transporter. *YS1* (*yellow stripe 1*); and various additional genes involved in metal transport and metabolism (Supplementary Table 1). M5 cells could either represent a cell type with a specific localization in the leaf or correspond to cells that contain different levels of iron.

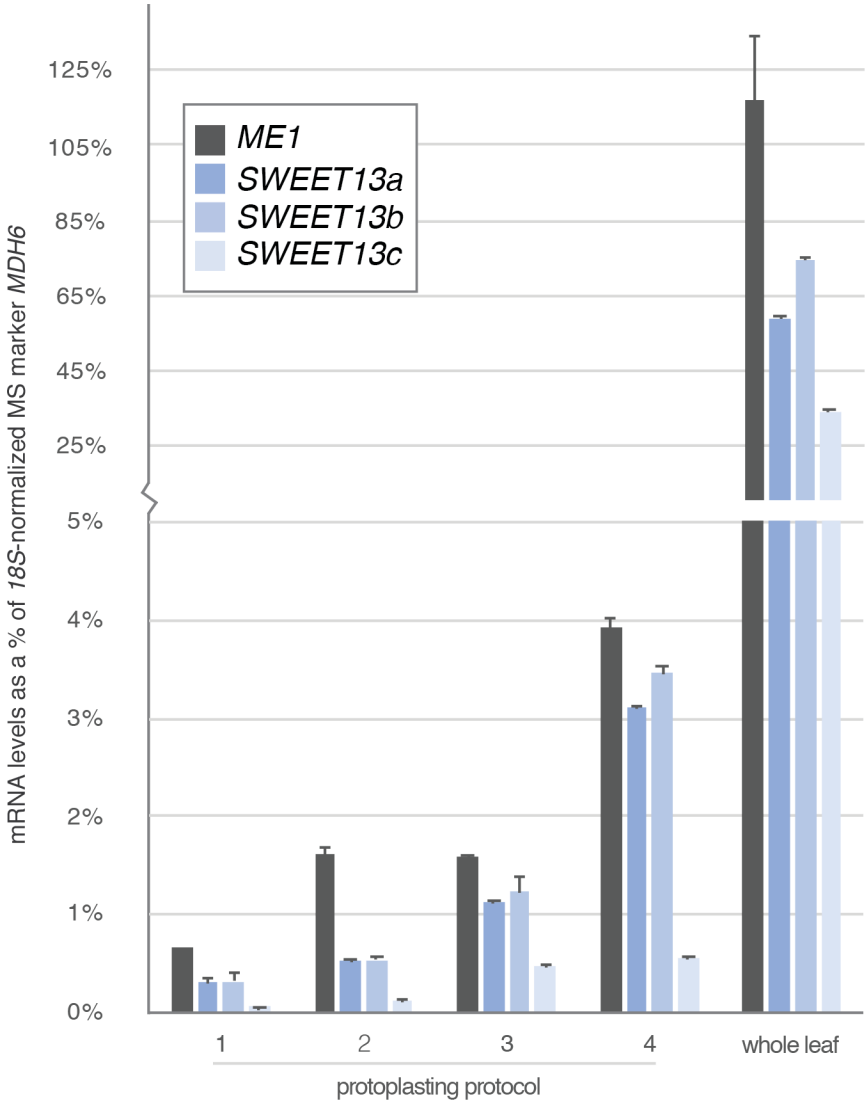

Supplementary Figure 1. qRT-PCR of putative BSC and vascular-expressed genes as an indication of protoplast cell type diversity prior to sequencing

Normalized mRNA levels of *ME1*, *SWEET13a*, *SWEET13b*, and *SWEET13c* shown as a percentage of *18S*-normalized expression of a mesophyll marker gene, *NADP-malate dehydrogenase6* (*MDH6*), after different protoplasting treatments. Error bars represent SEM of technical duplicates.

Protocol 1, standard enzyme cocktail (see Materials and Methods) with 3.5 h incubation. Protocol 2, doubled enzyme concentration. Protocol 3, isolated BS strands released after 2 h and continued protoplasting of filtered BS strands in fresh enzyme solution to deplete mesophyll cells. Protocol 4, incubated leaf tissue in pretreatment solution (2 mM L-cysteine and 164 mM sorbitol), which yielded the highest ratio of BS:MS marker genes.

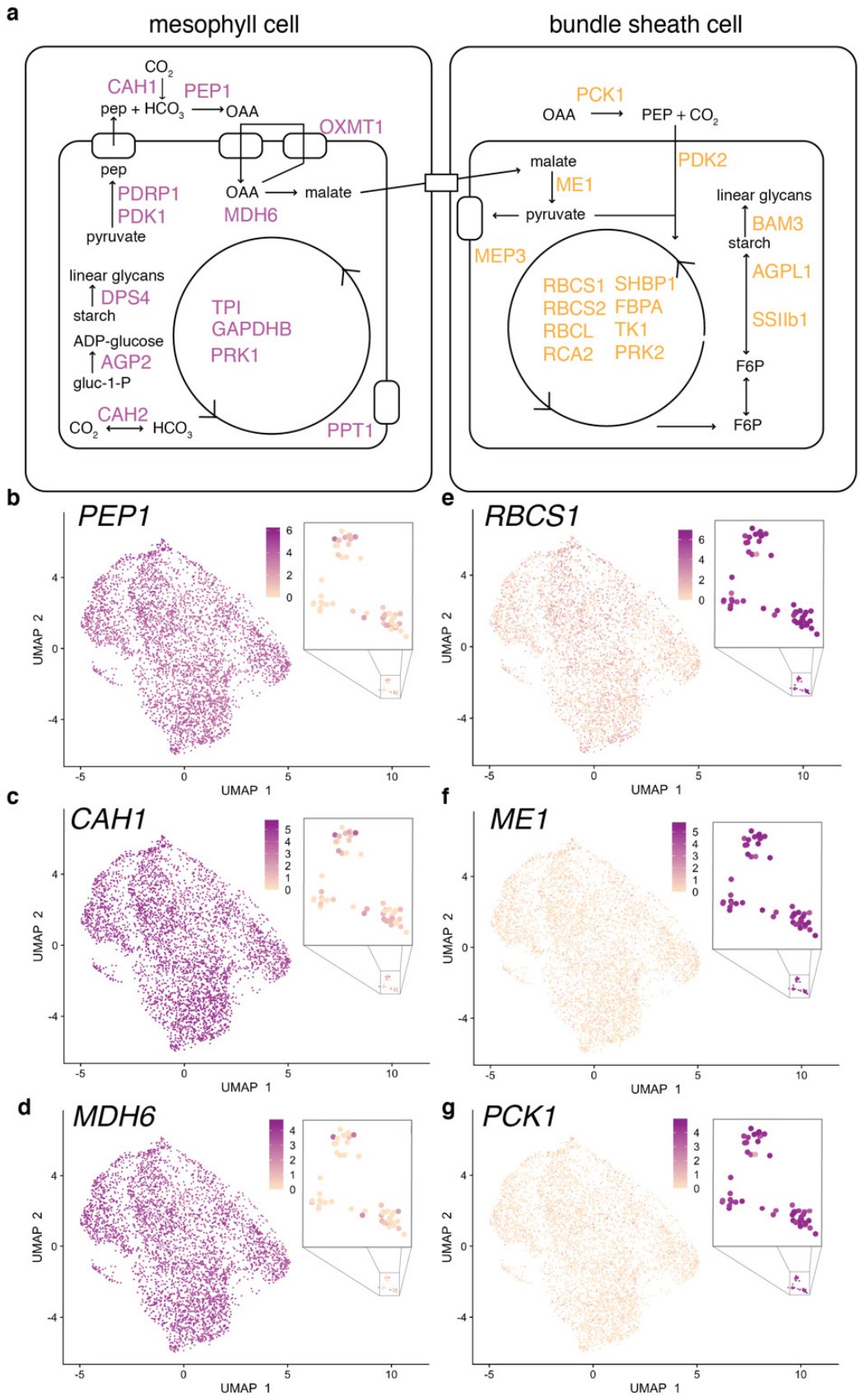
a
mesophyll cell
bundle sheath cell
CO2
CAH1
PEP1
pep + HCO3
OAA
OXMT1
pep
PDRP1
PDK1
pyruvate
OAA
malate
MDH6
linear glycans
DPS4
starch
ADP-glucose
AGP2
gluc-1-P
CO2
CAH2
HCO3
TPI
GAPDHB
PRK1
PPT1
PCK1
OAA
PEP + CO2
malate
ME1
pyruvate
PDK2
MEP3
RBCS1
RBCS2
RBCL
RCA2
SHBP1
FBPA
TK1
PRK2
linear glycans
BAM3
starch
AGPL1
SSIIb1
F6P
F6P
b
PEP1
e
RBCS1
c
CAH1
f
ME1
d
MDH6
g
PCK1
UMAP 1
UMAP 2

Supplementary Figure 2. Schematic of C4 photosynthesis related genes and relative expression in BS and MS clusters.

a. Partitioning of proteins involved in C4 photosynthesis between mesophyll and bundle sheath cells in maize(Friso et al., 2010). For all proteins displayed, mRNA expression in this scRNA-seq dataset was specific to either mesophyll or bundle sheath cells (logFC > 1.0; FDR-adjusted p-value < .05). **b**. Gene IDs, symbols, and full names are shown along with Log FC values in Supplementary Table 2. **b-g.** Feature plots show normalized levels of mRNAs for canonical C4 photosynthesis genes expressed differentially in mesophyll and bundle sheath. **b.** *PEP1* (Phosphoenolpyruvate carboxylase 1; Zm00001d046170) **c.** *CAH1* (Carbonic anhydrase 1; Zm00001d044099) **d.** *MDH6* (NADP-dependent malate dehydrogenase 6; Zm00001d031899) **e.** *RBCS1* (Ribulose bisphosphate carboxylase small subunit 1; Zm00001d052595) **f.** *ME1* (NADP-dependent malic enzyme 1; Zm00001d000316) **g.** *PCK1* (Phosphoenolpyruvate carboxykinase 1; Zm00001d028471)

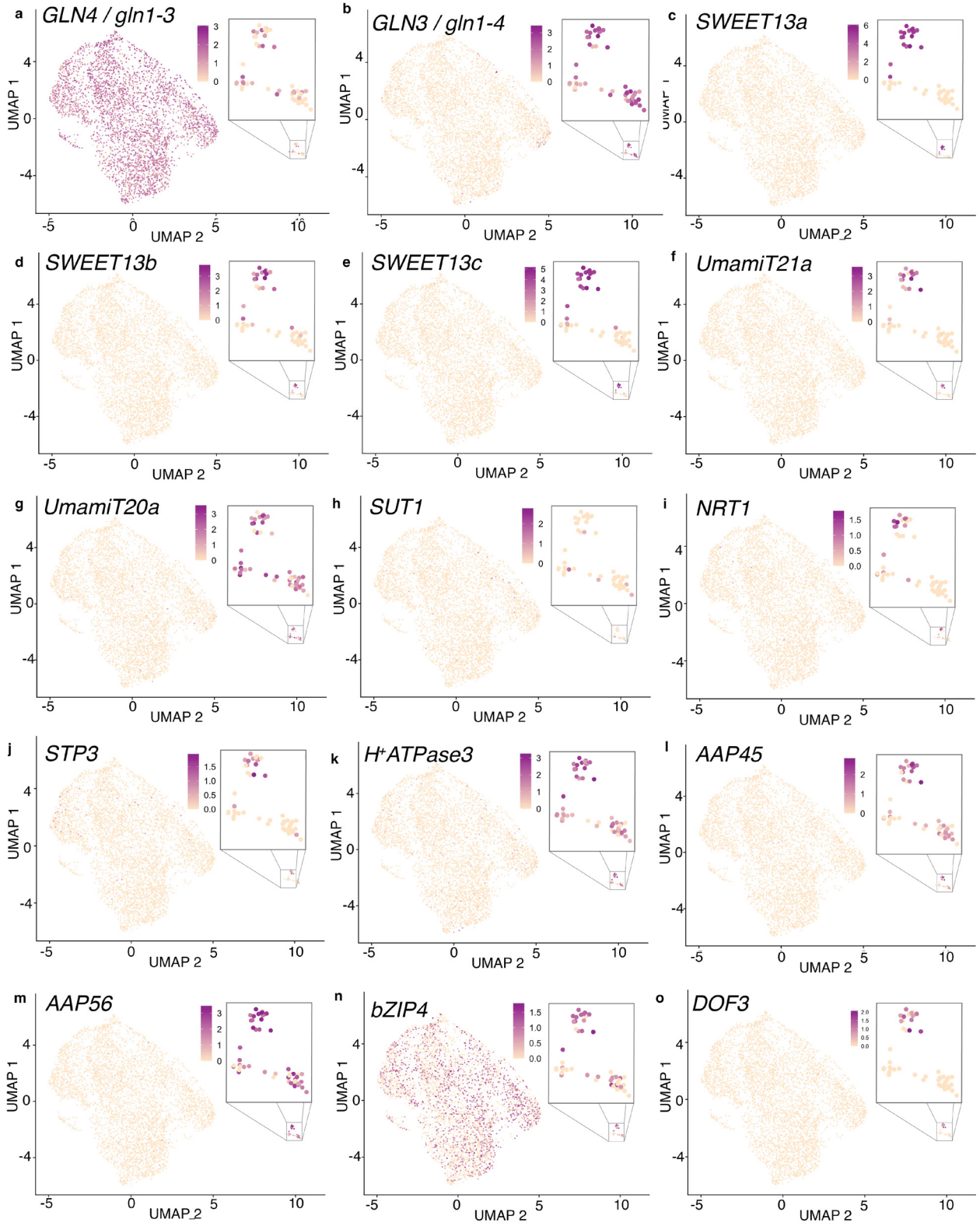
a
GLN4 / gln1-3
b
GLN3 / gln1-4
c
SWEET13a
d
SWEET13b
e
SWEET13c
f
UmamiT21a
g
UmamiT20a
h
SUT1
i
NRT1
j
STP3
k
H+ATPase3
l
AAP45
m
AAP56
n
bZIP4
o
DOF3
UMAP 1
UMAP 2

Supplementary Figure 3. UMAP plots of glutamine synthetase, transport-related proteins, and transcription factors in bundle sheath cells

a - b. Feature plots show normalized levels of mRNA transcripts for glutamine synthetase genes expressed differentially in mesophyll and bundle sheath. **a.** *GLN4 (gln1-3*, protein GS3, Zm00001d017958) is widely expressed in mesophyll cells and some bundle sheath cells. **b.** *GLN3 (gln1-4*, protein GS4, Zm00001d028260) is expressed in bundle sheath cells.

c – o. Feature plots show normalized levels of mRNA transcripts for transport-related genes and transcription factors expressed in ^{ad}BS or ^{ab}BS. **c.** *SWEET13a* (Zm00001d023677), **d.** *SWEET13b* (Zm00001d023673), **e.** *SWEET13c* (Zm00001d041067), and **f.** *UmamiT21a* (Zm00001d035717) are specific to ^{ab}BS. **g.** *UmamiT20a* (Zm00001d044951) is expressed in ^{ab}BS and ^{ad}BS. **h.** *SUT1* (Zm00001d027854) is not highly expressed in any cell type in this dataset. **i.** *NRT1* (Zm00001d044768), **j.** *STP3* (Zm00001d027268), **k.** *H^+ATPase3* (Zm00001d019062), **l.** *AAP45* (Zm00001d035243), **m.** *AAP56* (Zm00001d012231), **n.** *bZIP4* (Zm00001d018178) and **o.** *DOF3* (Zm00001d035651) are enriched in ^{ab}BS relative to ^{ad}BS.

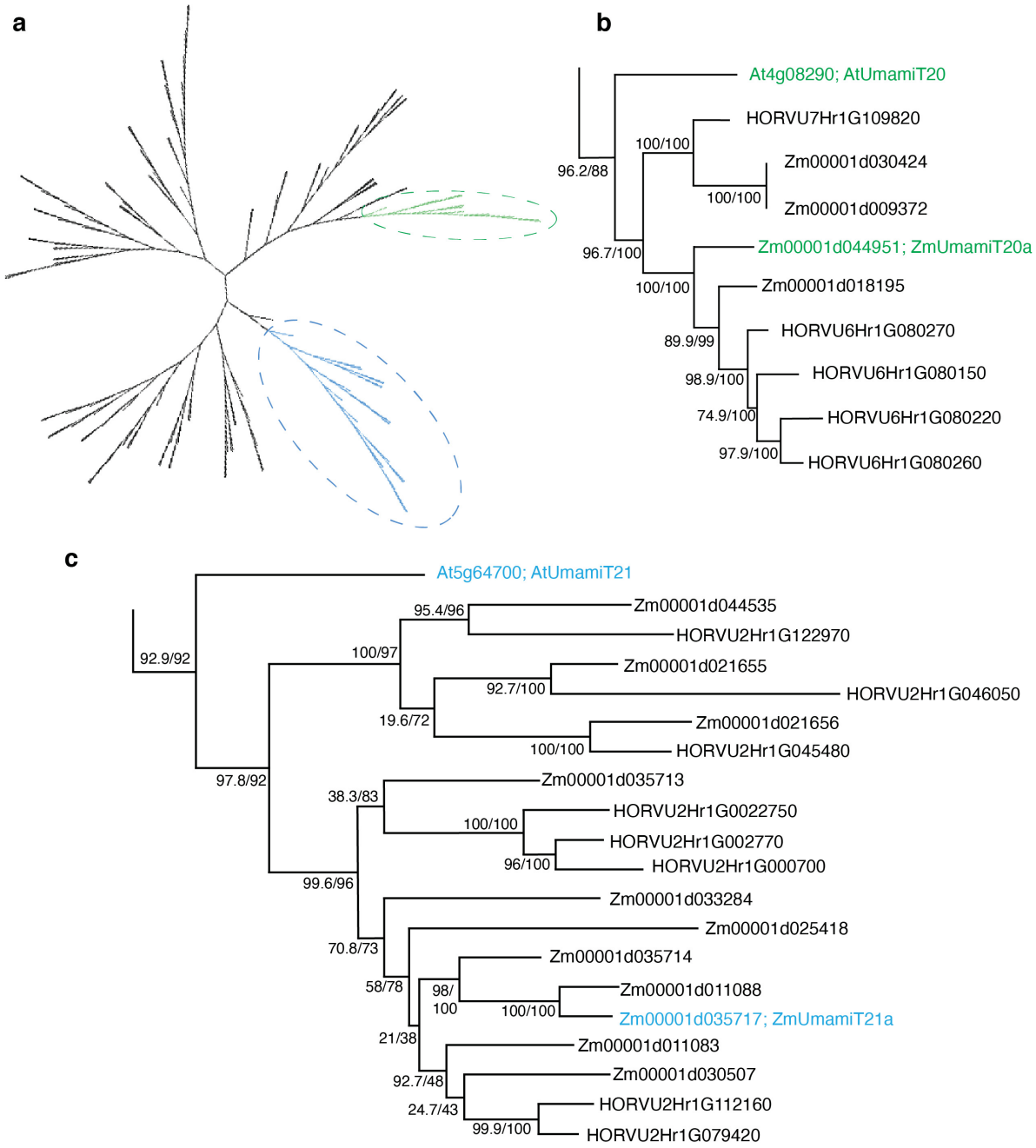

Supplementary Figure 4. Neighbor joining tree of family of UmamiT amino acid transporters in Arabidopsis, maize, and barley

a. Cladogram of all UmamiT amino acid sequences in maize, barley, and Arabidopsis **b.** Phylogram of green highlighted clade containing the ZmUmamiT expressed in all BSC types. Zm00001d44951 is most closely related to Arabidopsis UmamiT20. **c.** Phylogram of blue highlighted clade containing the ZmUmamiT expressed specifically in ^{ab}BSC. Zm00001d035717 is most closely related to Arabidopsis UmamiT21. Values at nodes are % UF-bootstraps out of 1000/% SH-aLRT.

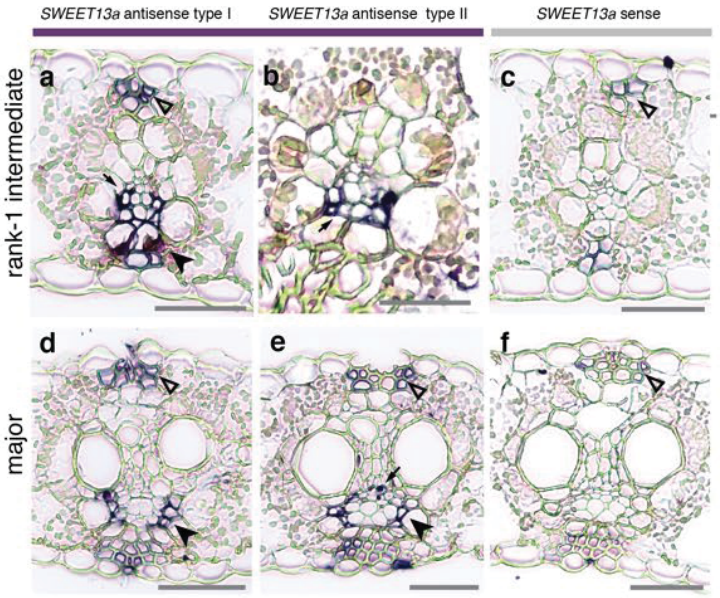

rank-1 intermediate		% veins
pattern I	BS + PP	85.2
pattern 2	PP only	14.8

major veins		% veins
pattern I	PP only	43.8
pattern 2	PP, medial VP	56.2

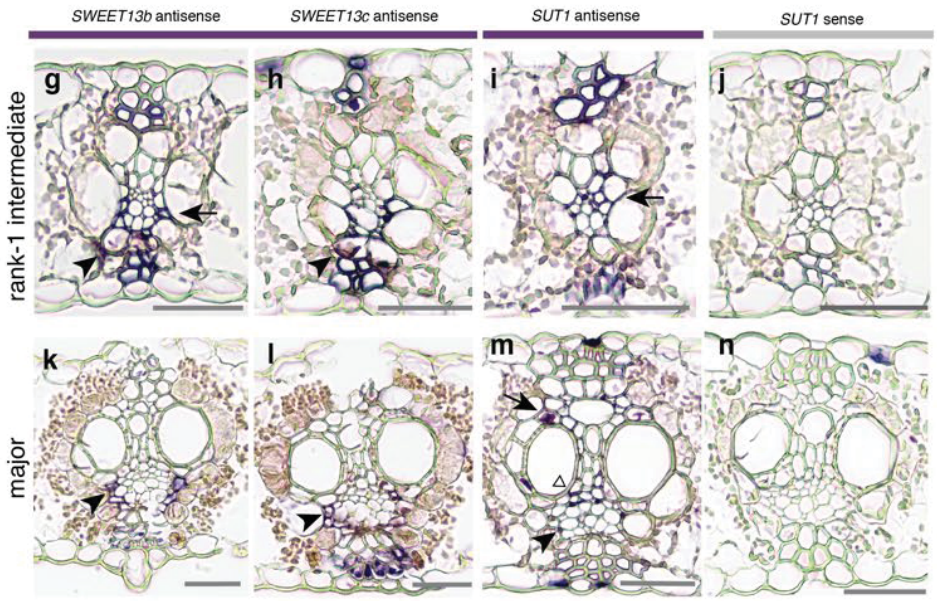

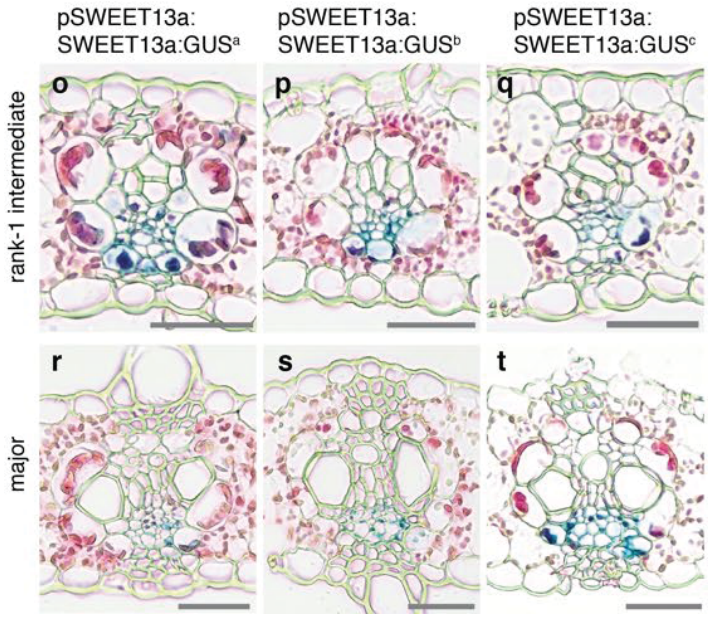

Supplementary Figure 5. SWEET and SUT mRNA localization and SWEET13a protein localization in rank-2 intermediate and major veins

a - c. SWEET13a mRNA localization in rank-1 intermediate veins **a.** Pattern 1: [ab]BSC (arrowhead) and vascular parenchyma (VP) (arrow), and **b.** Pattern 2: mainly in VP (arrow). **c**. rank-1 vein in sense-probe-hybridized section. **d-f.** SWEET13a mRNA localization in major veins **d.** Pattern 1: in phloem parenchyma (PP) only (arrow), and **e.** Pattern 2: in PP and medial VP (parenchyma between xylem and phloem) (arrow). **f.** *SWEET13a* major vein in sense-probe -hybridized section. Hypodermal sclerenchyma is considered background (open triangles). Table indicates percentage of veins meeting the above criteria for each vein type. Rank-1 intermediate, n = 196; and major veins, n = 98; variable n-numbers are due to relative proportions of each vein type in the leaf. Scale bars are 100 μm.

g - j. *SWEET13b*, *c*, and *SUT1* mRNA localization in rank-1 intermediate veins. **g.** For *SWEET13b* antisense probe-hybridized rank-1 intermediate veins, staining was in [ab]BS (arrowhead) and vascular parenchyma (arrow). **h.** For *SWEET13c* antisense probe-hybridized rank-1 intermediate veins, staining was in [ab]BS (arrowhead) and vascular parenchyma (arrow). **i.** For *SUT1* antisense probe-hybridized rank-1 intermediate veins, staining was in vasculature (arrow). **j.** *SUT1* sense probe-hybridized rank-1 intermediate vein.

k - n. *SWEET13b*, *c*, and *SUT1* mRNA localization in major veins. **k.** For *SWEET13b* antisense probe-hybridized major veins, staining was in phloem parenchyma (arrowhead). **l.** For *SWEET13c* antisense probe-hybridized major veins, staining was in phloem parenchyma (arrowhead). **m.** For *SUT1* antisense probe-hybridized major veins, staining was in companion cells (arrow), in vascular parenchyma between xylem and phloem (triangle), and in xylem parenchyma (arrowhead). **n.** *SUT1* sense probe-hybridized major vein. Scale bars are 100 μm.

o – t. SWEET13a protein localization as visualized by GUS staining of SWEET13a:GUS-transformed B104 plants . Chloro bromoindigo precipitate is localized to abaxial portion of veins in both rank-1 intermediate (**o – q**) and major veins (**r – t**) of all three independent transformation events. Scale bars are 100 μm; sections are counterstained with Eosin-Y.

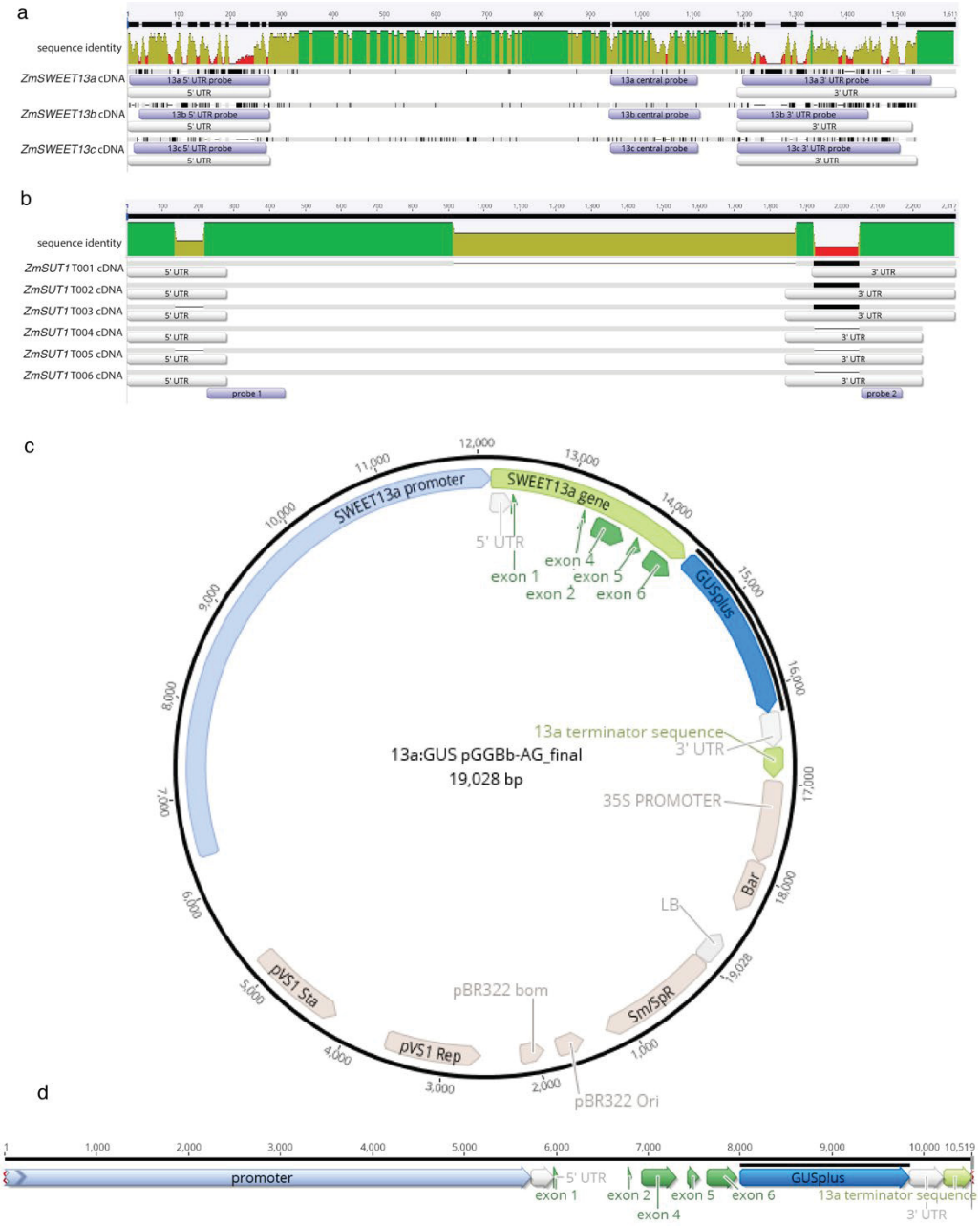

Supplementary Figure 6. Probe design for in situ hybridization and pSWEET13a:SWEET13a:GUS construct schematic

a. *ZmSWEET13a*, *b*, and *c* aligned using MUSCLE in Geneious. Regions used as templates for RNA probes are highlighted in purple. Three probes in unique regions of each gene allowed us to differentiate between the homologs. **b.** The six isoforms of *ZmSUT1* aligned using MUSCLE in Geneious; two regions common to all six isoforms were selected for probe templates. Two unique regions in ZmUMAMIT21a and ZmME1 were selected for probe templates.**c.** Circular schematic of plasmid used to transform B104. The construct included the 5751 bp upstream of the start codon (lavender), all exons and introns of the SWEET13a gene (green), a 9-alanine linker fused to GUSplus (blue), followed by 684 bp downstream of stop codon (green). d. linear schematic of the SWEET13a:GUS construct

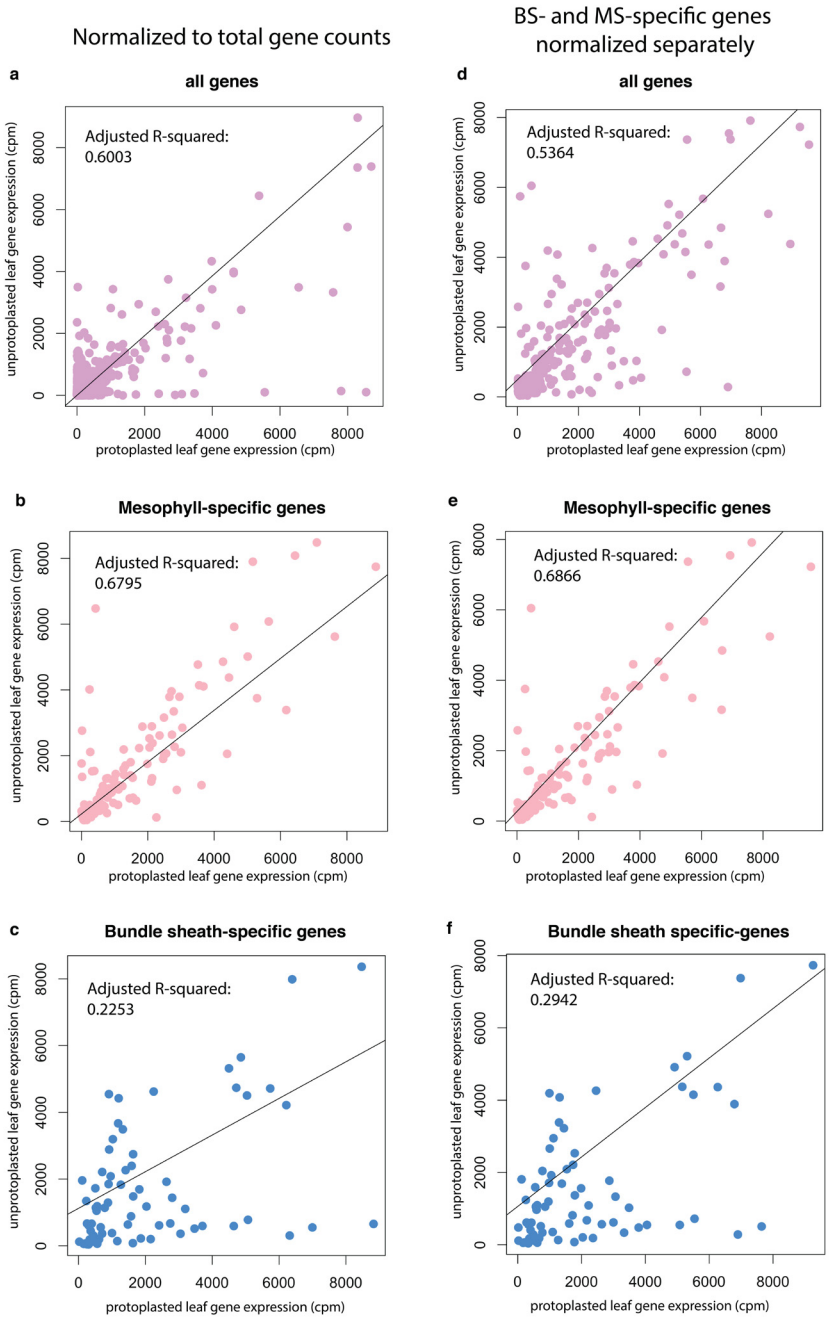

Supplementary Figure 7. Correlation of mRNA counts between protoplasted cells and whole leaf

a. mRNA counts in whole leaf and protoplasted leaf expressed as counts per million reads (cpm) with adjusted R-squared values. **b**. mRNA counts for mesophyll cell-specific genes, as determined by unsupervised marker gene discovery (see materials and methods). **c.** mRNA counts for bundle sheath-specific genes. In **d-f**: counts of MS- and BS-specific genes were normalized separately to compensate for differing ratios of cell types represented in bulk leaf and protoplast samples. **d.** MS- and BS-specific genes, normalized separately. **e.** MS-specific genes normalized to total counts of MS-specific genes. **f.** BS-specific genes normalized to total counts of BS-specific genes. TMM method of normalization.

Supplementary Table 2. mRNA enrichment of C4 photosynthesis-related genes in MS and BS clusters

mesophyll	Symbol or abbreviation	Log FC	Gene name
Zm00001d031899	*MDH6*	3.00	NADP-dependent malate dehydrogenase 6
Zm00001d046170	*PEP1*	3.20	Phosphoenolpyruvate carboxylase 1
Zm00001d044099	*CAH1*	3.58	Carbonic anhydrase 1
Zm00001d011454	*CAH6*	3.58	Carbonic anhydrase 6 (chloroplast localized)
Zm00001d023929	*OXMT1*	1.50	Oxo-glutarate/malate transporter1 (OMT)
Zm00001d038163	*PDK*	1.45	Pyruvate, phosphate dikinase 1
Zm00001d006520	*PDRP1*	2.95	Pyruvate, phosphate dikinase regulatory protein 1
Zm00001d032383	*PPT1*	0.99	Phosphate/phosphoenolpyruvate translocator 1
Zm00001d035737	*PRK1*	2.18	D-glycerate 3-kinase chloroplastic
Zm00001d027488	*GAPB1*	2.10	Glyceraldehyde phosphate dehydrogenase B1
Zm00001d021310	*TPI*	2.54	Triosephosphate isomerase
Zm00001d039131	*AGP2*	0.86	ADP glucose pyrophosphorylase 2
Zm00001d027309	*DPS4*	n/a	Phosphoglucan phosphatase DSP4 chloroplastic
bundle sheath	**Symbol or abbreviation**	**Log FC**	**Gene name**
Zm00001d004894	*RBCS2*	5.19	Ribulose biphosphate carboxylase small subunit 2
Zm00001d052595	*RBCS1*	5.18	Ribulose biphosphate carboxylase small subunit 1
Zm00001d006402	*RBCL*	2.08	Rubisco large chain (genomic, introns)
Zm00001d028471	*PCK1*	4.23	Phosphoenolpyruvate carboxykinase 1
Zm00001d000316	*ME1*	5.04	NADP-dependent malic enzyme
Zm00001d045451	*TK1*	2.20	Transketolase 1
Zm00001d010321	*PDK2*	1.58	Pyruvate orthophosphate dikinase 2
Zm00001d042050	*MEP3*	3.78	Protein RETICULATA-RELATED 4
Zm00001d000164	*PRK2*	1.14	Phosphoribulokinase chloroplastic 4
Zm00001d048593	*RCA2*	3.79	Rubisco activase 2
Zm00001d023559	*FBPA*	5.31	Fructose-bisphosphate aldolase
Zm00001d053015	*FBPA*	2.89	Fructose-bisphosphate aldolase
Zm00001d042840	*SHBP1*	3.78	Sedoheptulose-17-bisphosphatase 3 chloroplastic
Zm00001d018936	*RPE*	3.67	Probable ribose-5-phosphate isomerase 3 chloroplastic
Zm00001d033910	*AGPL1*	2.14	ADP glucose pyrophosphorylase large subunit leaf 1
Zm00001d047077	*BAM3*	1.09	Beta-amylase 3
Zm00001d026337	*SSIII1b*	0.60	Starch synthase IIIb-1

Supplementary Table 4. Genes used in this study

AGPv4 ID	gene	full name
Zm00001d023677	SWEET13a	SWEET13a
Zm00001d023673	SWEET3b	SWEET13b
Zm00001d041067	SWEET13c	SWEET13c
Zm00001d027854	SUT1	Sucrose Transporter 1
Zm00001d048611	MT1b	Metallothionein-like protein 1B
Zm00001d038558	CC3	Cystatin3
Zm00001d004894	RBCS2	ribulose bisphosphate carboxylase small subunit2
Zm00001d052595	RBCS1	ribulose bisphosphate carboxylase small subunit1
Zm00001d000316	ME1	NADP-dependent malic enzyme
Zm00001d053281	NAAT1	Nicotianamine aminotransferase
Zm00001d016441	TAAT	Tyrosine aminotransferase
Zm00001d044099	CAH1	Carbonic anhydrase 1
Zm00001d031899	MD6	NADP-dependent malate dehydrogenase 6
Zm00001d046170	PEP1	Phosphoenolpyruvate carboxylase 1
Zm00001d028471	PCK1	Phosphoenolpyruvate carboxykinase 1
Zm00001d047658	NAS10	Nicotianamine synthase10
Zm00001d047651	NAS1	Nicotianamine synthase 1
Zm00001d028887	NAS9	Nicotianamine synthase 9
Zm00001d028888	NAS2	Nicotianamine synthase2
Zm00001d017429	YS1	Iron-phytosiderophore transporter yellow stripe 1
Zm00001d033496	Nas3	Nicotianamine synthase 3
Zm00001d035243	AAAP45	Amino acid permease 45
Zm00001d012231	AAAP56	Amino acid permease 56
Zm00001d035717	UmamiT21a	UmamiT21a
Zm00001d044951	UmamiT20a	UmamiT20a
Zm00001d010321	PDK2	Pyruvate orthophosphate dikinase 2
Zm00001d038163	PDK1	Pyruvate orthophosphate dikinase1
Zm00001d031899	MDH6	NADP-dependent malate dehydrogenase 6
Zm00001d017958	GLN4	glutamine synthetase 4 (gln1-3)
Zm00001d033747	GLN2	glutamine synthetase 2 / Glutamine synthetase root isozyme 2
Zm00001d026501	GLN1	glutamine synthetase 1 leaf isozyme chloroplastic
Zm00001d028260	GLN3	glutamine synthetase 3 / 6 / root isozyme 5 (gln1-4)
Zm00001d044768	NRT1	Protein NRT1/ PTR FAMILY 5.8
Zm00001d027268	STP3	Sugar transport protein 3
Zm00001d019062	H+ATPase	membrane H(+)-ATPase3
Zm00001d018178	bZIP4	basic leucine zipper 4 / ABA-insensitive 5-like protein
Zm00001d010201	MYB25	Transcription repressor MYB6 / myb25

Phloem loading via the abaxial bundle sheath cells in maize leaves

SUPPLEMENTARY RESULTS

Analysis of an independent repeat of the maize leaf scRNA-seq dataset

Evidence from *in situ* hybridization supports the results from single-cell RNAseq (scRNA-seq), which indicate that a subset of bundle sheath cells shows high levels of mRNA encoding sugar and amino acid transport proteins. However, because the cells partitioned were all collected from plants grown under the same conditions on the same day, we cannot exclude the possibility that transcriptional states could be influenced by particular conditions such as undetected pathogen infection or differences in growth conditions. Therefore, a second scRNA-seq experiment was generated. Tissue from plants at the same developmental stage (B73, V2, leaf 2 tip) were harvested for protoplast release, and 10x Genomics Chromium GEM partitioning and sequencing were performed as described for the first replicate (Bezrutczyk et al., 2020). An estimated 7,000 cells were loaded in the 10x Chromium partitioning chip. However, this partitioning event resulted in only 0.16 ng/uL cDNA recovered after cell partitioning and cDNA synthesis, compared to 3.16 ng/uL cDNA in the first replicate. A cDNA library was generated and sequenced, but only 1,952 cells were assigned by the Cellranger software, compared to 5,655 in the first replicate. The reason for the low cDNA recovery is not known, though one potential reason is that the cell viability was only 70% based on the percentage of cells which absorbed trypan blue dye, an indicator of a compromised plasma membrane. As a comparison, 90% of protoplasts in the first replicate were viable. Because of the lower recovery, this dataset was not analyzed further, and a third experiment was performed. The third experiment (henceforth 'maize leaf R3') resulted in 3.6 ng/uL cDNA and 6,104 cells, and was used for further analysis.

Initial data processing was completed according to the methods described in Bezrutczyk et al., 2020, using 10x Genomics Cellranger to trim and align reads and generate a feature-barcode matrix. Downstream analysis was performed using the Seurat R package (v3.1) (Butler et al., 2018). The same parameters were used for filtering for both datasets: to remove cells with low mRNA count (nFeature_RNA) and doublets, as well as damaged cells with high chloroplast (pt) or mitochondria (mt) genome-derived transcripts, cells were filtered (percent.pt <4 & percent.mt <0.75 & nFeature_RNA >1800 & nFeature_RNA <7000). Normalization and scaling were performed using SCTransform (Hafemeister and Satija, 2019). Maize leaf R3 was

analyzed on its own using the identical analysis pipeline that was used on the first replicate (henceforth 'maize leaf R1'). In addition to separate analyses for each replicate, the two replicates were combined to create an integrated dataset, and the integrated dataset was analyzed.

Maize leaf R1 and R3 are broadly similar, with a few key differences

The dataset from maize leaf R3 is broadly similar to the dataset from maize leaf R1. The total number of cells was similar, but a lower percentage of cells in maize leaf R3 met pre-processing cell selection cutoffs (cells retained in dataset: genes detected per cell > 1800; % mitochondrial genome-derived mRNA <0.75; % chloroplast genome derived mRNA < 4). Ultimately, fewer cells were retained for further analysis after cell selection in maize leaf R3. Importantly, there were less than half the number of bundle sheath cells in maize leaf R3 as in maize leaf R1.

	Maize leaf R1	*Maize leaf R2*	*Maize leaf R3*
viability	90%	70%	90%
cDNA	3.16 ng/µL	0.16ng/µL	3.6 ng/µL
total cells	5655	1952	6104
low-UMI cells	1892	-	2862
% retained	67%	-	53%
total retained	3763	-	3242
BS cells	53	-	20

Similar to the maize leaf R1, maize leaf R3 mostly consisted of mesophyll (MS) cells, with a smaller number of bundle sheath (BS) cells. Unsupervised *k*-means clustering resulted in five mesophyll clusters in maize leaf R1 (Fig 1a), while maize leaf R3 had only four (Fig. 1b). The MS5 cluster (Fig. 1a, dark green cells), which was enriched for *nicotianamine synthase1* and other genes related to metal ion metabolism, was missing from maize leaf R3. The key marker genes which defined this cluster were present in maize leaf R3, but were found in cells distributed throughout the other mesophyll clusters. No cells in maize leaf R3 were enriched for multiple *nicotianamine synthase* genes. That no cells form a metal ion metabolism-specific cluster suggests that nutrient status or differences in growth conditions resulted in a small population of cells with an idiosyncratic transcriptional state in maize leaf R1. Additionally, in maize leaf R3, prior to cell selection, there were five cells which formed a very small, well-separated cluster with exclusive expression of *SUT1* (data not shown). These may be companion cells, but the *SUT1*-expressing cells' UMI counts were below the cell selection

cutoff. Additionally, differential gene expression analysis indicated that these cells did not have high levels of mRNAs for genes homologous to Arabidopsis companion cell marker genes, such as *ATPase* (Kim et al., 2020). Due to low UMI counts and lack of clear companion cell identity, the cells which contained *SUT1* mRNA were not analyzed further.

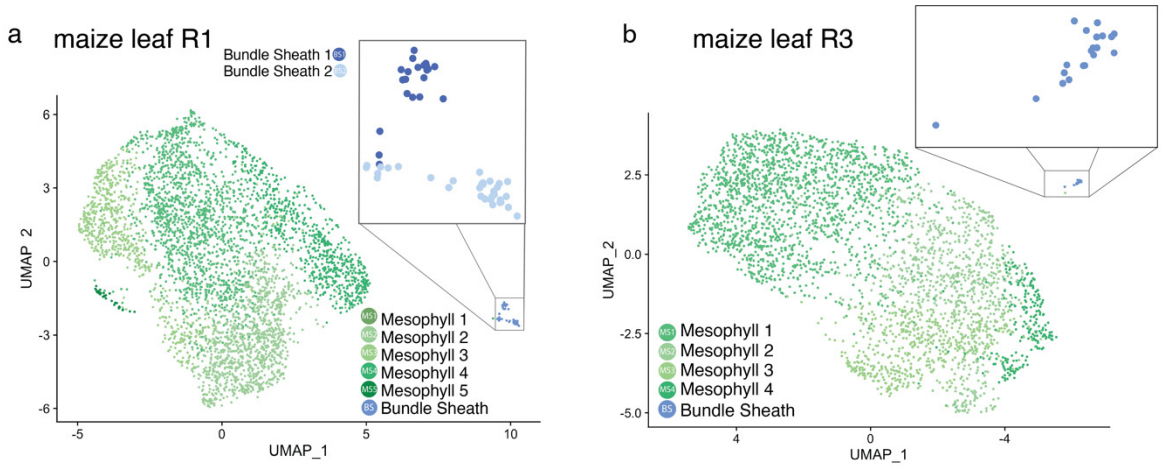

Figure 1. UMAP plots show 2D representation of cell relatedness in multidimensional space based on transcriptional profiles. **a.** Maize leaf R1 consists of six clusters at K-means clustering resolution 0.2. The BS cluster separates into two at higher resolution (inset). The "upper" and "lower" cluster were later determined to correspond to abaxial (^{ab}BS) and adaxial (^{ad}BS) (Bezrutczyk et al., 2020) and are therefore named ^{ab}BS and ^{ad}BS. **b.** Maize leaf R3 consists of five clusters at low resolution, but the BS cluster does not separate into two subclusters at higher resolution.

The bundle sheath cluster from maize leaf R3 was similar to that of maize leaf R1 in that a subset of BS cells showed high levels of *SWEET13a*, *b*, and *c* mRNA, as well as amino acid transporter *UmamiT21a*. All cells in the BS cluster showed high expression of canonical C4 marker genes, such as *RBCS1* (Fig 2). However, the cells of the BS cluster in maize leaf R3 did not separate into two clusters (Fig. 1a, b; inset panels), even at very high resolution (FindClusters resolution > 100). Separation of cells into clusters by *k*-means clustering is dependent on both cell number and the uniqueness of the cells' transcriptional profiles. In Arabidopsis root meristem, the transcriptomes of just two putative quiescent cells formed a cluster (Ryu et al., 2019), presumably because the transcriptional profile of these two cells was sufficiently unique. The differential expression of only 38 genes distinguished the abaxial and adaxial BS clusters in maize leaf R1, and the cells containing SWEET mRNAs in both maize leaf R1 and R3 predominantly contain genes characteristic of bundle sheath identity. Therefore, the bundle sheath cluster of maize leaf R3 cannot be resolved into two subclusters due to a combination of small number of cells and lack of sufficient defining transcriptional features. The results from maize leaf R3 do not, on their own, provide strong support for our hypothesis that a subset of bundle sheath cells is specialized for sucrose and amino acid transport.

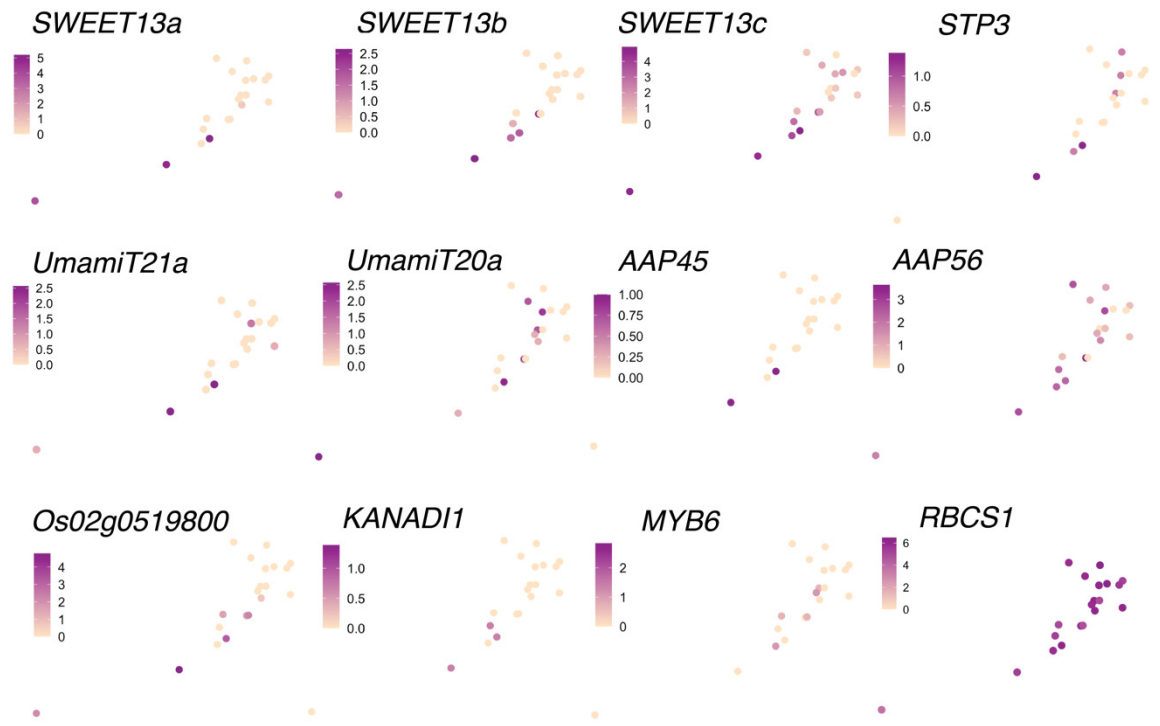

Figure 2. Maize leaf R3 feature plots show normalized mRNA levels plotted in UMAP space. Darker colors indicate higher mRNA levels. *SWEET13a*, *SWEET13b*, *SWEET13c*, *UmamiT21a, AAP45, STP3, Os02g0519800,* and *KANADI1* mRNAs are all highly enriched in a subset of cells. *AAP56, UmamiT20a,* and *MYB6*-enriched cells are distributed throughout the bundle sheath cluster. As in maize leaf R1, *RBCS1* and other canonical C4 photosynthesis marker genes are highly expressed in all BS cells.

Multiple methods for combining scRNA-seq datasets

The datasets from maize leaf R1 and maize leaf R3 were combined so that the transcriptional profiles of cells from both replicates could be directly compared. The greater number of cells in a combined dataset may also improve the statistical power to resolve subclusters of rare cell populations. The R package Seurat v3.1 provides tools for several methods of scRNA-seq dataset combination. The first method is to generate a single matrix of reads from two or more datasets, and 'merged' datasets are analyzed as if they were one. Seurat's 'merge' function has been used for experiments that were performed at the same time, such as protoplasts that were released on the same day from plants grown concurrently (Kim et al., 2020). The second method is to annotate the clusters of one dataset using marker genes derived from clusters of another dataset, without directly combining them. The third method is known as 'integration', in which shared cell states are identified across experiments. The identity of clusters from one dataset are then calculated based on 'anchor' features, and separate scaling parameters are applied to gene expression values from each dataset to compensate for batch effects (Butler et al., 2018). The advantage of integration is that it allows for pooling of all cells into a single

UMAP plot with coherent expression of marker genes in feature plots, even if UMI counts for some genes in a given cluster vary between experiments, as may be the case for datasets from plants grown on different days, or from analogous cell types in different species. Without the integration tool, batch effects can cause cells to cluster by both batch and cell identity; integration allows these independent experiments to be visualized as one and minimizes the differences between batches.

Merging datasets from maize leaf R1 and R3

To combine datasets from the two replicates, two different methods were tested: merging and integration. Merging the datasets from maize leaf R1 and R3 resulted in bundle sheath and mesophyll clusters which separated by both batch and cell identity: cells were clustered as MS and BS (cell identity), but also maize leaf R1 and maize leaf R3 (batch) (Fig. 3), therefore the dataset combined by merging was not used for further analysis.

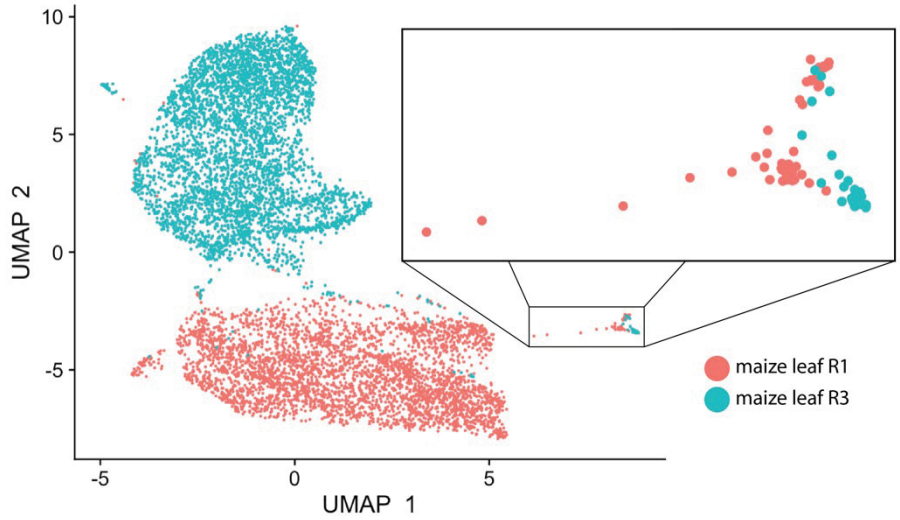

Figure 3. UMAP plot with cells colored by dataset. Merging datasets from maize leaf R1 and R3 by combining all reads into a single matrix results in clusters separating according to both cell type (MS cell clusters on the left, BS clusters on the right) as well as batch.

Combining datasets from maize leaf R1 and R3 using Seurat's 'integration' function

In order to determine whether the mesophyll and bundle sheath clusters in datasets from both replicates could be superimposed without separating by batch effects, the datasets were combined using Seurat's integration tool. To use anchors to integrate the two datasets, cell selection was performed as previously described (Bezrutczyk et al., 2020) and each dataset was separately scaled and normalized using SCTransform (Butler et al., 2018; Hafemeister and Satija, 2019). Integration was performed using nfeatures = 1000, and all features (genes) were used to find anchors. UMAP plots and feature plots were generated as previously described. The integrated dataset consisted of 7005 cells, with four MS clusters and one BS cluster at low

resolution (FindClusters resolution = 0.2) and two BS clusters at high resolution (FindClusters resolution = 26). These two BS clusters correspond to ^{ab}BS and ^{ad}BS, based on differential expression of abaxially-expressed transcription factor *KANADI1* and transporters such as *SWEET13a, b,* and *c,* the transcripts of which were found in the abaxial but not adaxial BS cells (Bezrutczyk et al., 2020).

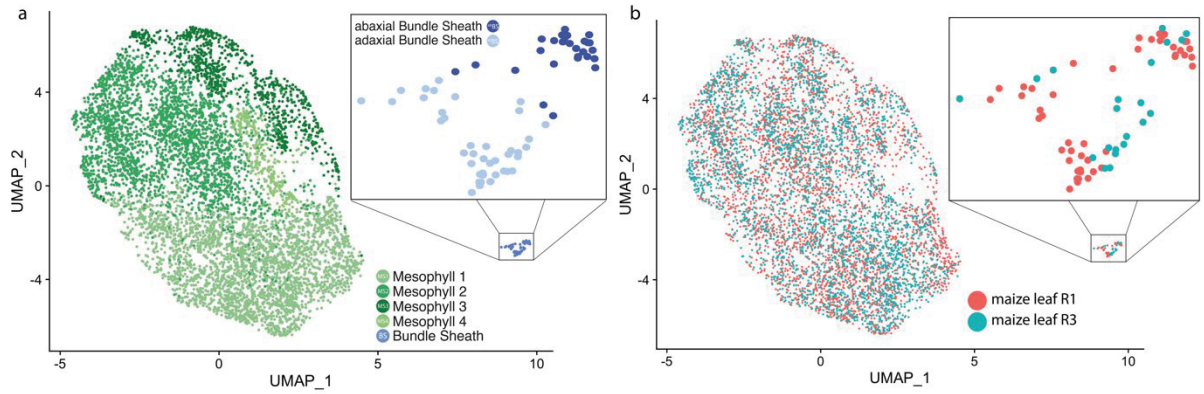

Figure 4. UMAP plot of the integrated dataset**. a.** The integrated dataset with cells colored by identity has four mesophyll clusters and one BS cluster at low resolution and two BS clusters at high resolution (inset panels) **b.** UMAP plot with cells colored by dataset shows that clusters from different experiments can be superimposed on each other based on shared cell states/identities.

Key marker genes which were specifically expressed in ^{ab}BS or ^{ad}BS in maize leaf R1 were also expressed in those clusters in the integrated dataset. Feature plots show cells in UMAP space with relative mRNA levels for a gene of interest indicated by color gradient. Feature plots for the integrated dataset were generated using UMI counts which have been scaled so that cells with detected shared identities show comparable levels of gene expression across datasets (assay: 'integrated').

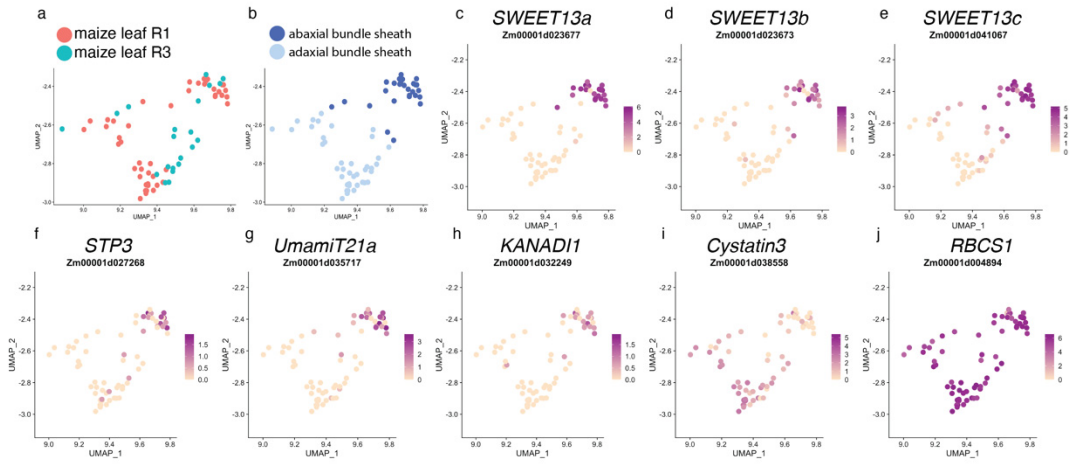

Figure 5. UMAP plots of BS subclusters in the integrated dataset. **a.** BS subclusters colored by replicate. **b**. BS subclusters colored by cell identity. **c-j.** Feature plots show normalized levels of mRNAs plotted in UMAP space. *SWEET13a*, *SWEET13b*, *SWEET13c*, *UmamiT21a, STP3,* and *KANADI1* are all highly expressed in the abaxial BS cluster. *Cystatin3* is one of the only genes expressed preferentially in the adaxial BS cluster, and *RBCS1* and other canonical C4 marker genes (not shown) are expressed in both clusters.

Similarities between transcription profiles of clusters from the two replicates can be visualized in a dot plot. This plot is generated using data in which SCTransform was used to scale UMI counts from each dataset separately (assay: 'SCT') so as not to introduce dependencies between the scaled UMI counts from different replicates. Mesophyll clusters share broadly similar mRNA levels of canonical C4 marker genes: *CARBONIC ANHYDRASE1* (*CA1*), *MALATE DEHYDROGENASE6* (*MDH6*), *PHOSPHOENOLPYRUVATE CARBOXYLASE1* (*PEPC*), and *OXO-GLUTARATE/MALATE TRANSPORTER1* (*OXMT1*) (Fig. 6). Both BS clusters from both datasets express *RuBisCO small subunit 1* and *2* (*RBCS1 and RBCS2*), *PHOSPHOENOLPYRUVATE CARBOXYKINASE1* (*PCK1*), and *NADP-MALATE DEHYDROGENASE* (*ME1*). *SWEET13a*, *SWEET13b*, and *SWEET13c* are enriched in the abaxial BS cells in datasets from both replicates.

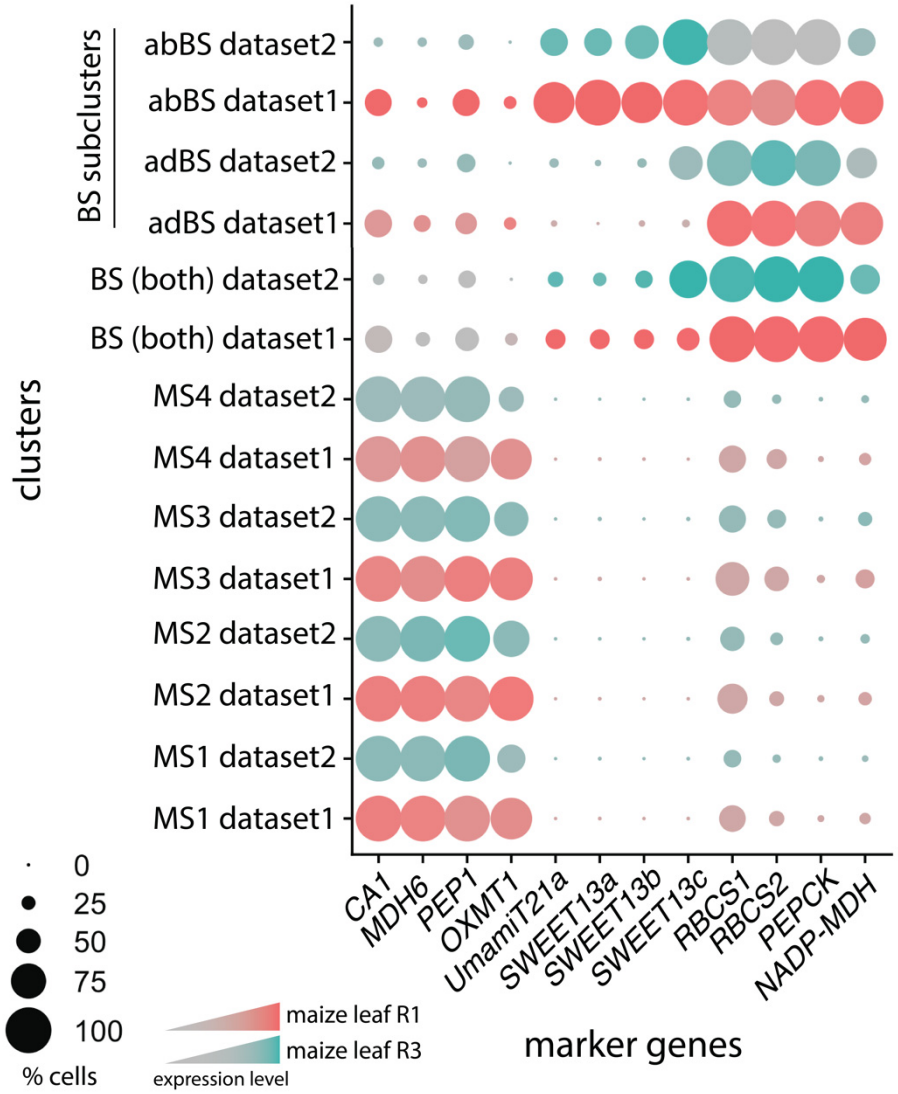

Figure 6. Marker gene expression in the first replicate (salmon) and the second replicate (turquoise) with normalized UMI count indicated by color intensity. The percentage of cells expressing the gene in a given cluster indicated by dot size examples of sizes from the continuous scale are shown on the lower left. C4 marker genes and abaxial vs adaxial bundle sheath marker genes were selected: *CA1*, *MDH6*, *PEP1*, and *OXMT1* are all highly expressed in all four MS clusters, which *rbcs1*, *rbcs2*, *PEPCK*, and *NADP-MDH* are all highly expressed in both BS clusters, while *SWEET13a*, *b*, and *c* are unique to the abaxial BS cluster.

In summary, though maize leaf R3 showed a pattern of gene expression that was largely consistent with maize leaf R1, it did not, on its own, provide strong evidence for the hypothesis that the abaxial bundle sheath cells are specialized for transport: maize leaf R3 had only 20 BS cells, while maize leaf R1 had 53, and there was insufficient statistical power to resolve the bundle sheath cells into two subclusters in maize leaf R3. However, there were important similarities between the replicates: *SWEET13a, b,* and *c* were expressed in a subset of BS cells in both replicates, and *RBCS* and other BS-specific C4 genes were highly expressed in all BS cells. Putative abaxial BS cells from R3 can be subclustered along with the abaxial BS cells from R1 in the integrated dataset, indicating that these cells can be divided into mathematically defined clusters when a larger number of cells display the abaxial BS transcriptional profile. Therefore, the *SWEET*-mRNA containing BS cells in R3 are likely ^{ab}BS cells, despite the fact that they cannot be defined as such based on the information in R3 alone.

IMPAIRED PHLOEM LOADING IN ZMSWEET13A,B,C, SUCROSE TRANSPORTER TRIPLE KNOCK-OUT MUTANTS IN ZEA MAYS

Bezrutczyk, M., Hartwig, T., Horschman, M., Char, S.N., Yang, J., Yang, B., Frommer, W.B. and Sosso, D.

Research

New Phytologist

Impaired phloem loading in *zmsweet13a,b,c* sucrose transporter triple knock-out mutants in *Zea mays*

Margaret Bezrutczyk[1,2,3], Thomas Hartwig[1,2,3], Marc Horschman[3], Si Nian Char[4], Jinliang Yang[5], Bing Yang[4], Wolf B. Frommer[1,2,3] and Davide Sosso[3]

[1]Institute for Molecular Physiology, Heinrich Heine University Düsseldorf, Düsseldorf 40225, Germany; [2]Max Planck Institute for Plant Breeding Research, Cologne 50829, Germany; [3]Department of Plant Biology, Carnegie Science, 260 Panama St, Stanford, CA 94305, USA; [4]Department of Genetics, Development, and Cell Biology, Iowa State University, Ames, IA 50011, USA; [5]Department of Agronomy and Horticulture, University of Nebraska-Lincoln, Lincoln, NE 68588, USA

Author for correspondence:
Wolf B. Frommer
Tel: +49 2118114826
Email: frommew@hhu.de

Received: *3 October 2017*
Accepted: *28 December 2017*

New Phytologist (2018) **218:** 594–603
doi: 10.1111/nph.15021

Key words: corn, efflux, export, leaf, maize (*Zea mays*), phloem loading, sucrose, transport.

Summary

- Crop yield depends on efficient allocation of sucrose from leaves to seeds. In Arabidopsis, phloem loading is mediated by a combination of SWEET sucrose effluxers and subsequent uptake by SUT1/SUC2 sucrose/H^+ symporters. ZmSUT1 is essential for carbon allocation in maize, but the relative contribution to apoplasmic phloem loading and retrieval of sucrose leaking from the translocation path is not known.
- Here we analysed the contribution of SWEETs to phloem loading in maize.
- We identified three leaf-expressed SWEET sucrose transporters as key components of apoplasmic phloem loading in *Zea mays* L. ZmSWEET13 paralogues (a, b, c) are among the most highly expressed genes in the leaf vasculature. Genome-edited triple knock-out mutants were severely stunted. Photosynthesis of mutants was impaired and leaves accumulated high levels of soluble sugars and starch. RNA-seq revealed profound transcriptional deregulation of genes associated with photosynthesis and carbohydrate metabolism. Genome-wide association study (GWAS) analyses may indicate that variability in ZmSWEET13s correlates with agronomical traits, especifically flowering time and leaf angle.
- This work provides support for cooperation of three ZmSWEET13s with ZmSUT1 in phloem loading in *Z. mays*.

Introduction

Crop yield is critical for human nutrition, yet the underlying machinery that ultimately determines yield potential is still not understood. Crop productivity under ideal conditions is determined by the efficiency with which plants intercept light, convert it into chemical energy, translocate photosynthates and convert these to storage products in harvestable organs (Zhu *et al.*, 2010). In many crops, sucrose is the primary form for translocation inside the conduit (i.e. the phloem). A combination of SWEET-mediated efflux from phloem parenchyma and subsequent secondary active sucrose import by SUT sucrose/H^+ symporters is thought to create the driving force for pressure gradient-driven phloem transport and retrieval of sucrose leaking along the translocation path (Chen *et al.*, 2015a).

Sucrose is thought to follow one of three routes during phloem loading: (1) apoplasmic loading via plasma membrane transporters, (2) symplasmic loading via diffusion through plasmodesmata or (3) polymer trapping via enzymatic addition of galactose, which is thought to impair back-diffusion through plasmodesmata (Turgeon & Wolf, 2009; Chen *et al.*, 2015a). Some mechanisms may coexist, as suggested by anatomical studies which have found thin- and thick-walled sieve tubes in monocots, cell types that may differ regarding the primary loading mechanism (Botha, 2013).

In Arabidopsis, a SWEET/SUT-mediated apoplasmic mechanism appears to be important for phloem loading (Chen *et al.*, 2012, 2015a). SWEETs are a class of transporters with seven transmembrane helices that function as hexose or sucrose uniporters (Xuan *et al.*, 2013). Multiple SemiSWEETs and SWEETs have been crystallized, and AtSWEET13 has been proposed to function in complexes via a 'revolving door' mechanism to accelerate transport efficacy (Feng & Frommer, 2015; Han *et al.*, 2017; Latorraca *et al.*, 2017). In Arabidopsis, SWEET roles include phloem loading, nectar secretion, pollen nutrition and seed filling (Chen *et al.*, 2012; Sun *et al.*, 2013; Lin *et al.*, 2014; Sosso *et al.*, 2015). In rice, cassava and cotton, SWEETs act as susceptibility factors for pathogen infections (Chen *et al.*, 2010; Cohn *et al.*, 2014; Cox *et al.*, 2017). AtSWEET11 and 12 are probably responsible for effluxing sucrose from the phloem parenchyma into the apoplasm (Chen *et al.*, 2012). Sucrose is subsequently loaded against a concentration gradient into the sieve element companion cell complex (SECC) via the SUT1 sucrose/H^+ symporter (a.k.a. AtSUC2), powered by the proton gradient created by co-localized H^+/ATPases (Riesmeier *et al.*, 1994; Gottwald *et al.*, 2000; Slewinski *et al.*, 2009; Srivastava *et al.*, 2009). Although the fundamental

involvement of SUT transporters in phloem loading has been demonstrated using RNA interference (RNAi) and knock-out mutants in Arabidopsis (also in potato, tobacco, tomato and maize) (Riesmeier *et al.*, 1994; Bürkle *et al.*, 1998; Srivastava *et al.*, 2009; Chen *et al.*, 2015a), *atsweet11,12* and *atsuc2 (sut1)* mutants were able to produce viable seeds and only showed a slight reduction in plant growth (Chen *et al.*, 2012).

In monocots, including all cereal crops, the situation is less clear. In maize, the phloem-expressed ZmSUT1 (Baker *et al.*, 2016) (phylogenetically in the SUT2 clade) appears to be critically important for phloem translocation (Slewinski *et al.*, 2009), whereas rice *ossut1* mutants and RNAi lines had no apparent growth or yield defects (Ishimaru *et al.*, 2001; Scofield *et al.*, 2002; Eom *et al.*, 2012). As a result, there is an ongoing debate regarding the mechanisms behind phloem loading in cereals (Braun *et al.*, 2014; Regmi *et al.*, 2016).

Here we identified a set of three close paralogs of SWEET13 from *Zea mays* L. as essential transporters for efflux of sucrose into the apoplasm before phloem loading.

Materials and Methods

Plant material and growth conditions

zmsweet13a, *zmsweet13b* and *zmsweet13c* alleles were obtained with a CRISPR-Cas9 construct targeting a sequence (5′-GCATCTACAAGAGCAAGTCGACGG-3′, the underlined CGG for PAM) conserved in all three paralogs in the 3rd exon using a CRISPR system and associated method as described (Char *et al.*, 2017). Briefly, a pair of 24-nt oligonucleotides matching to the target site were synthesized and annealed into a double-stranded DNA fragment. The DNA fragment was subcloned into an intermediate vector pgRNA1 and the resulting guide RNA expression cassette was mobilized into the Cas9 expressing binary vector pGW-Cas9 through the Gateway recombination reaction using the recombinase, resulting in pCas9-gRNA_SWEET13. The CRISPR construct was transformed into the *Agrobacterium tumefaciens* strain EHA101 for plant transformation. Maize transformation was performed at the Iowa State University Plant Transformation Facility. Hi-II calli were derived from the F_1 immature embryos of Hi-IIA and Hi-IIB plants, which are independent lines of a B73xA188 cross. Calli were transformed with *A. tumefaciens* containing plasmids for expressing guide RNAs and the Cas9 construct. T0 plantlets grown on sterile media from successfully transformed calli were transplanted to soil when 1 inch in height. T0 plants were selfed or outcrossed to B73, and plants which did not contain the CRISPR construct were selected by performing PCR using three different primer pairs targeting Cas9 (Supporting Information Table S1). T1, T2 and T3 plants homozygous for all three mutated genes (*zmsweet13abc*) were selected along with wild-type siblings. Height was assessed by weekly measurement from the soil surface to the top of the highest fully developed leaf. Wild-type 'siblings' were descendants of the Hi-II plants transformed and outcrossed once to B73, which in the T1 generation did not carry the CRISPR-Cas9 construct or any detectable mutations. Triple mutant plants either descended from selfed T0 Hi-II plants or outcrossed once to B73. The mutant phenotype was unaffected by the difference in genetic background. Mutants and wild-type plants were grown side by side, in glasshouses under long-day conditions (16 h : 8 h, day : night, 28–30°C), and in 2016 in a summer field at Carnegie Science (Stanford, CA, USA).

Genotyping of maize plants

Genomic DNA was extracted from leaves using a Qiagen Biosprint 96 device. PCR was performed with the Terra PCR Direct Red Dye Premix Protocol (Clontech Laboratories, Palo Alto, CA, USA) with melting temperatures of 60, 64 and 62.5°C for *ZmSWEET13a*, *b* and *c,* respectively (for primers see Table S1). Amplicons of relevant regions of the CRISPR-Cas9 targeted *ZmSWEET13* alleles were sequenced by Sequetech (Mountain View, CA, USA). Chromatograms were analysed using 4Peaks (www.nucleobytes.com/4peaks/).

Plastic embedding and sectioning

Flag leaves collected at 07:00 h were placed in 0.1 M cacodylate-buffered fixative with 2% paraformaldehyde and 2% glutaraldehyde, vacuum infiltrated for 15 min and incubated overnight. Sample dehydration was performed by a graded ethanol series (10, 30, 50, 70 and 95%). Sample embedding was performed according to the LR White embedding kit protocol (Electron Microscopy Science, Hatfield, PA, USA). Cross-sections (1.5 μm) were obtained on an Ultracut (Reichert, Depew, NY, USA), stained for 30 s with 0.1% toluidine blue and washed with double distilled H_2O (2×), followed by 5 min of starch staining with saturated Lugol's solution. Sections were mounted with CytoSeal 60 (Electron Microscopy Science).

Phylogenetic analyses

The evolutionary history was inferred by using maximum likelihood with a JTT matrix-based model. The tree with the highest log likelihood (−3000.1) is shown. The percentage of trees in which associated taxa clustered together is shown next to the branches. Initial tree(s) for the heuristic search were obtained by neighbour-joining to a matrix of pairwise distances with the JTT model used for estimation. The analysis involved 16 polypeptide sequences, derived from PHYTOZOME (https://phytozome.jgi.doe.gov) and GRAMENE (http://www.gramene.org/) using *ZmSWEET13a* as a template in a search for similar sequences in the genomes of *Z. mays*, *Sorghum bicolor*, *Setaria italica*, *Hordeum vulgare*, *Triticum urartu* (progenitor of A-genome of bread wheat *Triticum aestivum*), *Brachypodium distachyon* and *Oryza sativa.* A minimum of 95% site coverage was required so that no more than 5% alignment gaps, missing data and ambiguous bases were allowed at any position. There were a total of 252 positions in the final dataset. Evolutionary analyses were conducted in MEGA6.

Soluble sugar analyses

Flag leaves were harvested from mature plants at 07:00 h. In total, 70 mg of liquid nitrogen-ground tissue was incubated for

1 h with 1 ml of 80% ethanol on ice with frequent mixing. Samples were centrifuged for 5 min at 4°C at 13 000 ***g***, and supernatant was removed. This step was repeated once. The liquid supernatant was subsequently dried in a vacuum concentrator and re-suspended in water. Sucrose, glucose and fructose were measured using NADPH-coupled enzymatic methods using an M1000 plate reader (Tecan, Männedorf, Switzerland), with measured values normalized to fresh weight. Starch quantification was performed as previously described (Sosso *et al.*, 2015).

Starch staining

Flag leaves collected at 07:00 h were boiled in 95% ethanol for *c.* 30 min (until chlorophyll pigments disappeared). Cleared leaves were submerged in saturated Lugol's iodine solution for 15 min, rinsed twice with H_2O and imaged with a Lumix GF1 camera (Panasonci, Kadoma, Osaka, Japan). The IKI solution used for starch staining was made by adding 1 g of iodine and 1 g of potassium iodide to 100 ml H_2O.

qRT-PCR RNA isolation and transcript analyses

RNA was extracted using the Trizol method (Invitrogen). First-strand cDNA was synthesized using a Quantitect reverse transcription kit (Qiagen). Quantitative reverse transcriptase PCR (qRT-PCR) to determine expression level was performed using a LightCycler 480 (Roche), and the $2^{-\Delta Ct}$ method for relative quantification. Wild-type maize and *zmsweet13abc* flag leaves were sampled at 17:00 h. Primers in the last exon and the 3′ untranslated region of *ZmSWEET13a, b* and *c* (Table S1) were used for qRT-PCR to determine gene expression levels. Internal references were *Zm18s* and *ZmLUG*.

FRET sucrose sensor analysis in HEK293T cells

ZmSWEET13a, b and *c* coding sequences were cloned into the Gateway entry vector pDONR221f1, followed by LR (*att*L, *att*R) recombination into pcDNA3.2V5 for expression in HEK293T cells. HEK293T cells were co-transfected with *ZmSWEET13a, b* or *c* in *pcDNA3.2V5* and the sucrose sensor FLIPsuc90μΔ1V (Chen *et al.*, 2012) using Lipofectamine 2000 (Invitrogen). For fluorescence resonance energy transfer (FRET) imaging, Hank's balanced salt solution medium was used to perfuse HEK293T/FLIPsuc90μΔ1V cells with defined pulses containing 20 mM sucrose in buffer. Image acquisition and analysis were performed as previously described (Chen *et al.*, 2012). AtSWEET12 was used as a positive control. Negative controls were empty vector transfectants.

Transient gene expression in *Nicotiana benthamiana* leaves

The *A. tumefaciens* strain GV3101 was transformed with the binary expression clone (pAB117) carrying *ZmSWEET13a, b* or *c* C-terminally fused with enhanced green fluorescent protein (eGFP) and driven by the CaMV 35S promoter. *Agrobacterium* culture and tobacco leaf infiltration were performed as described (Sosso *et al.*, 2015). Chloroplast autofluorescence was detected on a Leica TCS SP8 confocal microscope with 488 nm excitation (eGFP) and 561 nm excitation (chlorophyll). Emission was detected at 522–572 nm (eGFP fluorescence) and 667–773 nm (chloroplast fluorescence). Epidermal leaf chloroplast fluorescence (Dupree *et al.*, 1991) allowed us to determine eGFP vacuolar localization (lining chloroplasts on the vacuolar side) and plasma membrane localization was deduced (peripheral to chloroplasts; according to bright-field image). Image analysis was performed using Fiji software (https://fiji.sc/).

Analyses of photosynthetic rates

Licor LI-6800 measurements were taken at mid-day under glasshouse conditions (28°C, photosynthetically active radiation (PAR) 1000 μE m^{-2} s^{-1}, 60% relative humidity). Two-centimetre-diameter discs of leaves were clamped in the Licor measurement chamber and relative concentrations of CO_2 inside and outside of the chamber were measured. CO_2 absorbed (μmol m^{-2} s^{-1}) by leaf segments in the chamber was used as a proxy for photosynthetic rate. Measurements were made at the tips of leaf 7 to leaf 10 at midday.

Candidate gene association study

To test whether sequences at *SWEET* loci are associated with phenotypic variations in the maize population, we analyzed a maize diversity panel composed of 282 inbred lines (HapMap3 SNP data (Bukowski *et al.*, 2017) for the panel from the Panzea database (www.panzea.org)). We filtered single nucleotide polymorphism (SNP) data (minor allele frequency (MAF) > 0.1; missing rate < 0.5) using Plink (Purcell *et al.*, 2007) and calculated a kinship matrix with Gemma (Zhou & Stephens, 2012) using the filtered SNP set. A genome-wide association study (GWAS) was performed by fitting a mixed linear model using Gemma, where the kinship matrix was fitted as random effects in the model. A false discovery rate (FDR) approach (Benjamini & Hochberg, 1995) was used to control the multiple test problem with a cut off of 0.05. Linkage disequilibrium of SNPs in our candidate genes with significant association SNPs was calculated using Plink (Purcell *et al.*, 2007).

RNA-seq and data analysis

zmsweet13abc triple mutants and wild-type siblings were grown in soil under glasshouse conditions. Total RNA was isolated from flag leaf tissues using acidic phenol extraction as described previously (Eggermont *et al.*, 1996). Purification of poly-adenylated mRNA using oligo(dT) beads, construction of barcoded libraries and sequencing using Illumina HiSeq technology (150 bp paired-end reads) were performed by Novogene (https://en.novogene.com/) using the manufacturer's recommendations. Trimmed and quality control-filtered sequence reads were mapped to the B73 AGPv3 genome using Star (v.2.54) (Dobin *et al.*, 2013) in two pass mode (parameters: –outFilterScoreMinOverLread 0.3, –outFilterMatchNminOverLread 0.3, –outSAMstrandField intronMotif, –outFilterType BySJout, –outFilterIntronMotifs RemoveNoncanonical, –quantMode TranscriptomeSAM GeneCounts). To obtain

uniquely mapping reads, these were filtered by mapping quality (q20), and PCR duplicates were removed using SAMTOOLS (v.1.3.1). Gene expression was analysed in R (v.3.4.1) using DESeq2 software (v.1.16.1) (Love *et al.*, 2014). Genes were defined as differentially expressed by a two-fold expression difference with a *P*-value, adjusted for multiple testing, of < 0.05 (Fig. S7; Table S2). RNA-seq data are available in the NCBI Gene Expression Omnibus database.

Results

To test whether SWEETs are involved in phloem loading in maize, we evaluated the role of leaf-expressed maize *SWEETs* in carbon allocation. We identified three *SWEET13* paralogs (GRMZM2G173669: *ZmSWEET13a*, GRMZM2G021706: *ZmSWEET13b*, GRMZM2G179349: *ZmSWEET13c*) as the most highly expressed SWEETs in maize leaves based on published expression values in four publicly available datasets (Denton *et al.*, 2017) (Fig. S1). *ZmSWEET13a* and *b* are located in tandem on chromosome 10 in a region syntenic with the *OsSWEET13* locus in rice, while *ZmSWEET13c* is on chromosome 3 (Fig. S2). Interestingly, maize is one of the few cereals having three *SWEET13* paralogs, along with *Sorghum bicolor* and *Triticum urartu* (Figs 1a, S3). Similar to ZmSUT1, *ZmSWEET13a, b* and *c* mRNA preferentially accumulated in bundle sheath/vein preparations rather than mesophyll (Fig. 2a). If the SWEETs were involved in phloem loading, one would expect that their mRNA levels would be highest in leaf domains that serve as sucrose sources, as compared to sink tissues. Consistent with a role in phloem loading, mRNA levels of all three *SWEET13*s (as well as *SUT1*) were highest in leaf tips (Fig. 2b). Analysis of independent RNA-seq experiments that had differentiated source and sink regions of maize leaves on the basis of radiotracer experiments also found *ZmSWEET13* transcripts to be ~ five-fold higher in source vs sink domains (Fig. S4) (Wang *et al.*, 2014). We tested the transport activity of the three SWEETs in human HEK293T cells coexpressing a genetically encoded sensor (Chen *et al.*, 2010, 2012). All three SWEETs mediated sucrose transport (Fig. 1b). To test whether these SWEETs were part of (1) intercellular translocation or (2) intracellular sugar sequestration similar to Arabidopsis SWEET2, 16 or 17 (Chardon *et al.*, 2013; Klemens *et al.*, 2013; Guo *et al.*, 2014; Chen *et al.*, 2015b), we tested their subcellular localization in transiently transformed tobacco cells, and found that they localized preferentially to the plasma membrane (Fig. 1c).

Recently, *ZmSWEET13* had been implicated as a possible key player in C_4-photosynthesis in grasses (Emms *et al.*, 2016). To test their role in maize, we designed guide RNAs that target a conserved region within a transmembrane domain, assuming that defects in the membrane domain would lead to complete loss of function. We generated single *knock-out* mutants, as well as

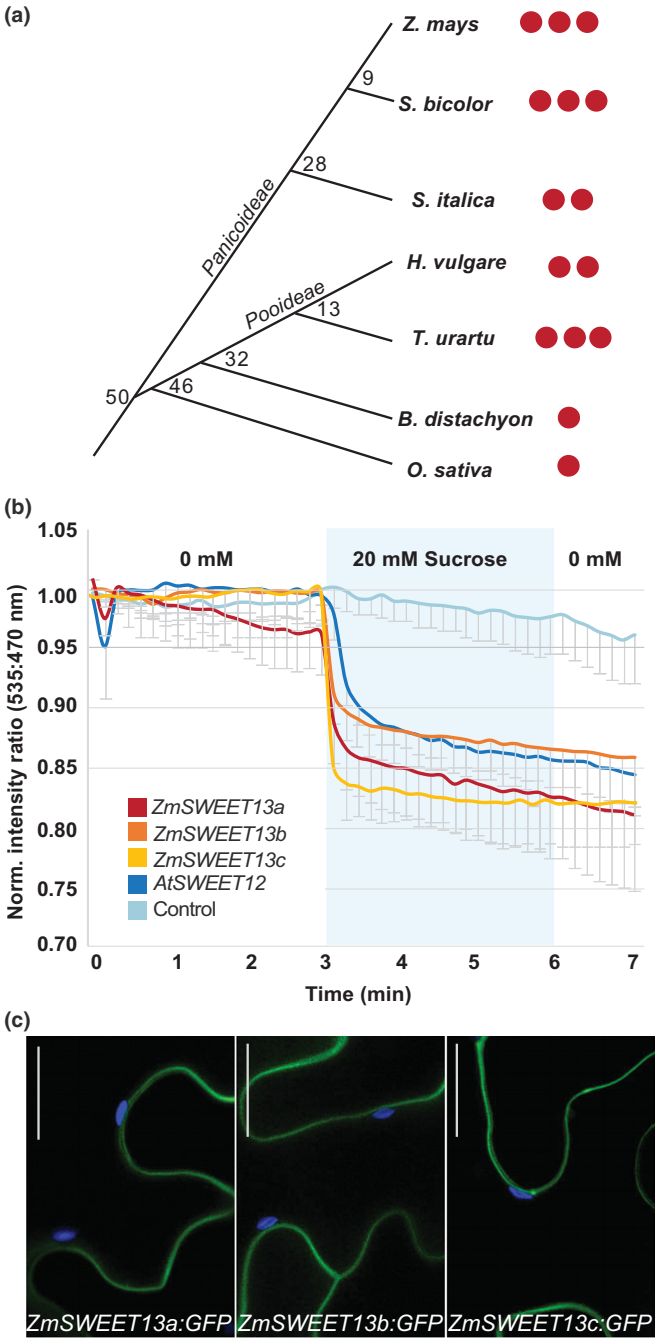

Fig. 1 Phylogeny, functional analysis and subcellular localization of SWEET13a,b,c. (a) Phylogenetic relationship between putative orthologs in the following grasses: *Zea mays* L., *Sorghum bicolor*, *Setaria italica*, *Hordeum vulgare, Triticum urartu* (progenitor of A-genome of bread wheat *Triticum aestivum*), *Brachypodium distachyon* and *Oryza sativa*. Chronogram branch divergence time-points are in million years (Emms *et al.*, 2016). Red dots represent the number of *SWEET13* paralogs for each species. (b) Sucrose transport activity by ZmSWEET13a, b and c in HEK293T cells coexpressing FLIPsuc90μΔ1V (fluorescent sucrose sensor). Cells were transfected to express sensors only as negative control, or to co-express *AtSWEET12* as a positive control. HEK293T cells were perfused with buffer, then subjected to a 3-min pulse of 20 mM sucrose (mean ± SEM, repeated independently four times with comparable results). (c) Confocal images (maximum projection of Z-stack) of *Agrobacterium*-infiltrated *Nicotiana benthamiana* epidermal leaf cells transiently expressing ZmSWEET13a-eGFP, ZmSWEET13b-eGFP or ZmSWEET13c-eGFP fusions. The eGFP emission (green, 522–572 nm) was merged with chloroplast fluorescence (blue, 667–773 nm). ZmSWEET13x-eGFP derived fluorescence between chloroplasts and the cell periphery indicates localization to the plasma membrane. Bars, 50 μm.

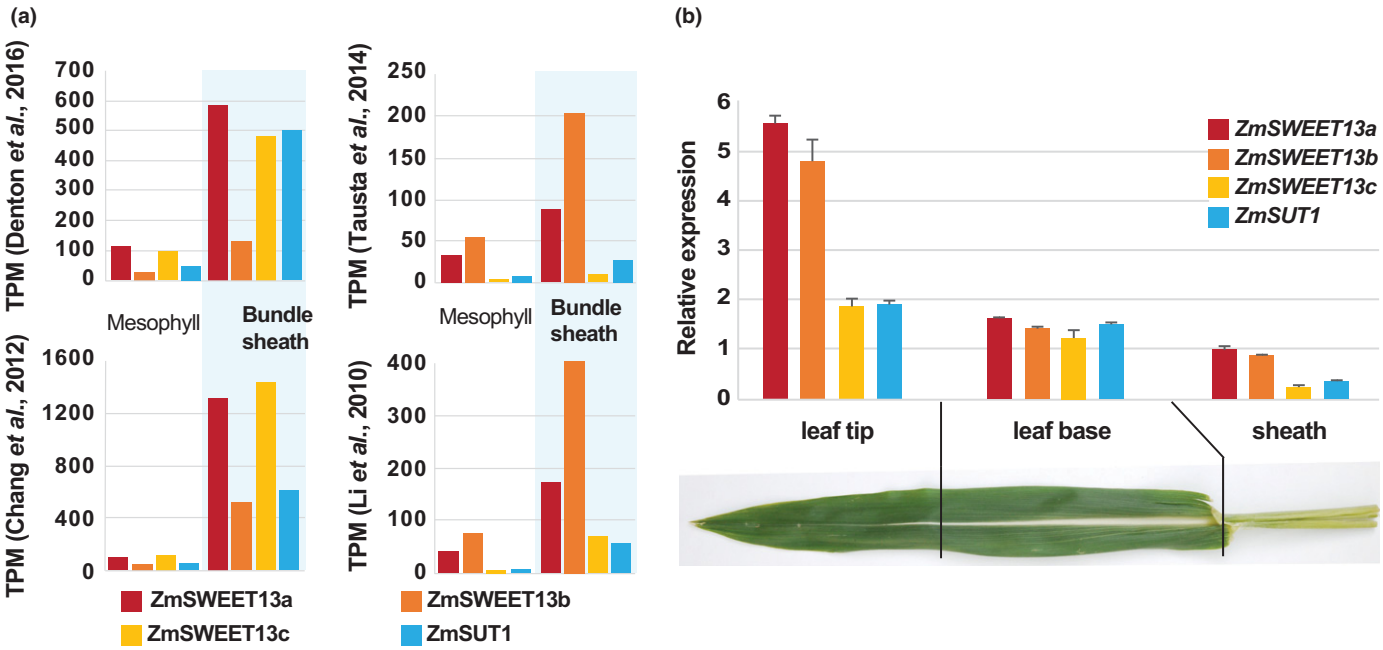

Fig. 2 *ZmSWEET13*s and *ZmSUT1* mRNA levels in flag leaves of *Zea mays* L. (a) *ZmSWEET13*a,b,c and *ZmSUT1* mRNAs accumulate preferentially in the bundle sheath and vein preparations, relative to mesophyll in four independent datasets (Li *et al.*, 2010; Chang *et al.*, 2012; Tausta *et al.*, 2014; Denton *et al.*, 2017) (TPM, transcripts per million; see also Supporting Information Fig. S1). (b) Relative mRNA levels (by qRT-PCR) of *ZmSWEET13a, b, c* and *ZmSUT1* in maize flag leaves. All four genes had highest mRNA levels in leaf tips (mean ± SEM, $n = 3$ technical replicates with expression normalized to *Zm18S* transcript levels, repeated independently four times with comparable results, see Fig. S13e, f).

combinations of mutant alleles, using CRISPR-Cas9 (Fig. 3). We recovered two mutant alleles of *ZmSWEET13a*, four of *ZmSWEET13b* and three of *ZmSWEET13c*. The majority of mutations were caused by single nucleotide insertions in the target sequence. All mutations created premature stop codons leading to truncated polypeptides at amino acid 129 in the fourth of seven transmembrane domains (Fig. 3). T2 lines carrying homozygous mutations in all three genes were characterized by severe growth defects (Fig. 4a). The growth phenotype was analyzed in subsequent generations in the glasshouse and in a single field season. Single and double mutants showed slight growth defects, while triple mutants had substantial defects: plants were severely stunted with shorter, narrower leaves (Fig. 4a–c). Leaves were chlorotic, and accumulated ~5× more starch and ~4× more soluble sugars compared to the wild-type (Fig. 5a–c), consistent with symptoms expected for impaired phloem loading. Accumulation of starch occurred primarily in mesophyll and bundle sheath cells (Fig. 5d, e). As observed in plants with impaired phloem loading, photosynthesis was also strongly impacted in glasshouse-grown *zmsweet13a,b,c* mutants (Fig. S5). In the field, triple mutants from five independent allelic combinations presented even more severe phenotypes, with extreme chlorosis, massive anthocyanin accumulation and extremely stunted growth; in several cases this resulted in lethality (Fig. 4e). *SWEET13* mRNA levels were drastically reduced in all three *ZmSWEET13s*, as quantified by RNA-seq and qRT-PCR (Figs 4d, S6). In summary, the strong phenotype of the triple mutants is consistent with maize using predominantly an apoplasmic phloem loading mechanism.

Despite the severe defects, triple mutant plants grown in the glasshouse (as well as a subset in the field) exported sufficient sugars from leaves to produce viable seeds. A possible explanation for the viability of the triple mutants could be compensation by other sucrose-transporting clade III SWEETs. To test this hypothesis and to obtain insights about possible physiological changes in the mutants, we performed an RNA-seq analysis of flag leaves of wild-type (Hi-II transformants outcrossed once to B73 and selfed that neither contain SWEET13 mutations nor contain Cas9 as verified by PCR) and triple mutant plants (Hi-II background) (Fig. S7). Notably, we did not observe significant enrichment of mRNA of any of the clade III *SWEETs*, arguing against transcriptional compensation by other clade III *SWEETs* (Fig. S6). Our data do not exclude the possibility that compensation occurs at the post-transcriptional level. We performed a pathway enrichment analysis using the Plant MetGenMap database (Joung *et al.*, 2009) and found that mRNA levels of multiple genes encoding functions in the light-harvesting complex and in chlorophyll/tetrapyrrole biosynthesis were substantially reduced in triple mutants, consistent with impaired photosynthesis and chlorosis (Figs S8, S9). Furthermore, in line with the accumulation of starch and soluble sugars in leaves, transcripts related to carbohydrate synthesis and degradation, in particular starch biosynthesis and sucrose degradation, were affected in the triple mutants (Fig. S10; Table S3).

A recent study has found that the Arabidopsis homolog AtSWEET13 (although phylogenetically not the closest homolog of ZmSWEET13) can also transport gibberellin (Kanno *et al.*, 2016). The observed phenotypes of the triple *zmsweet13 knock out* mutants in maize are consistent with a primary role in sucrose transport and distinct from those observed in the Arabidopsis

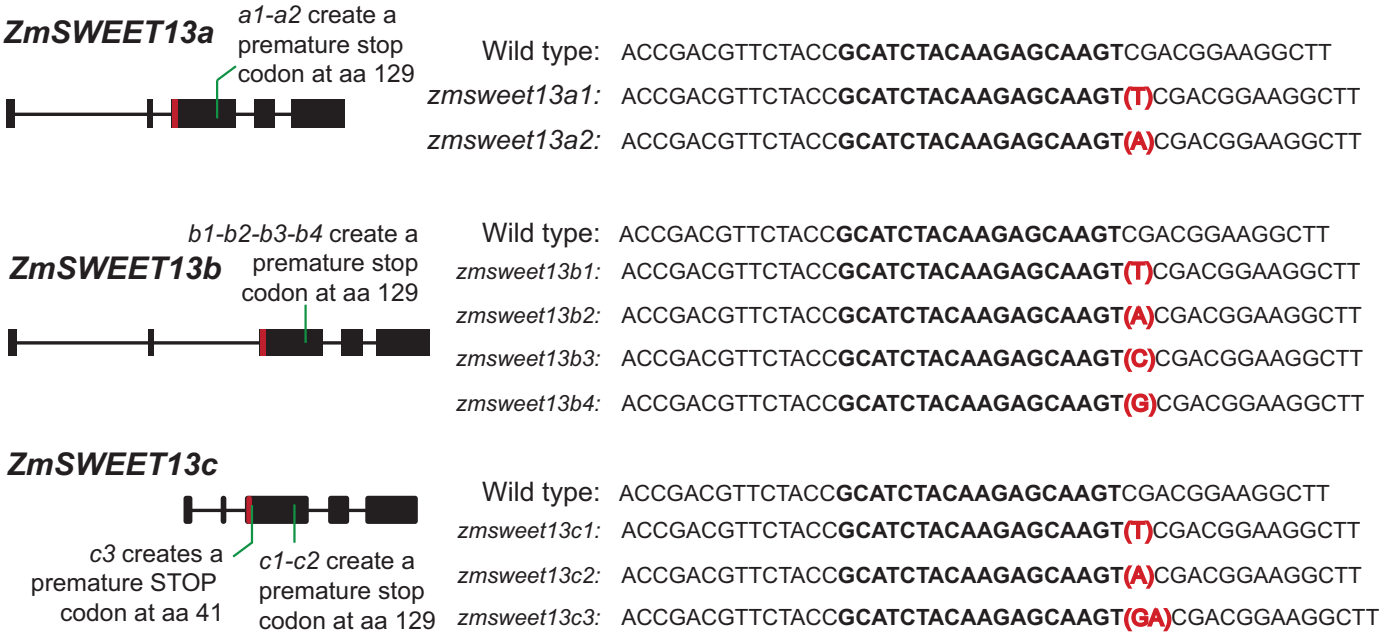

Fig. 3 CRISPR-Cas9-induced *ZmSWEET13a, b* and *c* mutations in *Zea mays* L. Schematic representation of *ZmSWEET13a*, *b* and *c* gene models, with exons displayed as black boxes. Schematics of the target site within the third exon (red) and sequences of the insertions obtained by genomic editing by CRISPR-Cas9, as determined in T3 homozygous lines, with guide RNAs marked in bold. The nine alleles carry frameshift mutations with insertions of either 1 or 2 nt, resulting in premature stop codons, as indicated within the gene model by a green line.

sweet13;14 double mutant, namely male sterility, and increased seedling and seed size (Kanno *et al.*, 2016).

To determine if variation in the *ZmSWEET13* genes may account for differences in agronomically important traits in existing maize lines, we conducted a GWAS using phenotypic traits obtained from a maize diversity panel (Flint-Garcia *et al.*, 2005). We obtained genotypic data from maize HapMap3 SNPs (Bukowski *et al.*, 2017) and filtered out SNPs with a minor allele frequency < 0.1 and missing rate > 0.5, leaving ~13 million SNPs for analyses. We performed GWAS using a mixed linear model approach (Zhou & Stephens, 2012), where kinship calculated from the genome-wide SNPs was fitted as the random effects. The SNPs that passed the FDR threshold of 0.05 and showed linkage disequilibrium ($R^2 > 0.8$) with *ZmSWEET13a,b,c* genes were considered significant associations. SNPs in *ZmSWEET13s* were significantly associated with ear-related traits (i.e. ear rank number and ear height) and developmental traits (i.e. days to silk, days to tassel, middle leaf angle and germination count) (Figs S11, S12). While these results are compatible with a key role of *ZmSWEET13s* in carbon allocation, it will be necessary to determine whether polymorphisms in these genes or flanking regions are causative for these traits.

Discussion

The phloem sap of many monocots and dicots contains high sucrose concentrations. The high sucrose contents in the loading zone are thought to create a pressure gradient that drives phloem translocation. Inhibition of the expression of the SUT1 sucrose/H^+ symporter by RNAi or T-DNA insertion typically leads to stunted growth and accumulation of carbohydrates in leaves (Riesmeier *et al.*, 1994; Bürkle *et al.*, 1998; Gottwald *et al.*, 2000; Slewinski *et al.*, 2009; Srivastava *et al.*, 2009). Chlorosis and inhibition of photosynthesis, which often accompany defects in phloem translocation, may either be due to feedback inhibition of photosynthesis or be a consequence of nutrient deficiencies caused by the reduced supply of carbohydrates to the root system (Ainsworth & Bush, 2011). SUTs function as sucrose/H^+ symporters and, at least in maize, appear to fulfil two roles: (1) loading of the SECC with sucrose in source leaves, and (2) retrieval of sucrose that diffuses out of the SECC, as a consequence of the high sucrose concentration in the SECC, relative to surrounding tissues. SUTs import sucrose from the cell wall space, implying the existence of transporters that efflux sucrose into the cell wall space preceding uptake by SUTs. AtSWEET11 and 12 are candidates for such an efflux role in Arabidopsis: they appear to function as uniporters and can thus serve as cellular efflux systems when sucrose gradients are suitable. Both SWEETs were highly expressed in leaves, localized most likely to the phloem parenchyma, and *atsweet11;12* mutants were smaller and accumulated starch in leaves (Chen *et al.*, 2012). However, the phenotype of *atsweet11;12* mutants was relatively weak, implying leaky mutations, compensation by other transporters or the coexistence of other phloem loading mechanisms. Other mechanisms could include symplasmic transport, or yet unknown processes.

Here, we show that maize has three closely related clade III SWEETs (named SWEET13a, b and c) that are encoded by some of the most highly expressed genes in the leaf. The three genes possibly derive from relatively recent gene duplication events: sorghum and wheat have three copies per genome, while

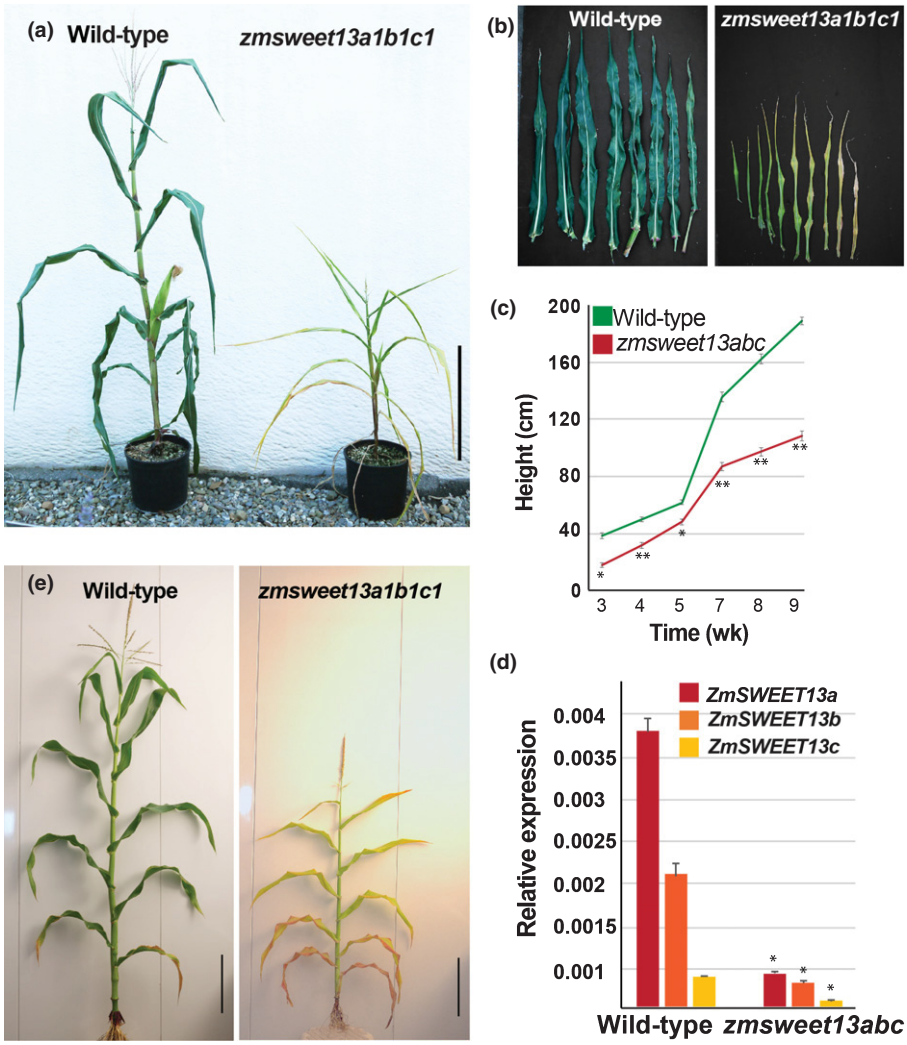

Fig. 4 Characterization *of ZmSWEET13abc* triple *Zea mays* L. mutants. (a) Mature wild-type and same-age *zmsweet13a1b1c1* triple mutant, showing reduced growth and leaf chlorosis. Bar, 50 cm. (b) Leaf phenotype of plants presented in Fig. 2(a), showing reduced length, width and chlorosis in leaves of the *zmsweet13a1b1c1* triple mutant. (c) Growth of wild-type and triple mutants in glasshouse conditions (mean ± SEM, $n = 17$ and 15, two-tailed *t*-test performed between wild-type and *zmsweet13abc*: *, $P < 0.005$; **, $P < 0.001$). (d) Relative mRNA levels (by qRT-PCR) of *ZmSWEET13* paralogs in maize flag leaves from wild-type and *zmsweet13abc*. Samples were harvested at 16:00 h (mean ± SEM, $n = 3$ technical replicates with expression normalized to 18S levels, repeated independently five times with comparable results, see Fig. S13(e, f)). Two-tailed *t*-test performed between wild-type and *zmsweet13abc* for each gene: four pools of four (16 plants) for each genotype: *, $P < .0001$. (e) Mature field-grown *zmsweet13a1b4c1* plants under field conditions (Carnegie field 2016). Mutants were stunted, showed severe chlorosis of all leaves, and anthocyanin accumulation in the oldest leaves.

Brachypodium and rice each have only one. The comparatively high number of *SWEET13s* had been attributed to specific roles in C_4 photosynthesis (Emms *et al.*, 2016), but the presence of three *SWEET13s* in *T. urartu* (Fig. 1a), the progenitor of the A-genome of bread wheat *T. aestivum*, both of which are C_3 plants, puts this interpretation into question. Evidence that maize SWEET13s cooperate in phloem loading is based on two key observations: the severe growth defect of *zmsweet13abc* mutants is similar to that of *zmsut1* mutants (Slewinski *et al.*, 2009), and a massive accumulation of free sugars and starch in leaves is also consistent with a defect in phloem translocation. These phenotypic effects are also similar to the RNAi-mediated SUT1 knockdown phenotypes in potato and tobacco (Riesmeier *et al.*, 1994; Bürkle *et al.*, 1998). The observed growth defect in maize is much more severe than that of the *atsweet11;12* mutant in Arabidopsis, and comparable to that of the *zmsut1* mutant (Slewinski *et al.*, 2009; Chen *et al.*, 2012). We thus propose that the three ZmSWEET13s and ZmSUT1 play dominant roles in phloem loading, probably in the same pathway.

Notably, the combined *zmsweet13abc* mutations were not lethal, because the plants still produced fertile viable offspring, implying compensatory or alternative mechanisms for phloem loading. While it is possible that other transporters might compensate, it is unlikely that other clade III SWEETs take over such roles, as judged by the lack of induction of other clade III SWEET genes in the mutants. Maize may thus either also have parallel symplasmic or other yet unknown loading mechanisms.

It is still not clear whether *SWEET13* triplication mainly serves to increase the amount of SWEET protein in the same cells (e.g. phloem parenchyma), or if each SWEET13 transporter mediates

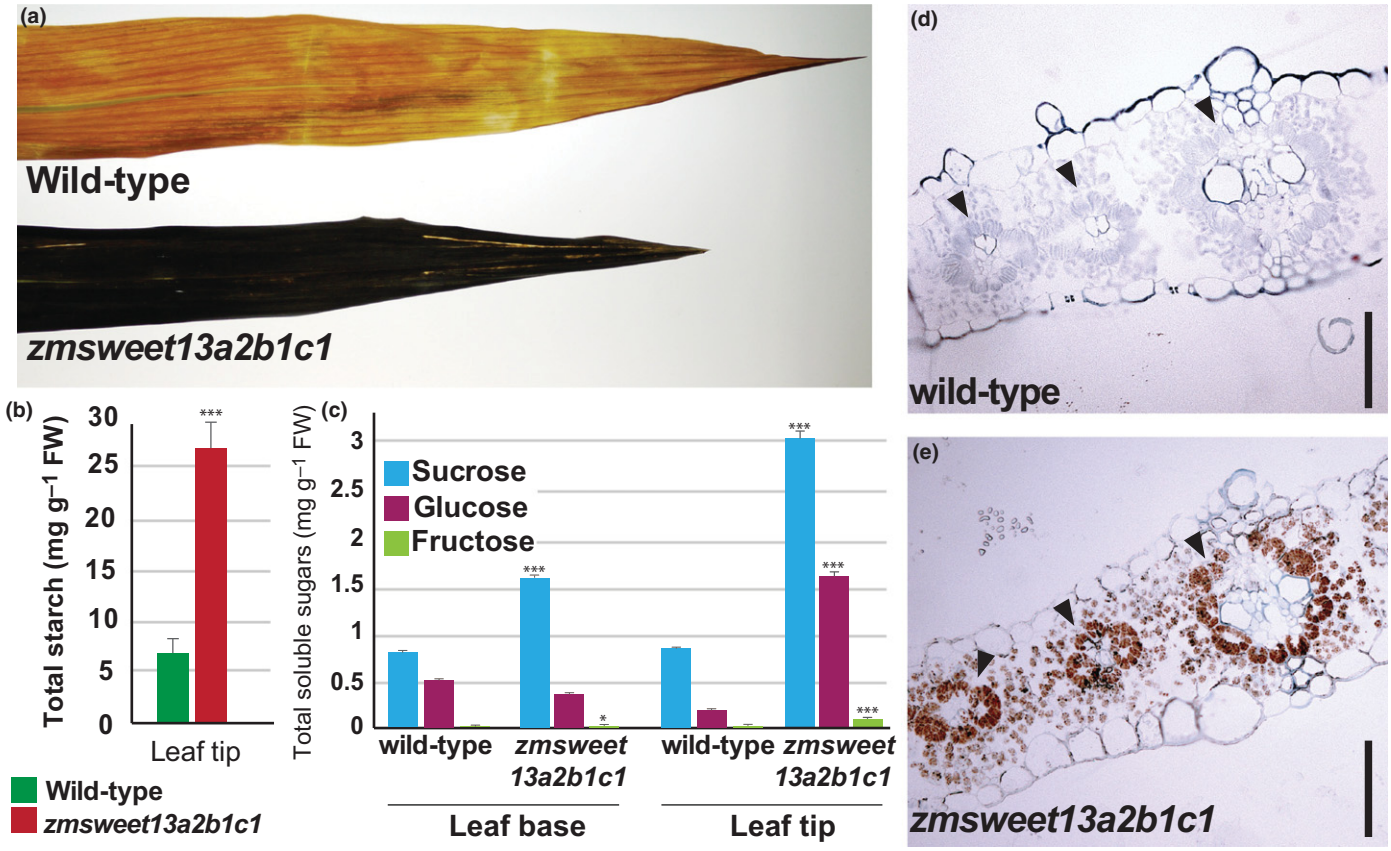

Fig. 5 Starch and soluble sugar accumulation in *zmsweet13abc Zea mays* L. triple mutants. (a) Flag leaves were collected at dawn (07:00 h), cleared with boiling ethanol and stained for 15 min with Lugol's solution. (b) Starch quantification from the same leaves as displayed in (a). The triple mutant contained ~5× more starch compared to wild-type in leaf tips. No significant differences were measured in the sheath or base (mean ± SEM, two-tailed *t*-test performed between wild-type and *zmsweet13abc*: *, $P < 0.05$; **, $P < 0.001$; ***, $P < 0.0001$; $n = 3$ technical replicates, repeated independently three times with comparable results, see Fig. S13a, b). (c) Quantification of soluble sugars in the flag leaf of *zmsweet13a2b1c1* mutants. The triple mutant contained higher sugar levels in both tip and base of the leaf. Samples were harvested at 07:00 h (mean ± SEM, two-tailed *t*-test performed between wild-type and *zmsweet13abc* for each sugar: *, $P < 0.05$; **, $P < 0.001$; ***, $P < 0.0001$; $n = 3$ technical replicates, repeated independently three times with comparable results, see Fig. S13b,c). (d, e) Starch accumulation in leaves from wild-type (d) and the triple mutant (e) harvested at the end of the night. Leaves were fixed, embedded and stained with Lugol's solution for starch. Starch grains accumulated in both mesophyll and bundle sheath cells in the *zmsweet13a2b1c1* mutant, while wild-type controls showed no detectable starch accumulation at this time point (arrowheads indicate vascular bundles). Bar, 75 mm.

efflux from a specific cell type and loading is achieved in a multi-tier manner. This question is of particular interest because *in situ* hybridization experiments identified SUT1 in companion cells, xylem and phloem parenchyma, as well as bundle sheath (Baker *et al.*, 2016). With the intent of localizing SWEET13 paralogs, we had generated translational reporter gene fusions that included the first three introns. However, neither GUS activity nor GFP fluorescence were detectable in any of the transformants carrying fusions for either of the three SWEET13s (data not shown). We therefore hypothesize that additional regulatory elements that were lacking from our chimeras must be required for proper expression.

Another interesting question is whether maize can serve as a model for phloem loading in rice, barley and wheat. Surprisingly, RNAi of the rice homolog of *ZmSUT1* did not lead to a detectable effect on the phenotype of the sporophyte (Ishimaru *et al.*, 2001). Thus, it remains a matter of debate whether rice uses predominantly apoplasmic and symplasmic or other mechanisms simultaneously (Eom *et al.*, 2012; Braun *et al.*, 2014). It will therefore be important to study the role of SWEET homologs in rice and other crops. It is noteworthy in this context that the clade III sucrose transporters OsSWEET11 and 15 are expressed preferentially in the caryopsis and act as key players in apoplasmic unloading processes in developing rice grains (Ma *et al.*, 2017; Yang *et al.*, 2018).

Data from the GWAS analysis indicate that genetic variation at the *ZmSWEET13s* loci in the maize diversity panels is significantly associated with several phenotypic traits, including ear- and developmental-related traits. Although the causality needs to be validated, the identified SNP markers might be useful for marker-assisted selection for further crop improvement. A better understanding of the role of SWEET sugar transporters in phloem loading in maize may guide future engineering efforts to improve yield potential.

Acknowledgements

We thank Joelle Sasse, Bi-Huei Hou, Aurélie Grimault, Franklin Talavera-Rauh, Xiao-Qing Xu, Grayson Badgley and Guido Grossmann for experimental support during various analyses. We thank Ari Kornfeld (Department of Global Ecology,

Carnegie Science) for help and advice with photosynthesis measurements. This work was made possible by research grants from Syngenta Crop Protection, LLC (WBF), the Office of Basic Energy Sciences of the US Department of Energy (DE-FG02-04ER15542; W.B.F.), the Bill and Melinda Gates Foundation, and the National Science Foundation (IOS-1258018; B.Y., W.B.F.). W.B.F.'s lab is supported by the Alexander von Humboldt Foundation.

Author contributions

M.B., S.N.C., B.Y., W.B.F. and D.S. conceived and designed experiments. M.B., M.H., T.H., S.N.C., B.Y. and D.S. performed experiments. M.B., T.H., B.Y., J.Y., W.B.F. and D.S. analysed the data. D.S. and W.B.F. wrote the manuscript, M.B. and B.Y. helped with revisions.

Competing financial interests

The authors (D.S. and W.B.F., on behalf of Carnegie Science) have filed a PCT patent application based in part on this work with the US Patent and Trademark Office.

References

Ainsworth EA, Bush DR. 2011. Carbohydrate export from the leaf: a highly regulated process and target to enhance photosynthesis and productivity. *Plant Physiology* **155**: 64.

Baker RF, Leach KA, Boyer NR, Swyers MJ, Benitez-Alfonso Y, Skopelitis T, Luo A, Sylvester A, Jackson D, Braun DM. 2016. Sucrose transporter ZmSut1 expression and localization uncover new insights into sucrose phloem loading. *Plant Physiology* **172**: 1876–1898.

Benjamini Y, Hochberg Y. 1995. Controlling the false discovery rate: a practical and powerful approach to multiple testing. *Journal of the Royal Statistical Society Series B (Methodological)* **57**: 289–300.

Botha CEJ. 2013. A tale of two neglected systems-structure and function of the thin- and thick-walled sieve tubes in monocotyledonous leaves. *Frontiers in Plant Science* **4**: 297.

Braun DM, Wang L, Ruan Y-L. 2014. Understanding and manipulating sucrose phloem loading, unloading, metabolism, and signalling to enhance crop yield and food security. *Journal of Experimental Botany* **65**: 1713–1735.

Bukowski R, Guo X, Lu Y, Zou C, He B, Rong Z, Wang B, Xu D, Yang B, Xie C *et al.* 2017. Construction of the third generation *Zea mays* haplotype map. *GigaScience*: gix134.

Bürkle L, Hibberd JM, Quick WP, Kühn C, Hirner B, Frommer WB. 1998. The H^+-sucrose cotransporter NtSUT1 is essential for sugar export from tobacco leaves. *Plant Physiology* **118**: 59–68.

Chang Y-M, Liu W-Y, Shih AC-C, Shen M-N, Lu C-H, Lu M-YJ, Yang H-W, Wang T-Y, Chen SC-C, Chen SM *et al.* 2012. Characterizing regulatory and functional differentiation between maize mesophyll and bundle sheath cells by transcriptomic analysis. *Plant Physiology* **160**: 165.

Char SN, Neelakandan AK, Nahampun H, Frame B, Main M, Spalding MH, Becraft PW, Meyers BC, Walbot V, Wang K *et al.* 2017. An *Agrobacterium*-delivered CRISPR/Cas9 system for high-frequency targeted mutagenesis in maize. *Plant Biotechnology Journal* **15**: 257–268.

Chardon F, Bedu M, Calenge F, Klemens PA, Spinner L, Clement G, Chietera G, Leran S, Ferrand M, Lacombe B *et al.* 2013. Leaf fructose content is controlled by the vacuolar transporter SWEET17 in Arabidopsis. *Current Biology* **23**: 697–702.

Chen L-Q, Cheung LS, Feng L, Tanner W, Frommer WB. 2015a. Transport of sugars. *Annual Review of Biochemistry* **84**: 865–894.

Chen LQ, Hou BH, Lalonde S, Takanaga H, Hartung ML, Qu XQ, Guo WJ, Kim JG, Underwood W, Chaudhuri B *et al.* 2010. Sugar transporters for intercellular exchange and nutrition of pathogens. *Nature* **468**: 527–532.

Chen H-Y, Huh J-H, Yu Y-C, Ho L-H, Chen L-Q, Tholl D, Frommer WB, Guo W-J. 2015b. The Arabidopsis vacuolar sugar transporter SWEET2 limits carbon sequestration from roots and restricts *Pythium* infection. *Plant Journal* **83**: 1046–1058.

Chen LQ, Qu XQ, Hou BH, Sosso D, Osorio S, Fernie AR, Frommer WB. 2012. Sucrose efflux mediated by SWEET proteins as a key step for phloem transport. *Science* **335**: 207–211.

Cohn M, Bart RS, Shybut M, Dahlbeck D, Gomez M, Morbitzer R, Hou B-H, Frommer WB, Lahaye T, Staskawicz BJ. 2014. *Xanthomonas axonopodis* virulence is promoted by a transcription activator-like effector-mediated induction of a SWEET sugar transporter in cassava. *Molecular Plant–Microbe Interactions: MPMI* **27**: 1186–1198.

Cox KL, Meng F, Wilkins KE, Li F, Wang P, Booher NJ, Carpenter SCD, Chen L-Q, Zheng H, Gao X *et al.* 2017. TAL effector driven induction of a SWEET gene confers susceptibility to bacterial blight of cotton. *Nature Communications* **8**: 15588.

Denton AK, Maß J, Külahoglu C, Lercher MJ, Bräutigam A, Weber APM. 2017. Freeze-quenched maize mesophyll and bundle sheath separation uncovers bias in previous tissue-specific RNA-Seq data. *Journal of Experimental Botany* **68**: 147–160.

Dobin A, Davis CA, Schlesinger F, Drenkow J, Zaleski C, Jha S, Batut P, Chaisson M, Gingeras TR. 2013. STAR: ultrafast universal RNA-seq aligner. *Bioinformatics* **29**: 15–21.

Dupree P, Pwee K-H, Gray JC. 1991. Expression of photosynthesis gene-promoter fusions in leaf epidermal cells of transgenic tobacco plants. *Plant Journal* **1**: 115–120.

Eggermont K, Goderis IJ, Broekaert WF. 1996. High-throughput RNA extraction from plant samples based on homogenisation by reciprocal shaking in the presence of a mixture of sand and glass beads. *Plant Molecular Biology* **14**: 273–279.

Emms DM, Covshoff S, Hibberd JM, Kelly S. 2016. Independent and parallel evolution of new genes by gene duplication in two origins of C_4 photosynthesis provides new insight into the mechanism of phloem loading in C_4 species. *Molecular Biology and Evolution* **33**: 1796–1806.

Eom J-S, Choi S-B, Ward JM, Jeon J-S. 2012. The mechanism of phloem loading in rice (*Oryza sativa*). *Molecules and Cells* **33**: 431–438.

Feng L, Frommer WB. 2015. Structure and function of SemiSWEET and SWEET sugar transporters. *Trends in Biochemical Sciences* **40**: 480–486.

Flint-Garcia SA, Thuillet A-C, Yu J, Pressoir G, Romero SM, Mitchell SE, Doebley J, Kresovich S, Goodman MM, Buckler ES. 2005. Maize association population: a high-resolution platform for quantitative trait locus dissection. *Plant Journal* **44**: 1054–1064.

Gottwald JR, Krysan PJ, Young JC, Evert RF, Sussman MR. 2000. Genetic evidence for the in planta role of phloem-specific plasma membrane sucrose transporters. *Proceedings of the National Academy of Sciences, USA* **97**: 13979–13984.

Guo W-J, Nagy R, Chen H-Y, Pfrunder S, Yu Y-C, Santelia D, Frommer WB, Martinoia E. 2014. SWEET17, a facilitative transporter, mediates fructose transport across the tonoplast of Arabidopsis roots and leaves. *Plant Physiology* **164**: 777–789.

Han L, Zhu Y, Liu M, Zhou Y, Lu G, Lan L, Wang X, Zhao Y, Zhang XC. 2017. Molecular mechanism of substrate recognition and transport by the AtSWEET13 sugar transporter. *Proceedings of the National Academy of Sciences, USA* **114**: 10089–10094.

Ishimaru K, Hirose T, Aoki N, Takahashi S, Ono K, Yamamoto S, Wu J, Saji S, Baba T, Ugaki M *et al.* 2001. Antisense expression of a rice sucrose transporter OsSUT1 in rice (*Oryza sativa* L.). *Plant & Cell Physiology* **42**: 1181–1185.

Joung J-G, Corbett AM, Fellman SM, Tieman DM, Klee HJ, Giovannoni JJ, Fei Z. 2009. Plant MetGenMAP: an integrative analysis system for plant systems biology. *Plant Physiology* **151**: 1758.

Kanno Y, Oikawa T, Chiba Y, Ishimaru Y, Shimizu T, Sano N, Koshiba T, Kamiya Y, Ueda M, Seo M. 2016. AtSWEET13 and AtSWEET14 regulate gibberellin-mediated physiological processes. *Nature Communications* **7**: 13245.

Klemens PAW, Patzke K, Deitmer J, Spinner L, Le Hir R, Bellini C, Bedu M, Chardon F, Krapp A, Neuhaus HE. 2013. Overexpression of the vacuolar sugar carrier AtSWEET16 modifies germination, growth, and stress tolerance in Arabidopsis. *Plant Physiology* **163**: 1338–1352.

Latorraca NR, Fastman NM, Venkatakrishnan AJ, Frommer WB, Dror RO, Feng L. 2017. Mechanism of substrate translocation in an alternating access transporter. *Cell* **169**: 96–107.

Li P, Ponnala L, Gandotra N, Wang L, Si Y, Tausta SL, Kebrom TH, Provart N, Patel R, Myers CR *et al.* 2010. The developmental dynamics of the maize leaf transcriptome. *Nature Genetics* **42**: 1060–1067.

Lin IW, Sosso D, Chen L-Q, Gase K, Kim S-G, Kessler D, Klinkenberg PM, Gorder MK, Hou B-H, Qu X-Q *et al.* 2014. Nectar secretion requires sucrose phosphate synthases and the sugar transporter SWEET9. *Nature* **508**: 546–549.

Love MI, Huber W, Anders S. 2014. Moderated estimation of fold change and dispersion for RNA-seq data with DESeq2. *Genome Biology* **15**: 550.

Ma L, Zhang D, Miao Q, Yang J, Xuan Y, Hu Y. 2017. Essential role of sugar transporter OsSWEET11 during the early stage of rice grain filling. *Plant & Cell Physiology* **58**: 863–873.

Purcell S, Neale B, Todd-Brown K, Thomas L, Ferreira MAR, Bender D, Maller J, Sklar P, de Bakker PIW, Daly MJ *et al.* 2007. PLINK: a tool set for whole-genome association and population-based linkage analyses. *American Journal of Human Genetics* **81**: 559–575.

Regmi KC, Zhang S, Gaxiola RA. 2016. Apoplasmic loading in the rice phloem supported by the presence of sucrose synthase and plasma membrane-localized proton pyrophosphatase. *Annals of Botany* **117**: 257–268.

Riesmeier JW, Willmitzer L, Frommer WB. 1994. Evidence for an essential role of the sucrose transporter in phloem loading and assimilate partitioning. *EMBO Journal* **13**: 1–7.

Scofield GN, Hirose T, Gaudron JA, Furbank RT, Upadhyaya NM, Ohsugi R. 2002. Antisense suppression of the rice transporter gene, OsSUT1, leads to impaired grain filling and germination but does not affect photosynthesis. *Functional Plant Biology* **29**: 815–826.

Slewinski TL, Meeley R, Braun DM. 2009. Sucrose transporter1 functions in phloem loading in maize leaves. *Journal of Experimental Botany* **60**: 881–892.

Sosso D, Luo D, Li Q-B, Sasse J, Yang J, Gendrot G, Suzuki M, Koch KE, McCarty DR, Chourey PS *et al.* 2015. Seed filling in domesticated maize and rice depends on SWEET-mediated hexose transport. *Nature Genetics* **47**: 1489–1493.

Srivastava AC, Dasgupta K, Ajieren E, Costilla G, McGarry RC, Ayre BG. 2009. Arabidopsis plants harbouring a mutation in AtSUC2, encoding the predominant sucrose/proton symporter necessary for efficient phloem transport, are able to complete their life cycle and produce viable seed. *Annals of Botany* **104**: 1121–1128.

Sun MX, Huang XY, Yang J, Guan YF, Yang ZN. 2013. Arabidopsis RPG1 is important for primexine deposition and functions redundantly with RPG2 for plant fertility at the late reproductive stage. *Plant Reproduction* **26**: 83–91.

Tausta SL, Li P, Si Y, Gandotra N, Liu P, Sun Q, Brutnell TP, Nelson T. 2014. Developmental dynamics of Kranz cell transcriptional specificity in maize leaf reveals early onset of C_4-related processes. *Journal of Experimental Botany* **65**: 3543–3555.

Turgeon R, Wolf S. 2009. Phloem transport: cellular pathways and molecular trafficking. *Annual Review of Plant Biology* **60**: 207–221.

Wang L, Czedik-Eysenberg A, Mertz RA, Si Y, Tohge T, Nunes-Nesi A, Arrivault S, Dedow LK, Bryant DW, Zhou W *et al.* 2014. Comparative analyses of C_4 and C_3 photosynthesis in developing leaves of maize and rice. *Nature Biotechnology* **32**: 1158.

Xuan YH, Hu YB, Chen LQ, Sosso D, Ducat DC, Hou BH, Frommer WB. 2013. Functional role of oligomerization for bacterial and plant SWEET sugar transporter family. *Proceedings of the National Academy of Sciences, USA* **110**: E3685–E3694.

Yang J, Luo D, Yang B, Frommer WB, Eom J-S. 2018. SWEET11 and 15 as key players in seed filling in rice. *New Phytologist* **218**: 604–615.

Zhou X, Stephens M. 2012. Genome-wide efficient mixed-model analysis for association studies. *Nature Genetics* **44**: 821–824.

Zhu XG, Long SP, Ort DR. 2010. Improving photosynthetic efficiency for greater yield. *Annual Review of Plant Biology* **61**: 235–261.

Supporting Information

Additional Supporting Information may be found online in the Supporting Information tab for this article:

Fig. S1 Expression pattern of SWEET genes in *Zea mays* L. across four leaf-specific RNA-seq datasets.

Fig. S2 Chromosomal localization and potential synteny of *ZmSWEET13s* in *Zea mays* L. and *Oryza sativa.*

Fig. S3 SWEET13 orthologs in different grasses.

Fig. S4 Expression of *ZmSWEET13a*, *b* and *c* in sink and source tissues of *Zea mays* L.

Fig. S5 Photosynthetic rates in *Zea mays* L. *zmsweet13abc* mutants.

Fig. S6 *ZmSWEET* mRNA levels in *Zea mays* L. *zmsweet13abc* mutants.

Fig. S7 Principal component analysis of differentially expressed genes in *zmsweet13* mutants and wild type

Fig. S8 Differentially expressed genes in *Zea mays* L. *zmsweet13abc* mutants involved in light-harvesting processes.

Fig. S9 Differentially expressed genes in *Zea mays* L. *zmsweet13abc* mutants involved in chlorophyll and tetrapyrrole biosynthesis.

Fig. S10 Differentially expressed genes in *Zea mays* L. *zmsweet13abc* mutants involved in sucrose and starch biosynthesis.

Fig. S11 GWAS results for *ZmSWEET13c* genes in *Zea mays* L.

Fig. S12 GWAS results for ZmSWEET13a and ZmSWEET13b genes in *Zea mays* L.

Fig. S13 Biological repeats of sugar quantification and qRT-PCR of *Zea mays* L. leaves.

Table S1 List of primers

Table S2 Read statistics of RNA-seq experiments

Table S3 Significantly affected pathways in *Zea mays* L. zm*sweet-13abc* mutants

Please note: Wiley Blackwell are not responsible for the content or functionality of any Supporting Information supplied by the authors. Any queries (other than missing material) should be directed to the *New Phytologist* Central Office.

SUGAR FLUX AND SIGNALING IN PLANT-MICROBE INTERACTIONS

Bezrutczyk, M., Yang, J., Eom, J.-S., Prior, M., Sosso, D., Hartwig, T., Szurek, B., Oliva, R., Vera-Cruz, C., White, F.F., Yang, B. and Frommer, W.B.

the plant journal

SEB Society for Experimental Biology

The Plant Journal (2018) **93,** 675–685 doi: 10.1111/tpj.13775

SI PLANT BIOTIC INTERACTIONS

Sugar flux and signaling in plant–microbe interactions

Margaret Bezrutczyk[1,2], Jungil Yang[1,2], Joon-Seob Eom[1,2], Matthew Prior[4], Davide Sosso[5], Thomas Hartwig[1,2], Boris Szurek[6], Ricardo Oliva[7], Casiana Vera-Cruz[7], Frank F. White[8], Bing Yang[9] and Wolf B. Frommer[1,2,3,*]

[1]*Institute for Molecular Physiology, Heinrich Heine Universität Düsseldorf, Universiätsstr. 1, 40225, Düsseldorf, Germany,*
[2]*Max Planck Institute for Plant Breeding Research, Carl von Linné Weg 10, 50829, Köln, Germany,*
[3]*Institute for Transformative Biomolecules (ITbM), Nagoya University, JapanITbM Building 6F, Furo, Chikusa, Nagoya 464-8602, Japan,*
[4]*Center for Plant Cell Biology and Department of Botany and Plant Sciences, University of California, 900 University Ave., Riverside, CA, 92521, USA,*
[5]*Inari Agriculture Inc., 200 Sidney Street, Cambridge, MA, 02139, USA,*
[6]*IRD, Cirad, University of Montpellier, BP 64501, 911 Avenue Agropolis, 34394, Montpellier Cedex 5, France,*
[7]*International Rice Research Institute, DAPO Box 7777, Metro Manila, Philippines,*
[8]*Department of Plant Pathology, University of Florida, 1449 Fifield Hall, 2550 Hull Road, PO Box 110680, Gainesville, FL, 32611, USA, and*
[9]*Department of Genetics, Development, and Cell Biology, Iowa State University, Ames, IA 50011, USA*

Received 15 August 2017; revised 29 October 2017; accepted 1 November 2017; published online 21 November 2017.
*For correspondence (e-mail frommew@hhu.de).

SUMMARY

Plant breeders have developed crop plants that are resistant to pests, but the continual evolution of pathogens creates the need to iteratively develop new control strategies. Molecular tools have allowed us to gain deep insights into disease responses, allowing for more efficient, rational engineering of crops that are more robust or resistant to a greater number of pathogen variants. Here we describe the roles of SWEET and STP transporters, membrane proteins that mediate transport of sugars across the plasma membrane. We discuss how these transporters may enhance or restrict disease through controlling the level of nutrients provided to pathogens and whether the transporters play a role in sugar signaling for disease resistance. This review indicates open questions that require further research and proposes the use of genome editing technologies for engineering disease resistance.

Keywords: pathogen, symbiosis, sucrose, transport, nutrition, signaling, *Arabidopsis thaliana*, *Oryza sativa*, Triticum sp.

INTRODUCTION

Plant pathogens cause massive yield losses in all crops, and thus contribute to food insecurity and shortages (Oerke, 2006). Both full-blown diseases and subclinical infections (low-level infestation without major disease symptoms) cause substantial yield losses (Popp and Hantos, 2011). The health and economic consequences of food security cannot be overstated. Thus, the development of effective disease resistance within food crops is of fundamental importance to both subsistence farmers and agribusiness. A major task has to be the development of effective strategies to reduce disease losses and the associated social instability. This difficult task requires effective collaboration among diverse disciplines in order to develop new technologies. Bioengineering requires extensive knowledge gleaned from fundamental research in the field of plant–pathogen interactions (Jones and Dangl, 2006; Jones *et al.*, 2016). Many promising solutions are on the horizon, including greatly expanded accessibility to R genes and an improved understanding of disease susceptibility (Boutrot and Zipfel, 2017). Anecdotal examples and recent research indicate that the rational manipulation of host susceptibility can contribute to development of effective disease management strategies. This review focuses on recent groundbreaking discoveries regarding the role of

host sugar transporters in disease progression. We propose two hypotheses regarding the roles of sugar transporters in pathogen defense, which are not mutually exclusive, and can serve as guides for future research and engineering (subsequently referred to as 'pathogen-starvation' and 'apoplasmic sugar signaling' hypotheses).

SUTs, SWEETs and STPs: gate keepers of sugar allocation

The identification of the role that sugar transporters play in pathogen susceptibility should not come as a surprise, as it had been predicted 30 years ago (Patrick, 1989). At that time, none of the plant genes encoding sugar transporters was known. Since then, many of the transporters that distribute the carbon resources of a plant, including those for phloem loading and seed filling, have been identified at the molecular level (Chandran, 2015; Chen *et al.*, 2015a). Sugar uptake transporters, or SUTs, were the first sucrose transporters characterized (Riesmeier *et al.*, 1992, 1994). SUT1 homologs from a variety of species are now known to function as proton symporters, which use the proton gradient to import sucrose into the sieve element companion cell complex (SECC) for phloem loading (Boorer *et al.*, 1996; Carpaneto *et al.*, 2005). In Arabidopsis, corn and several solanaceous species, SUT1 has been shown to import sucrose into the SECC conduits from the cell wall space (Riesmeier *et al.*, 1994; Bürkle *et al.*, 1998; Gottwald *et al.*, 2000; Slewinski *et al.*, 2009). Since the discovery of SUT1, the search was on for the mechanism responsible for efflux of sucrose from the cytosol, where sucrose is made by photosynthesis, into the cell wall space. Genetically encoded FRET sensors proved pivotal to identifying proteins that had such properties, the so-called SWEETs (Chen *et al.*, 2010, 2012, 2015a,b). Each plant contains about two dozen SWEET paralogs, which predominantly transport hexoses or sucrose. Of note, several SWEETs play critical roles in the cellular efflux of sugars, in phloem (AtSWEET11, 12, ZmSWEET13a, b, and c; Chen *et al.*, 2012; Bezrutczyk *et al.*, 2017), seeds (AtSWEET11, 12 and 15; OsSWEET11 and 15; Chen *et al.*, 2015b; Yang *et al.*, 2017) and nectaries (AtSWEET9, BrSWEET9 and NtSWEET9; Lin *et al.*, 2014). In the context of pathogen susceptibility (discussed below), the efflux of sucrose in uninfected leaves by SWEETs appears to be limited to phloem parenchyma cells, at least in Arabidopsis. One may speculate that sugar release occurs in the few micrometers between phloem parenchyma and the SECC, and in close vicinity to the subsequent active uptake by SUTs in the SECC, potentially limiting the release of sucrose to a tiny interface in leaves. In one case, a hexose-transporting SWEET appears to be responsible for cellular uptake of hexoses to serve seed filling in corn (Sosso *et al.*, 2015).

A third class of sugar transporters that will be addressed in this review are STPs (sugar transport proteins, sometimes also MSTs), monosaccharide/H^+ symporters first described in Chlorella and Arabidopsis (Sauer and Tanner, 1989; Sauer *et al.*, 1990; Boorer *et al.*, 1994). As is the case with SWEET proteins, each plant contains multiple paralogs. STPs are 12-transmembrane domain transporters that play vital roles in sugar retrieval from the cell wall space (Lemonnier *et al.*, 2014; Yamada *et al.*, 2016).

PLANT PHYSIOLOGY, ONE R GENE AT A TIME

SWEETs also play a role in pathogen susceptibility. The recessive *xa13* bacterial blight resistance locus was first described in 1987 in rice (Ogawa *et al.*, 1987). It took almost 20 years before the underlying gene was identified, and another 4 years until the function of Xa13 as a SWEET sucrose transporter became clear (OsSWEET11; Chu *et al.*, 2006; Yang *et al.*, 2006; Chen *et al.*, 2010). Chromatin-immunoprecipitation experiments demonstrated that the bacterial type III TAL (Transcription Activation-Like) effector PthXo1 from the *Xanthomonas oryzae* pv. *oryzae* (Xoo) strain PXO99 bound directly to the Xa13/OsSWEET11 promoter, providing us with the mechanism that explains the gene-for-gene susceptibility and recessive resistance (Chen *et al.*, 2010; Römer *et al.*, 2010).

Xa13 (also called *Os8N3*) was separately cloned by two independent groups – one comprised of Bing Yang, Akiko Sugio and Frank White, and the other of Shiping Wang and Jeff Bennetzen (Chu *et al.*, 2006; Yang *et al.*, 2006). Resistance due to *xa13* occurs only in the recessive homozygote, and is due to nucleotide polymorphisms in the promoter that prevents PthXo1-induction of the associated *Xa13* gene (Yang *et al.*, 2006). Xa13 is a homolog of nodulin number 3 (MtN3), which is induced during nodulation of *Medicago truncatula* roots (Gamas *et al.*, 1996).

More recently, other rice SWEETs were associated with host susceptibility, and other TAL effectors were found to target different promoter regions of several SWEET loci (Antony *et al.*, 2010; Yu *et al.*, 2011; Zhou *et al.*, 2015). In fact, artificial TAL effector-induced expression of any member of a subset of phylogenetically related SWEETs (clade III) with sucrose transport ability is able to trigger susceptibility to the bacterial pathogen, although only three of them have been observed as targets by natural *Xoo* field strains so far (Streubel *et al.*, 2013; Zhou *et al.*, 2015).

The characterization of *xa13*, the associated *OsSWEET11* locus, and the PthXo1 TAL effector stood the classical gene-for-gene paradigm for resistance on its proverbial head. In the conventional resistance gene model, bacterial type III effectors (avr genes) are associated with specific resistance (R) genes. Strains with a specific avr gene are considered races within a specific pathogen and can find a host in a plant lacking the corresponding R gene. While gene-for-gene resistance is a condition of an R gene/avr gene pair, in this case susceptibility is a condition of a susceptibility (S) gene and a virulence gene pair. A failure of

the SWEET gene to respond to the induction by the TAL effector confers resistance in rice to bacterial blight. At the moment, the recessive *xa13* is bred into elite rice lines as an effective R gene, particularly in India (Lore *et al.*, 2011; Mishra *et al.*, 2013; Laha *et al.*, 2016). However, the gene is only effective against strains of the bacterium that rely on the TAL effector PthXo1 for ectopic induction of *OsSWEET11* expression; strains that have other TAL effector genes that target *OsSWEET13* or *OsSWEET14* are still virulent. The *xa13* resistance locus represents a series of alleles that have arisen naturally. Importantly, it appears that *xa13* mutations cause little to no impairment of physiological function or yield. While the alleles of *xa13* are the only known SWEET promoter mutations that have been historically used in breeding efforts, screening of rice germplasm has revealed additional recessive alleles at *OsSWEET13* and *OsSWEET14* (Liu *et al.*, 2011; Hutin *et al.*, 2015). More recently, the recessive resistance gene *b6* in cotton has been associated with alterations of the GhSWEET10 promoter, which is targeted by the TAL effector Avrb6 of *Xanthomonas citri* subsp. *malvacearum*, the causal agent of cotton blight (Cox *et al.*, 2017). Originally, SWEET-based susceptibility had been thought to be a unique feature of a xylem pathogen. However, *X. citri* does not appear to be restricted to xylem in cotton. It remains to be determined if this case is possibly a violation to that concept or if it is a more widespread phenomenon. The fact that SWEETs are induced during many other plant–pathogen interactions also challenges the 'xylem pathogen' hypothesis.

Interference with the binding of the TAL effectors is a promising avenue for blocking the induction of SWEET genes. TAL effectors are prokaryotic transcription factors that bind to sequence-specific effector-binding elements (EBEs) of the eukaryotic host (Boch *et al.*, 2009; for review, see Bogdanove and Voytas, 2011). TAL effectors bind to the promoter regions, commonly the TATAA box itself, and direct expression of the respective downstream SWEETs (Antony *et al.*, 2010; Chen *et al.*, 2010; Römer *et al.*, 2010). Mutations involving the EBE reduce or eliminate effector binding, preventing *SWEET* gene induction. TALEN-mediated deletions directed at *OsSWEET14* and, more recently, CRISPR-Cas9-mediated mutations at *OsSWEET13* have produced plants that are resistant to strains of *Xoo* (Li *et al.*, 2013; Zhou *et al.*, 2015; Blanvillain-Baufumé *et al.*, 2017). Alteration of promoter mutations, either present in natural variants of *OsSWEET11*/Xa13 as well as those obtained by genome editing, prevent binding of the TAL effectors and their usurpation of SWEET gene regulation in infected cells, which leads to a recessive 'gain of function' resistance that does not noticeably impair normal SWEET function, and importantly has no negative effects on yield potential (Chen *et al.*, 2010). The discovery that plant SWEETs are co-opted during Xanthomonas infection revealed a step within the plant–pathogen dance that, as a target, can be engineered to trip up the pathogen.

TWO HYPOTHETICAL MODELS FOR HOW SUGARS INFLUENCE PATHOGEN RESISTANCE

The two primary working models of sugar-mediated pathogen resistance are currently 'pathogen starvation' and 'sugar signaling'. The first hypothesis is the simplest: that pathogens infect plants with the primary goal of gaining access to the resources (sucrose) needed for reproduction, a process that proceeds from a few cells at the time of infection to billions of bacteria when symptoms become apparent. There is no doubt that host-derived sugars are transferred to the pathogen, at least in the case of fungi (Aked and Hall, 1993; Sutton *et al.*, 1999). One step of this is the ectopic induction of SWEETs, which results in leakage of sugars into the apoplasmic space. This hypothesis depends on the assumption that apoplasmic sugar pools are low, thereby limiting pathogen growth. An alternative is a 'sugar signaling' hypothesis, in which altered levels of sugar at the infection site trigger signaling cascades that result in salicylic acid (SA) pathway activation and defense gene upregulation, ultimately generating physiological changes that repel pathogens (Gebauer *et al.*, 2017).

The sugar transporters described earlier fit both hypotheses: SWEET sugar transporters can be upregulated during pathogen attack and export sugars out of cells into extracellular spaces, where pathogens are known to feed (Asai *et al.*, 2016); SWEETs could also be upregulated to help translocate sugars to infection sites to fuel the host defense metabolism (Tadege *et al.*, 1998). STPs, as proton hexose symporters, are known to take up hexoses from apoplasmic space and have been found to be induced during pathogen challenge (Lemonnier *et al.*, 2014), supporting the pathogen starvation hypothesis. On the other hand, sugars themselves can act as signals that induce defense genes (Herbers *et al.*, 1996; Herbers and Sonnewald, 1998; Gebauer *et al.*, 2017), supporting a 'sugar signaling' hypothesis.

One of the assumptions of the 'pathogen starvation' hypothesis is that plants do not volunteer sugars passively, so bacteria had to evolve elegant mechanisms to induce SWEETs and cellular efflux of sucrose (Figure 1). Given the complex defense machinery developed by plants to prevent and suppress infections, the host likely uses all possible means to restrict pathogen reproduction, including the limitation of resources for growth in the apoplasmic space. It is possible that the restriction of sugar transfer to the interface between phloem parenchyma and the SECC complex, deep inside the leaf, originally evolved to limit sugar availability in the cell wall space (Chen *et al.*, 2012). This hypothesis may explain the recessive nature of *xa13*-mediated resistance and, importantly, predicts elevated sugar flux towards the apoplasmic space during pathogen infection.

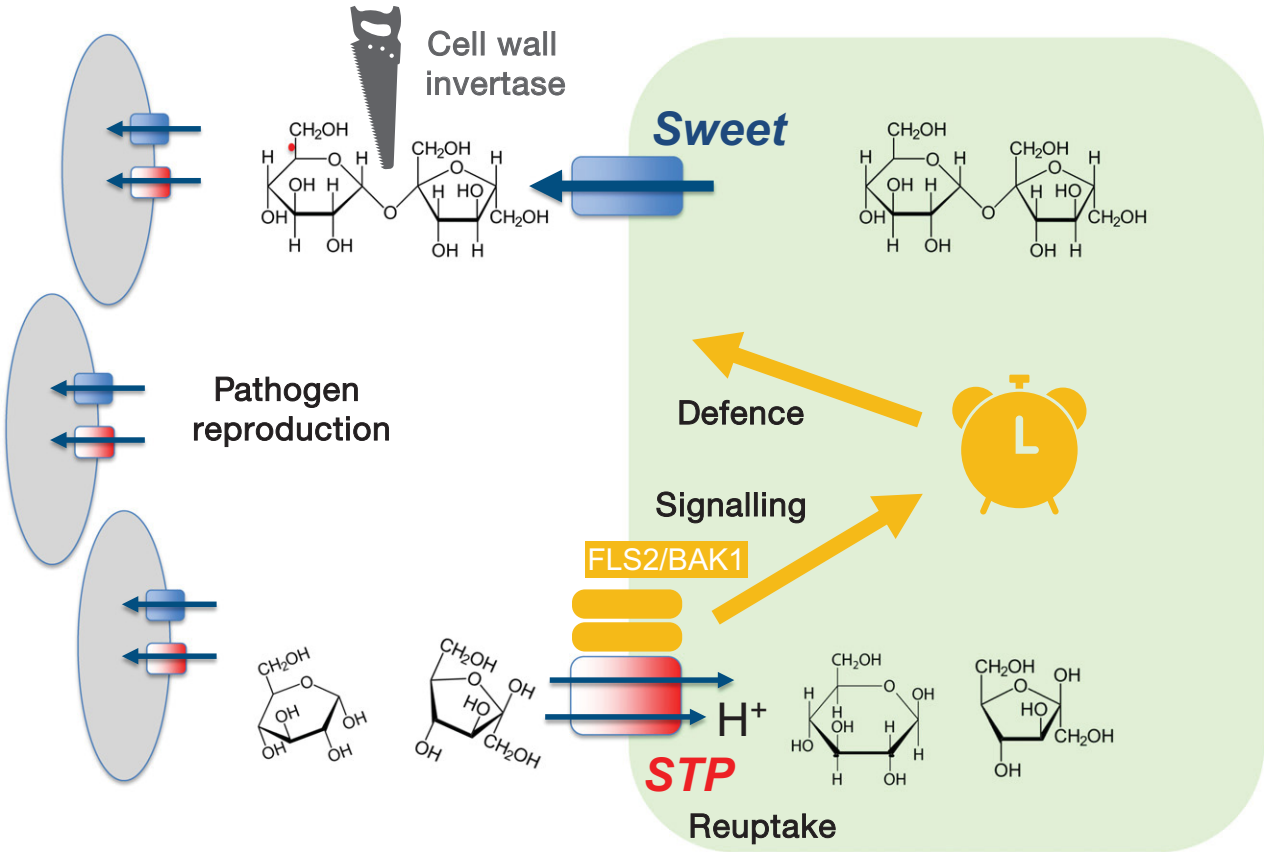

Figure 1. Cartoon illustrating two alternative pathways for SWEET- and STP-mediated pathogen susceptibility/resistance.
In the 'sugar starvation' hypothesis of disease resistance, the microbial pathogen induces SWEETs (sucrose uniporters) using effectors. In parallel, the plant recognizes the pathogen elicitors, which induce STPs (hexose/H^+ symporters). SWEET induction leads to secretion of sucrose into the cell wall space, where it is partially cleaved by cell wall invertases. The microbe uses sucrose and/or hexoses for nutrition/reproduction. STPs counteract the accumulation of sugars in the cell wall space by secondary active retrieval. In the 'sugar signaling' hypothesis of disease resistance, either the external accumulation of sugars or other signaling events, perhaps mediated via STPs by interaction with other proteins such as FLS2 and BAK1, signal an infection and trigger defense responses. These hypotheses are not mutually exclusive, and may function at the same or different times during the course of infection.

So far, experiments that test this hypothesis have not found elevated apoplasmic sugar levels, as measured by assays that typically detect sucrose and hexoses in leaves in the low millimolar range (Lohaus *et al.*, 2001). One explanation is that sugars may pass briefly from host cells to pathogens without accumulating substantially in the apoplasmic space. Flux can change without affecting pool sizes. Multiple Arabidopsis *SWEETs* are induced during Pseudomonas infection (Chen *et al.*, 2010), and higher hexose levels were not found in apoplasmic wash fluids despite induction of cell wall invertase activity (Yamada *et al.*, 2016). Cell wall invertase genes are induced in other some bacterial diseases, for example, cassava blight (Cohn *et al.*, 2014) and powdery mildew in wheat (Sutton *et al.*, 2007). Plants also respond to the bacterial pathogen-associated molecular pattern (PAMP) signals with induction of hexose/H^+ symporters, such as STP1, 4 and 13, that may counteract the SWEET-mediated secretion (Fotopoulos *et al.*, 2003; Yamada *et al.*, 2016), and thus limit apoplasmic sugar accumulation. STP13 appears to play such a role during infections with the fungus *Botrytis cinerea* (Lemonnier *et al.*, 2014).

The only method used for determining sugar pools in the cell wall space is based on infiltration of the apoplasmic space with solutions followed by centrifugation of the tissues (Lohaus *et al.*, 2001; Araya *et al.*, 2015). Potential issues with this apoplasmic wash technique could also be limiting the information on apoplasmic sugar accumulation: the technique has no temporal or spatial resolution, therefore cannot capture dynamics or local differences. It is generally assumed to measure the apoplasmic sugar pools. Pool size may also be less relevant than fluxes (Patrick, 1989). However, the technique is likely measuring also the efflux capacity of the tissues as the cells are exposed to medium that lacks sugars, creating an infinite gradient across the cell membranes. Incubation of cells in substrate-free medium is typically used to measure cellular efflux from the cytoplasm. Efflux of radiolabeled sugars was used to characterize efflux mediated by SWEETs when expressed in Xenopus oocytes (Chen *et al.*, 2010, 2012). Therefore,

Box 1 Some critical questions

- *Xoo* induces OsSWEET11 to extreme levels – are high SWEET activity levels necessary for infection and, if true, why are such high levels required?
- Only Clade 3 SWEETs are susceptibility loci for *Xoo* – why can only this subset fulfill the role and not the others?
- *xa13* (*OsSWEET11* promoter variant) has been used as a key resistance gene for many decades – can we generate robust resistance by combining SWEET promoter mutations?
- If we assume that *Xoo* does not require its SucX sucrose and GLT glucose transporters for pathogenicity, do they use a combination of sucrose and hexoses or are there other sugar uptake systems present in planta?
- SWEETs are also induced in other pathogen systems – are SWEETs critical in plant pathogen systems beyond Xanthomonas? If so, how do they induce SWEETs in the absence of TAL effectors? And, can we engineer resistance against a wide range of pathogens by restricting SWEET induction?
- If SWEETs serve predominantly in pathogen nutrition – what are the pools of sugars in the apoplasm, what are the fluxes, and what are the sources?
- Have plants evolved to limit apoplasmic sugar availability? Does the plant restrict access to nutrients by moving sugars predominantly via plasmodesmata and by restricting apoplasmic loading to the interface between phloem parenchyma and the sieve element companion cell complex (SECC)?
- Direct evidence for sugar movement through plasmodesmata is lacking – how can we test whether sugars traffic through plasmodesmata?
- What is the spatial distribution of sugars in the apoplasm of uninfected and infected plants?
- If the apoplasmic space contains substantial amounts of sugars – would these apoplasmic sugars be carried to the stomata by the water flux from xylem to stomata in leaves? Is there a retrieval system to avoid such issues?
- STP H^+-symporters could serve as hexose retrieval systems during infection – does the plant use STPs to counteract SWEET activity?
- The STP13 conundrum – why is the effect of inhibition of STP13 sugar transport activity the opposite in wheat rust compared with *Botrytis cinerea* infection of Arabidopsis?
- No one feeds on sugars alone – are transporters for other nutrients also required for susceptibility? In other words, can we block growth of pathogens by preventing access to nutrients in general?

there is a distinct need for better tools that have a high spatial resolution, the ability to separate cytosolic from apoplasmic concentrations, and the ability to measure dynamics in response to infection. Local changes in sugar availability have been predicted from photosynthesis imaging experiments in infected leaves (Siebke and Weis, 1995; Rolfe and Scholes, 2010). One potentially suitable technology may be the use of genetically encoded sensors (Okumoto, 2010) that can be expressed *in planta* to assess sugar flux during pathogen infection, or in the pathogen itself to visualize the nutritional status of the invading fungus or bacteria. Other methods such as mass spectrometry imaging, Raman spectroscopy or other tools not yet developed may help in addressing this important set of questions. Despite progress over the past decade, many questions remain open, a subset of which is summarized in Box 1.

SWEETs — SELECTIVE SUGARS TRANSPORTERS OR TRANSPORTERS OF OTHER SUBSTRATES?

During evolution, transporters have been optimized for the recognition of specific substrates. However, it is now evident that many, if not all, transporters can translocate many compounds, including natural and artificial drugs. For example, SUTs, which have a primary physiological role in importing sucrose into the SECC, can also transport a variety of glucosides such as helicin and salicin (Sun *et al.*, 2010). Another example is NTR1/PTR1, a transporter originally identified as a weak amino acid transporter, but this activity was later shown to likely be a side activity of a di- and tripeptide transporter that has no physiological relevance (Rentsch *et al.*, 1995). The related human peptide transporter PepT1 also transports a wide range of drugs (Brandsch, 2013). Recent findings indicate that the nitrate/peptide transporters mediate transport of compounds with highly diverse structures, such as nitrate, peptides, plant hormones and specialized metabolites (Kanno *et al.*, 2012; Nour-Eldin *et al.*, 2012; Chiba *et al.*, 2015). Of particular note in the context of this review, is that SWEETs transport gibberellins (Kanno *et al.*, 2016). Could gibberellin transport be key to the roles SWEETs play in pathogen resistance? Although this hypothesis does need to be tested, it must be noted that SWEET transport of sugars is well established, the physiological phenotypes of mutants are compatible with sugar transport function, and only

sucrose-transporting SWEETs have been shown to confer pathogen susceptibility.

Many SWEETs have been shown to transport glucose and/or sucrose, and even the bacterial ancestors are sugar transporters (Chen *et al.*, 2015a). SWEET mutant phenotypes are consistent with physiological roles in sugar transport during nectar secretion, phloem loading and seed filling (Chen *et al.*, 2012; Lin *et al.*, 2014; Sosso *et al.*, 2015; Bezrutczyk *et al.*, 2017; Yang *et al.*, 2017). However, Shiping Wang's lab indicated that a number of SWEETs did not complement a yeast sugar transport mutant (Yuan *et al.*, 2014). Negative results obtained with functional assays in heterologous systems can be due to a variety of issues. For instance, vacuolar SWEETs do not localize to the yeast plasma membrane and thus are unable complement the yeast mutant that rely on proper plasma membrane targeting of the heterologous transporters (Chardon *et al.*, 2013; Guo *et al.*, 2014; Chen *et al.*, 2015c). More generally, the detection of transport activity in any heterologous expression depends on adequate targeting of the proteins to the respective compartments in the host: however heterologous systems often fail to traffic sufficient numbers of transporters for example to the cell membrane (yeast, human cells, Xenopus oocytes). These negative results cannot definitively eliminate these proteins as functional transporters, as shown for the human glucose transporter GLUT1 in yeast (Kasahara and Kasahara, 1996). Different assays may be required to evaluate the transport properties of proteins that do not reach the cell membrane in the currently prevalent test systems. Moreover, some SWEETs preferentially transport sucrose over hexoses, rendering activity not testable in the hexose-deficient yeast strain (Wieczorke *et al.*, 1999).

Another interesting angle in the alternate-substrate model comes from the work of Shiping Wang and colleagues. Wang's lab found that OsSWEET11 can interact with apparently non-functional members of the COPT copper transporter family (Yuan *et al.*, 2010, 2011). Using the yeast mutant MPY17, which only shows copper-dependent growth when grown on non-fermentable carbon sources (Puig *et al.*, 2002), copper auxotrophy was only complemented by co-expression of two COPT proteins with OsSWEET11. Because two COPT homologs are involved, OsSWEET11 may not contribute to copper transport itself: rather it could affect the growth phenotype of the yeast mutant in an indirect way, either by increasing the activity of the two COPTs in the complex or by importing trace amounts of soluble carbohydrates derived from the agar, which could partially relieve the conditional copper dependence of the mutant.

Wang's group proposes that Xanthomonas susceptibility in rice is due to the ability of a COPT–SWEET complex to remove copper from the xylem sap, which would otherwise be toxic to the bacteria. This reduction in copper toxicity specifically occurs during infection with the disease-causing strain PXO99, but not for other tested strains (PXO86 and PXO61, which depend on *OsSWEET14* for virulence; Yuan *et al.*, 2010, 2011). One interpretation of this result is that SWEETs transport copper; another is that SWEETs are required for COPT transporter complex function because sugars are needed for its assembly or another energy-consuming process.

Wang's hypothesis appears to be able to explain the susceptibility caused by *Xa13/OsSWEET11*, because PXO99 is particularly sensitive to copper. However, it has been shown that other *Xoo* strains target *OsSWEET11* paralogs like *OsSWEET13* and *14* with closely related TAL effectors (Antony *et al.*, 2010; Yu *et al.*, 2011; Zhou *et al.*, 2015). Notably, transgenic PXO99 carrying TAL effectors targeting *OsSWEET14* overcome the resistance (or copper toxicity) conferred by either *xa13* (mutated alleles of *OsSWEET11* promoter) or RNAi-silenced *OsSWEET13* (Yang *et al.*, 2006; Antony *et al.*, 2010). If copper homeostasis is the key to explaining resistance to each strain in a gene-for-gene manner, all five SWEETs must be able to contribute to copper transport in a similar way as they all can cause susceptibility (Streubel *et al.*, 2013) and all the strains that induce other SWEETs must also be hypersensitive to copper. More work will be required to determine the mechanisms of SWEET interaction with COPT transporters and of copper-mediated resistance: whether SWEETs transport copper or if the sugar that they transport is required for COPT function. These hypotheses are testable – by analyzing copper availability in cell wall space, by determining local copper levels with biosensors, by detailed and more direct characterization of the complex and its copper transport activity, by analysis of copper transport by SWEETs, and by analysis of copper susceptibility of the other strains. Also, copper resistance is a common trait of xanthomonads in fields where copper-based treatments are applied (Behlau *et al.*, 2013). Presumably, Xoo would only have to acquire copper resistance to regain virulence in the face of limited SWEET expression. Nonetheless, further support for this interesting hypothesis would shed new light on the multiple roles of transporters in disease resistance.

A CLOSER LOOK AT THE SUGAR SIGNALING HYPOTHESIS

Extensive co-adaptation has occurred between plant hosts and pathogens. The plant host recognizes a pathogen by molecular patterns at its surface or by its secreted compounds, some of which the pathogen has little freedom to change in order to avoid recognition. While most pathology work has concentrated on processes unrelated to metabolism, a series of studies examined how sugars could serve as potential signals during pathogen interactions. 'High sugar resistance' has been mentioned in a variety of systems (Horsfall and Dimond, 1957). Notably, addition of sucrose to rice plants led to increased

resistance to rice blast (Gómez-Ariza *et al.*, 2007). While supporting a sugar signaling model, the external application of sucrose is fundamentally different from local induction of transporters, thus this observation should be interpreted with care. Sonnewald's group put forward a 'priming' hypothesis, in which hexose sensing in the secretory pathway mediates the induction of defense genes (Herbers *et al.*, 1996). More recently, they showed that defects in phloem loading can trigger SA-mediated priming of defense during infection of Arabidopsis by *Colletotrichum higginsianum*, further supporting the 'sugar signaling' hypothesis (Gebauer *et al.*, 2017).

One way that sugar signaling could mediate resistance is through modulation of the ability of bacterial pathogens to inject effector molecules into the host via Type III secretion systems (TTSS). Sugars are known to affect the expression of TTSS, at least in Pseudomonas (Wengelnik *et al.*, 1996; Stauber *et al.*, 2012). It is apparent that sugar homeostasis in the plant apoplasm directly affects pathogen virulence (Figure 2). Scott Peck's group also showed that extracellular metabolites are necessary for the assembly of TTSS (Anderson *et al.*, 2014). Further exploration in this area could include testing if altered sugar levels in the apoplasm change the induction or assembly of TTSS components. Again, additional work is required to dissect the specific roles of the metabolites and ultimately differentiate between alternate hypotheses, i.e. the signaling and starvation models of plant resistance.

Proton symporters of the MST/STP (monosaccharide transporter/sugar transporter) family are induced during pathogen infection in many systems, from Pseudomonas and *B. cinerea* in Arabidopsis (Fotopoulos *et al.*, 2003; Lemonnier *et al.*, 2014; Yamada *et al.*, 2016) to multiple pathogens (causal agents of leaf, stripe and stem rusts; powdery mildew) in wheat (Moore *et al.*, 2015; White and Frommer, 2015; Ding and Jones, 2017). Several members of the MST family (STP1, 4 and 13) were induced during bacterial infections, most likely as part of the PAMP response (Fotopoulos *et al.*, 2003; Yamada *et al.*, 2016). STPs as proton symporters likely move hexoses from the cell wall into the cell. The most parsimonious hypothesis for sugar-mediated resistance is that STPs act as a defense system to counteract the hijacked SWEET sugar secretion by reimporting hexoses (derived from invertase-mediated hydrolysis of sucrose). Surprisingly, STP13 appears to interact with FLS2, the BAK1 complex and two other PRRs. Moreover, BAK1 phosphorylates STP13, which in turn alters STP13 glucose transport activity. Yamada *et al.* concluded that phospho-dependent regulation of STP13 activity changes apoplasmic sugar levels and thereby inhibits TTSS-mediated effector secretion from the bacteria (Figure 1). Remarkably, however, STP13 is also a key factor for resistance to fungal pathogens such as Botrytis (Lemonnier *et al.*, 2014). Arabidopsis plants overexpressing STP13 were more resistant, while knockout mutants were more susceptible, to Botrytis. Because at least one SWEET is also induced by Botrytis, STP13 could counteract SWEET-mediated sugar availability in the apoplasm (Chong *et al.*, 2014). In the case of the broad-spectrum fungal resistance caused by mutations in STP13 in wheat, transport-deficient STP13 confers dominant resistance in wheat (Moore *et al.*, 2015). Dominance of resistance has been linked to dominant negative inhibition of functional copies of STP13 by the mutated form.

In yeast, select homologs of the STPs can function as sugar sensors rather than transporters (Thevelein and Voordeckers, 2009). We had previously speculated that the Arabidopsis SUT2 may also function as a sensor (based on the presence of extended cytosolic domains, as found in yeast sugar sensors SNF3 and RGT2; Barker *et al.*, 2000). Because there is no convincing evidence so far, it is also pure speculation whether STPs or SWEETs may have additional activities. Over the past decade, other transporters have been identified that have sensor functions (Ho *et al.*, 2009; Thevelein and Voordeckers, 2009). Key evidence needed to prove transceptor activity is a separation of the two functions, as changes in nutrient levels generated by the transporter could act as signals. One would need to identify mutations that affect only the transport function to thereby uncouple transport from signaling. Testing such a hypothesis is substantially more feasible in single-cell organisms, where large numbers of mutations can be generated and tested rapidly to distinguish if additional activities other than transport are at work. Eventually, manipulation of STP13 function, whether in transport and/or signaling activities, may help the development of broad-spectrum resistance against bacterial and fungal pathogens.

PROVIDING NUTRITION FOR SYMBIONTS AND MICROBIOTA

Symbionts have co-evolved with their hosts to expand their range and supply nutrients. Rhizobia fix atmospheric N_2 and provide fixed N to their hosts, in return for carbon skeletons. The nodules in which they live require a constant supply of energy supplied either as carbohydrates or in the form of organic acids. Udvardi and Day showed that bacteroids in nodules take up organic acids preferentially, while transport of sugars is comparatively low and non-saturable for sucrose and glucose (Udvardi *et al.*, 1990). As already mentioned, SWEETs were first found as nodulins (genes induced during nodulation) and named MtN3 (*M. truncatula* nodulin number 3). Low-affinity transporters such as the SWEETs could mediate the above-mentioned, non-saturable uptake of glucose and sucrose. Alternatively, SWEETs could provide sugars to the nodule. Two studies recently demonstrated that multiple SWEETs capable of transporting either hexoses or sucrose are indeed

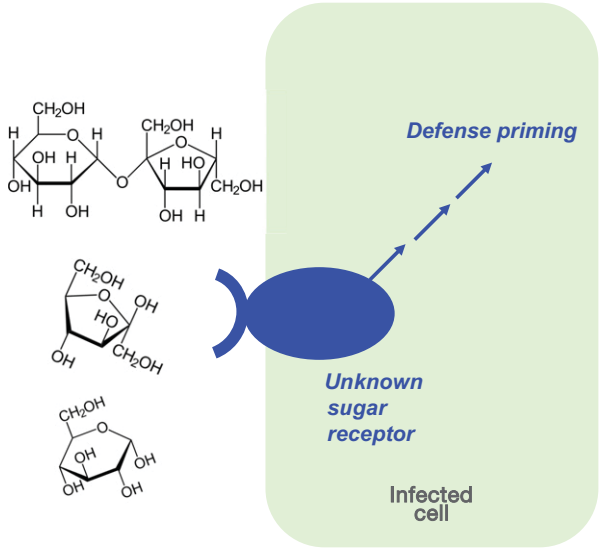

Figure 2. Hypothetical model for high sugar resistance.
Elevation of the levels of extracellular sugars, either through increased SWEET activity or through blockage of STP13, might be detected by a yet unknown sugar receptor that is somehow coupled to a signaling cascade that triggers defense priming (Gebauer *et al.*, 2017).

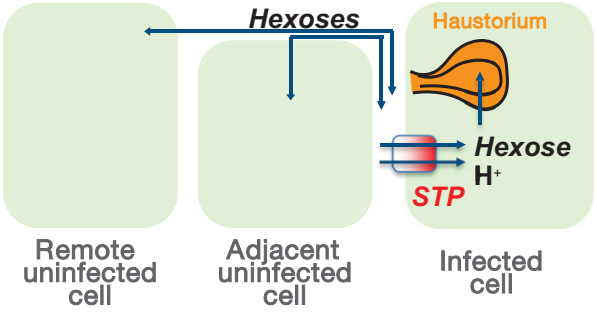

Figure 3. One possible model of the apparently different roles of STP13 in Arabidopsis and wheat.
During infection with a biotrophic pathogen that uses haustoria as feeding structures, STP13 expression and activity are induced as part of the defense response, thereby counteracting SWEET-mediated sugar accumulation in the apoplasm. In such systems, the pathogen has hijacked STP13 to import sugars into the haustorium or import sugars into the cell that feeds the haustorium with sugars provided from adjacent cells as part of the defense mechanism, thereby increasing the availability of sugars in the infected cell, which then can be used to feed the pathogen via the haustorium. This model is based on a concept presented by Yamada *et al.* (2016), but separates the source of sugars from the site of infection.

expressed in nodules, possibly providing sugars to the nodule (Kryvoruchko *et al.*, 2016; Sugiyama *et al.*, 2017). The presence of multiple SWEETs will require a careful analysis of all nodule-expressed members as well as the construction of mutant lines carrying knockouts of multiple family members in order to obtain clear insights into the roles of SWEETs in nitrogen fixation and nodule nutrition.

Mycorrhiza, with their fine hyphal networks, are thought to provide nutrients to their hosts in return for sugar supply (Schüssler *et al.*, 2006). Not surprisingly, SWEETs are also induced during mycorrhization and may thus be responsible for the sugar efflux that feeds the symbionts (Manck-Götzenberger and Requena, 2016).

Plants are colonized by complex communities of microbes, which colonize both their surface and apoplasm (Müller *et al.*, 2016; Andreote and Pereira E Silva, 2017). Presumably, these communities are fed by the plant host. The analysis of microbial communities in the gut and in plant roots provides circumstantial evidence that carbon availability may be important (Hacquard *et al.*, 2015). Could basal levels of SWEET expression provide sufficient nutrition to those that depend on sugars? If this is the case, could one strain take over during pathogenesis by using the available basal levels and outcompete the others without changing host supply? Computational approaches will have to be at the core of examining the effect of manipulation of nutrient secretion on these communities (Succurro *et al.*, 2017).

Microbes, whether symbionts or pathogens, need access to more than just sugars: they need to be supplied with all essential nutrients, and they likely prefer reduced forms. It is thus conceivable that many other host nutrient efflux systems, for example for amino acids, are manipulated by pathogens and symbionts in a similar fashion.

When we distinguish between the 'pathogen starvation' and 'sugar signaling' hypotheses, it is important to be aware that nutrient acquisition by symbiotic bacteria and the necrotrophic and biotrophic pathogens could differ in important ways. In its necrotrophic phase, *B. cinerea* causes cells to rupture and then feeds on the released nutrients (Lemonnier *et al.*, 2014), which is substantially different from the situation in extracellular appressoria-mediated feeding of, for example, corn smut *Ustilago maydis* (Wahl *et al.*, 2010) or the extrahaustorial-matrix feeding in the case of wheat stem rust *Puccinia graminis* (Voegele and Mendgen, 2003). Yamada *et al.* provided a possible model in which fungal pathogens that form haustorial feeding structures may use STP13 as a way to import sugars either into the haustoria or into the cells that contain the haustoria, possibly also explaining the differences observed for STPs in Botrytis and rust (Yamada *et al.*, 2016; Figure 3).

SUMMARY AND OUTLOOK

While there are many open questions (Box 1), the systematic identification of R genes has brought us substantially closer to being able to rationally engineer pathogen resistance in crop plants. Importantly, knowledge of the fact that different *Xoo* strains use different TAL effectors to induce particular SWEETs now allows the construction of elite rice lines that are resistant to particular *Xoo* isolates.

The combination of mutations in SWEET promoters may be a path towards broad-spectrum *Xoo* resistance. Because we are now able to rapidly identify which SWEETs are induced by a particular isolate, and can rapidly determine the TAL effector active in such a strain, it is conceivable that we can breed resistance towards newly emerging isolates more quickly than they can evolve and spread. Breeders have made extensive use of SWEET-based resistance, providing essentially proof-of-concept for approaches in which genome editing is used to engineer resistance. The approach is rather straightforward – TALEN or CRISPR technology is now effectively applied to obtain mutations in the effector molecule-binding sites in the SWEET promoters, thereby creating resistance without yield penalty (Bi and Yang, 2017). Advances in this field will rely heavily on collaborations between plant pathologists and physiologists. Moreover, the combination of different types of resistance mechanisms may help to increase the robustness of resistance as well as the spectrum. In addition to resistance to many diseases, subclinical infections (low-level infestation without major disease symptoms) also cause substantial yield losses (Popp and Hantos, 2011), thus there is an opportunity to even generate lines with increased yield.

ACKNOWLEDGEMENTS

The authors gratefully acknowledge grant support from the Bill and Melinda Gates Foundation (Grand Challenge program, WBF), the Office of Basic Energy Sciences of the US Department of Energy (DE-FG02-04ER15542; WBF), the National Science Foundation (IOS-1258018, WBF; 2012-1238189, BY, FFW; IOS-1258103, BY; and IOS-1258028, FFW), and the Alexander von Humboldt Foundation (WBF).

CONFLICT OF INTEREST

The authors declare no conflict of interest.

REFERENCES

Aked, J. and Hall, J.L. (1993) The uptake of glucose, fructose and sucrose into the lower epidermis of leaf discs of pea (Pisum sativum L. cv. Argenteum). *New Phytol.* **123**, 271–276.

Anderson, J.C., Wan, Y., Kim, Y.-M., Pasa-Tolic, L., Metz, T.O. and Peck, S.C. (2014) Decreased abundance of type III secretion system-inducing signals in *Arabidopsis* mkp1 enhances resistance against *Pseudomonas syringae*. *Proc. Natl Acad. Sci. USA*, **111**, 6846–6851.

Andreote, F.D. and Pereira E Silva, M.C. (2017) Microbial communities associated with plants: learning from nature to apply it in agriculture. *Curr. Opin. Microbiol.* **37**, 29–34.

Antony, G., Zhou, J., Huang, S., Li, T., Liu, B., White, F. and Yang, B. (2010) Rice xa13 recessive resistance to bacterial blight is defeated by induction of the disease susceptibility gene *Os-11N3*. *Plant Cell*, **22**, 3864–3876.

Araya, T., Bohner, A. and von Wirén, N. (2015) Extraction of apoplastic wash fluids and leaf petiole exudates from leaves of *Arabidopsis thaliana*. *Bio-Protoc.* **5**, e1691.

Asai, Y., Kobayashi, Y. and Kobayashi, I. (2016) Increased expression of the tomato *SlSWEET15* gene during grey mold infection and the possible involvement of the sugar efflux to apoplasm in the disease susceptibility. *J. Plant Pathol. Microbiol.* **7**, 1–8.

Barker, L., Kühn, C., Weise, A. *et al.* (2000) SUT2, a putative sucrose sensor in sieve elements. *Plant Cell*, **12**, 1153–1164.

Behlau, F., Hong, J.C., Jones, J.B. and Graham, J.H. (2013) Evidence for acquisition of copper resistance genes from different sources in citrus-associated Xanthomonads. *Phytopathology*, **103**, 409–418.

Bezrutczyk, M., Hartwig, T., Horschman, M., Char, S.N., Yang, J., Yang, B., Frommer, W. and Sosso, D. (2017) Impaired phloem loading in genome-edited triple knock-out mutants of SWEET13 sucrose transporters. *bioRxiv*. Available at: http://biorxiv.org/content/early/2017/10/03/197921. abstract.

Bi, H. and Yang, B. (2017) Gene editing with TALEN and CRISPR/Cas in rice. *Prog. Mol. Biol. Transl. Sci.* **149**, 81–98.

Blanvillain-Baufumé, S., Reschke, M., Solé, M. *et al.* (2017) Targeted promoter editing for rice resistance to *Xanthomonas oryzae* pv. *oryzae* reveals differential activities for *SWEET14*-inducing TAL effectors. *Plant Biotechnol. J.* **15**, 306–317.

Boch, J., Scholze, H., Schornack, S., Landgraf, A., Hahn, S., Kay, S., Lahaye, T., Nickstadt, A. and Bonas, U. (2009) Breaking the code of DNA binding specificity of TAL-type III effectors. *Science*, **326**, 1509–1512.

Bogdanove, A.J. and Voytas, D.F. (2011) TAL effectors: customizable proteins for DNA targeting. *Science*, **333**, 1843–1846.

Boorer, K.J., Loo, D.D. and Wright, E.M. (1994) Steady-state and pre-steady-state kinetics of the H+/hexose cotransporter (STP1) from *Arabidopsis thaliana* expressed in Xenopus oocytes. *J. Biol. Chem.* **269**, 20417–20424.

Boorer, K.J., Loo, D.D.F., Frommer, W.B. and Wright, E.M. (1996) Transport mechanism of the cloned potato H+/sucrose cotransporter StSUT1. *J. Biol. Chem.* **271**, 25139–25144.

Boutrot, F. and Zipfel, C. (2017) Function, discovery, and exploitation of plant pattern recognition receptors for broad-spectrum disease resistance. *Annu. Rev. Phytopathol.* **55**, 257–286.

Brandsch, M. (2013) Drug transport via the intestinal peptide transporter PepT1. *Curr. Opin. Pharmacol.* **13**, 881–887.

Bürkle, L., Hibberd, J.M., Quick, W.P., Kühn, C., Hirner, B. and Frommer, W.B. (1998) The H^+-sucrose cotransporter NtSUT1 is essential for sugar export from tobacco leaves. *Plant Physiol.* **118**, 59–68.

Carpaneto, A., Geiger, D., Bamberg, E., Sauer, N., Fromm, J. and Hedrich, R. (2005) Phloem-localized, proton-coupled sucrose carrier ZmSUT1 mediates sucrose efflux under the control of the sucrose gradient and the proton motive force. *J. Biol. Chem.* **280**, 21437–21443.

Chandran, D. (2015) Co-option of developmentally regulated plant SWEET transporters for pathogen nutrition and abiotic stress tolerance. *IUBMB Life*, **67**, 461–471.

Chardon, F., Bedu, M., Calenge, F. *et al.* (2013) Leaf fructose content is controlled by the vacuolar transporter SWEET17 in *Arabidopsis*. *Curr. Biol.* **23**, 697–702.

Chen, L.Q., Hou, B.H., Lalonde, S. *et al.* (2010) Sugar transporters for intercellular exchange and nutrition of pathogens. *Nature*, **468**, 527–532.

Chen, L.Q., Qu, X.Q., Hou, B.H., Sosso, D., Osorio, S., Fernie, A.R. and Frommer, W.B. (2012) Sucrose efflux mediated by SWEET proteins as a key step for phloem transport. *Science*, **335**, 207–211.

Chen, L.-Q., Cheung, L.S., Feng, L., Tanner, W. and Frommer, W.B. (2015a) Transport of sugars. *Annu. Rev. Biochem.* **84**, 865–894.

Chen, L.-Q., Lin, I.W., Qu, X.-Q., Sosso, D., McFarlane, H.E., Londoño, A., Samuels, A.L. and Frommer, W.B. (2015b) A cascade of sequentially expressed sucrose transporters in the seed coat and endosperm provides nutrition for the *Arabidopsis* embryo. *Plant Cell*, **27**, 607–619.

Chen, H.-Y., Huh, J.-H., Yu, Y.-C., Ho, L.-H., Chen, L.-Q., Tholl, D., Frommer, W.B. and Guo, W.-J. (2015c) The *Arabidopsis* vacuolar sugar transporter SWEET2 limits carbon sequestration from roots and restricts *Pythium* infection. *Plant J.* **83**, 1046–1058.

Chiba, Y., Shimizu, T., Miyakawa, S., Kanno, Y., Koshiba, T., Kamiya, Y. and Seo, M. (2015) Identification of *Arabidopsis thaliana* NRT1/PTR FAMILY (NPF) proteins capable of transporting plant hormones. *J. Plant. Res.* **128**, 679–686.

Chong, J., Piron, M.-C., Meyer, S., Merdinoglu, D., Bertsch, C. and Mestre, P. (2014) The SWEET family of sugar transporters in grapevine: VvSWEET4 is involved in the interaction with *Botrytis cinerea*. *J. Exp. Bot.* **65**, 6589–6601.

Chu, Z., Yuan, M., Yao, J. *et al.* (2006) Promoter mutations of an essential gene for pollen development result in disease resistance in rice. *Genes Dev.* **20**, 1250–1255.

Cohn, M., Bart, R.S., Shybut, M. *et al.* (2014) *Xanthomonas axonopodis* virulence is promoted by a transcription activator-like effector-mediated induction of a SWEET sugar transporter in cassava. *Mol. Plant-Microbe Interact.* **27**, 1186–1198.

Cox, K.L., Meng, F., Wilkins, K.E. *et al.* (2017) TAL effector driven induction of a SWEET gene confers susceptibility to bacterial blight of cotton. *Nat. Commun.* **8**, 15588.

Ding, P. and Jones, J.D.G. (2017) Mis-placed congeniality: when pathogens ask their plant hosts for another drink. *Dev. Cell*, **40**, 116–117.

Fotopoulos, V., Gilbert, M.J., Pittman, J.K., Marvier, A.C., Buchanan, A.J., Sauer, N., Hall, J.L. and Williams, L.E. (2003) The monosaccharide transporter gene, *AtSTP4*, and the cell-wall invertase, Atbetafruct1, are induced in *Arabidopsis* during infection with the fungal biotroph *Erysiphe cichoracearum*. *Plant Physiol.* **132**, 821–829.

Gamas, P., Niebel Fde, C., Lescure, N. and Cullimore, J. (1996) Use of a subtractive hybridization approach to identify new Medicago truncatula genes induced during root nodule development. *Mol. Plant Microbe Interact.* **9**, 233–242.

Gebauer, P., Korn, M., Engelsdorf, T., Sonnewald, U., Koch, C. and Voll, L.M. (2017) Sugar accumulation in leaves of *Arabidopsis sweet11/sweet12* double mutants enhances priming of the salicylic acid-mediated defense response. *Front. Plant Sci.* **8**. Available at: http://www.ncbi.nlm.nih.gov/pmc/articles/PMC5550771/ (accessed 5 September 2017).

Gómez-Ariza, J., Campo, S., Rufat, M., Estopà, M., Messeguer, J., Segundo, B.S. and Coca, M. (2007) Sucrose-mediated priming of plant defense responses and broad-spectrum disease resistance by overexpression of the maize pathogenesis-related PRms protein in rice plants. *Mol. Plant Microbe Interact.* **20**, 832–842.

Gottwald, J.R., Krysan, P.J., Young, J.C., Evert, R.F. and Sussman, M.R. (2000) Genetic evidence for the in planta role of phloem-specific plasma membrane sucrose transporters. *Proc. Natl Acad. Sci. USA*, **97**, 13979–13984.

Guo, W.-J., Nagy, R., Chen, H.-Y., Pfrunder, S., Yu, Y.-C., Santelia, D., Frommer, W.B. and Martinoia, E. (2014) SWEET17, a facilitative transporter, mediates fructose transport across the tonoplast of *Arabidopsis* roots and leaves. *Plant Physiol.* **164**, 777–789.

Hacquard, S., Garrido-Oter, R., González, A. *et al.* (2015) Microbiota and host nutrition across plant and animal kingdoms. *Cell Host Microbe*, **17**, 603–616.

Herbers, K. and Sonnewald, U. (1998) Altered gene expression brought about by inter- and intracellularly formed hexoses and its possible implications for plant-pathogen interactions. *J. Plant. Res.* **111**, 323–328.

Herbers, K., Meuwly, P., Frommer, W.B., Metraux, J.P. and Sonnewald, U. (1996) Systemic acquired resistance mediated by the ectopic expression of invertase: possible hexose sensing in the secretory pathway. *Plant Cell*, **8**, 793–803.

Ho, C.H., Lin, S.H., Hu, H.C. and Tsay, Y.F. (2009) CHL1 functions as a nitrate sensor in plants. *Cell*, **138**, 1184–1194.

Horsfall, J.G. and Dimond, A.E. (1957) Interactions of tissue sugar, growth substances, and disease susceptibility. *Z. Pflanzenkr. Pflanzenschutz.* **64**, 415–421.

Hutin, M., Sabot, F., Ghesquière, A., Koebnik, R. and Szurek, B. (2015) A knowledge-based molecular screen uncovers a broad-spectrum *OsSWEET14* resistance allele to bacterial blight from wild rice. *Plant J. Cell Mol. Biol.* **84**, 694–703.

Jones, J.D.G. and Dangl, J.L. (2006) The plant immune system. *Nature*, **444**, 323–329.

Jones, J.D.G., Vance, R.E. and Dangl, J.L. (2016) Intracellular innate immune surveillance devices in plants and animals. *Science*, **354**, aaf6395.

Kanno, Y., Hanada, A., Chiba, Y., Ichikawa, T., Nakazawa, M., Matsui, M., Koshiba, T., Kamiya, Y. and Seo, M. (2012) Identification of an abscisic acid transporter by functional screening using the receptor complex as a sensor. *Proc. Natl Acad. Sci. USA*, **109**, 9653–9658.

Kanno, Y., Oikawa, T., Chiba, Y. *et al.* (2016) AtSWEET13 and AtSWEET14 regulate gibberellin-mediated physiological processes. *Nat. Commun.* **7**, 13245.

Kasahara, T. and Kasahara, M. (1996) Expression of the rat GLUT1 glucose transporter in the yeast Saccharomyces cerevisiae. *Biochem. J.* **315**(Pt 1), 177–182.

Kryvoruchko, I.S., Sinharoy, S., Torres-Jerez, I. *et al.* (2016) MtSWEET11, a nodule-specific sucrose transporter of *Medicago truncatula*. *Plant Physiol.* **171**, 554–565.

Laha, G.S., Sailaja, B., Srinivas Prasad, M. *et al.* (2016) *Changes in Rice Disease Scenario in India: An Analysis from Production Oriented Survey*. Rajendranagar, Hyderabad: ICAR-Indian Institute of Rice Research. Available at: http://www.academia.edu/25006198/Changes_in_Rice_Disease_Scenario_in_India_An_Analysis_from_Production_Oriented_Survey._Technical_Bulletin_No._91_ICAR-IIRR_Hyderabad-500_030_Telangana_State_India_95_pp (accessed 25 February 2017).

Lemonnier, P., Gaillard, C., Veillet, F., Verbeke, J., Lemoine, R., Coutos-Thévenot, P. and La Camera, S. (2014) Expression of *Arabidopsis* sugar transport protein STP13 differentially affects glucose transport activity and basal resistance to *Botrytis cinerea*. *Plant Mol. Biol.* **85**, 473–484.

Li, T., Huang, S., Zhou, J. and Yang, B. (2013) Designer TAL effectors induce disease susceptibility and resistance to *Xanthomonas oryzae* pv. *oryzae* in rice. *Mol. Plant*, **6**, 781–789.

Lin, I.W., Sosso, D., Chen, L.-Q. *et al.* (2014) Nectar secretion requires sucrose phosphate synthases and the sugar transporter SWEET9. *Nature*, **508**, 546–549.

Liu, Q., Yuan, M., Zhou, Y., Li, X., Xiao, J. and Wang, S. (2011) A paralog of the MtN3/saliva family recessively confers race-specific resistance to *Xanthomonas oryzae* in rice. *Plant Cell Environ.* **34**, 1958–1969.

Lohaus, G., Pennewiss, K., Sattelmacher, B., Hussmann, M. and Hermann Muehling, K. (2001) Is the infiltration-centrifugation technique appropriate for the isolation of apoplastic fluid? A critical evaluation with different plant species. *Physiol. Plant.* **111**, 457–465.

Lore, J.S., Vikal, Y., Hunjan, M.S., Goel, R.K., Bharaj, T.S. and Raina, G.L. (2011) Genotypic and pathotypic diversity of *Xanthomonas oryzae* pv. *oryzae*, the cause of bacterial blight of rice in Punjab state of India. *J. Phytopathol.* **159**, 479–487.

Manck-Götzenberger, J. and Requena, N. (2016) Arbuscular mycorrhiza symbiosis induces a major transcriptional reprogramming of the potato SWEET sugar transporter family. *Front. Plant Sci.* **7**. Available at: http://www.ncbi.nlm.nih.gov/pmc/articles/PMC4830831/ (accessed 10 August 2017).

Mishra, D., Vishnupriya, M.R., Anil, M.G., Konda, K., Raj, Y. and Sonti, R.V. (2013) Pathotype and genetic diversity amongst Indian isolates of *Xanthomonas oryzae* pv. *oryzae*. *PLoS ONE*, **8**, e81996.

Moore, J.W., Herrera-Foessel, S., Lan, C. *et al.* (2015) A recently evolved hexose transporter variant confers resistance to multiple pathogens in wheat. *Nat. Genet.* **47**, 1494–1498.

Müller, D.B., Vogel, C., Bai, Y. and Vorholt, J.A. (2016) The plant microbiota: systems-level insights and perspectives. *Annu. Rev. Genet.* **50**, 211–234.

Nour-Eldin, H.H., Andersen, T.G., Burow, M. *et al.* (2012) NRT/PTR transporters are essential for translocation of glucosinolate defence compounds to seeds. *Nature*, **488**, 531–534.

Oerke, E.C. (2006) Crop losses to pests. *J. Agric. Sci.* **144**, 31–43.

Ogawa, T., Lin, L., Tabien, R.E. and Kush, G.S. (1987) A new recessive gene for resistance to bacterial blight of rice. *Rice Genet. Newsl.* **4**, 98–100.

Okumoto, S. (2010) Imaging approach for monitoring cellular metabolites and ions using genetically encoded biosensors. *Curr. Opin. Biotechnol.* **21**, 45–54.

Patrick, J.W. (1989) Solute efflux from the host at plant microorganism interfaces. *Aust. J. Plant Physiol.* **16**, 53–67.

Popp, J. and Hantos, K. (2011) The impact of crop protection on agricultural production. *Stud. Agric. Econ.* **113**, 47–66.

Puig, S., Lee, J., Lau, M. and Thiele, D.J. (2002) Biochemical and genetic analyses of yeast and human high affinity copper transporters suggest a conserved mechanism for copper uptake. *J. Biol. Chem.* **277**, 26021–26030.

Rentsch, D., Laloi, M., Rouhara, I., Schmelzer, E., Delrot, S. and Frommer, W.B. (1995) *NTR1* encodes a high affinity oligopeptide transporter in *Arabidopsis*. *FEBS Lett.* **370**, 264–268.

Riesmeier, J.W., Willmitzer, L. and Frommer, W.B. (1992) Isolation and characterization of a sucrose carrier cDNA from spinach by functional expression in yeast. *EMBO J.* **11**, 4705–4713.

Riesmeier, J.W., Willmitzer, L. and Frommer, W.B. (1994) Evidence for an essential role of the sucrose transporter in phloem loading and assimilate partitioning. *EMBO J.* **13**, 1–7.

Rolfe, S.A. and Scholes, J.D. (2010) Chlorophyll fluorescence imaging of plant-pathogen interactions. *Protoplasma*, **247**, 163–175.

Römer, P., Recht, S., Strauß, T., Elsaesser, J., Schornack, S., Boch, B., Wang, S. and Lahaye, T. (2010) Promoter elements of rice susceptibility

genes are bound and activated by specific TAL effectors from the bacterial blight pathogen, *Xanthomonas oryzae* pv. *oryzae*. *New Phytol.* **187**, 1048–1057.

Sauer, N. and Tanner, W. (1989) The hexose carrier from *Chlorella*. cDNA cloning of a eucaryotic H^+cotransporter. *FEBS Lett.* **259**, 43–46.

Sauer, N., Friedländer, K. and Gräml-Wicke, U. (1990) Primary structure, genomic organization and heterologous expression of a glucose transporter from *Arabidopsis thaliana*. *EMBO J.* **9**, 3045–3050.

Schüssler, A., Martin, H., Cohen, D., Fitz, M. and Wipf, D. (2006) Characterization of a carbohydrate transporter from symbiotic glomeromycotan fungi. *Nature*, **444**, 933–936.

Siebke, K. and Weis, E. (1995) Assimilation images of leaves of Glechoma hederacea: analysis of non-synchronous stomata related oscillations. *Planta*, **196**, 155–165.

Slewinski, T.L., Meeley, R. and Braun, D.M. (2009) Sucrose transporter1 functions in phloem loading in maize leaves. *J. Exp. Bot.* **60**, 881–892.

Sosso, D., Luo, D., Li, Q.-B. *et al.* (2015) Seed filling in domesticated maize and rice depends on SWEET-mediated hexose transport. *Nat. Genet.* **47**, 1489–1493.

Stauber, J.L., Loginicheva, E. and Schechter, L.M. (2012) Carbon source and cell density-dependent regulation of type III secretion system gene expression in *Pseudomonas syringae* pathovar tomato DC3000. *Res. Microbiol.* **163**, 531–539.

Streubel, J., Pesce, C., Hutin, M., Koebnik, R., Boch, J. and Szurek, B. (2013) Five phylogenetically close rice SWEET genes confer TAL effector-mediated susceptibility to *Xanthomonas oryzae* pv. *oryzae*. *New Phytol.* **200**, 808–819.

Succurro, A., Moejes, F.W. and Ebenhöh, O. (2017) A diverse community to study communities: integration of experiments and mathematical models to study microbial consortia. *J. Bacteriol.* **199**, e00865–16.

Sugiyama, A., Saida, Y., Yoshimizu, M., Takanashi, K., Sosso, D., Frommer, W.B. and Yazaki, K. (2017) Molecular characterization of LjSWEET3, a sugar transporter in nodules of *Lotus japonicus*. *Plant Cell Physiol.* **58**, 298–306.

Sun, Y., Reinders, A., LaFleur, K.R., Mori, T. and Ward, J.M. (2010) Transport activity of rice sucrose transporters OsSUT1 and OsSUT5. *Plant Cell Physiol.* **51**, 114–795.122.

Sutton, P.N., Henry, M.J. and Hall, J.L. (1999) Glucose, and not sucrose, is transported from wheat to wheat powdery mildew. *Planta*, **208**, 426–430.

Sutton, P.N., Gilbert, M.J., Williams, L.E. and Hall, J.L. (2007) Powdery mildew infection of wheat leaves changes host solute transport and invertase activity. *Physiol. Plant.* **129**, 787–795.

Tadege, M., Bucher, M., Stähli, W., Suter, M., Dupuis, I. and Kuhlemeier, C. (1998) Activation of plant defense responses and sugar efflux by expression of pyruvate decarboxylase in potato leaves. *Plant J.* **16**, 661–671.

Thevelein, J.M. and Voordeckers, K. (2009) Functioning and evolutionary significance of nutrient transceptors. *Mol. Biol. Evol.* **26**, 2407–2414.

Udvardi, M.K., Yang, L.-J.O., Young, S. and Day, D.A. (1990) Sugar and amino acid transport across symbiotic membranes from soybean nodules. *Mol. Plant Microbe Interact.* **3**, 334–340.

Voegele, R.T. and Mendgen, K. (2003) Rust haustoria: nutrient uptake and beyond. *New Phytol.* **159**, 93–100.

Wahl, R., Wippel, K., Goos, S., Kamper, J. and Sauer, N. (2010) A novel high-affinity sucrose transporter is required for virulence of the plant pathogen *Ustilago maydis*. *PLoS Biol.* **8**, e1000303.

Wengelnik, K., Marie, C., Russel, M. and Bonas, U. (1996) Expression and localization of HrpA1, a protein of Xanthomonas campestris pv. vesicatoria essential for pathogenicity and induction of the hypersensitive reaction. *J. Bacteriol.* **178**, 1061–1069.

White, F.F. and Frommer, W. (2015) Deciphering durable resistance one R gene at a time. *Nat. Genet.* **47**, 1376–1377.

Wieczorke, R., Krampe, S., Weierstall, T., Freidel, K., Hollenberg, C.P. and Boles, E. (1999) Concurrent knock-out of at least 20 transporter genes is required to block uptake of hexoses in *Saccharomyces cerevisiae*. *FEBS Lett.* **464**, 123–128.

Yamada, K., Saijo, Y., Nakagami, H. and Takano, Y. (2016) Regulation of sugar transporter activity for antibacterial defense in Arabidopsis. *Science*, **354**, 1427–1430.

Yang, B., Sugio, A. and White, F.F. (2006) *Os8N3* is a host disease-susceptibility gene for bacterial blight of rice. *Proc. Natl Acad. Sci. USA*, **103**, 10503–10508.

Yang, J., Luo, D., Yang, B., Frommer, W. and Eom, J.-S. (2017) SWEET11 and 15 as key players in seed filling in rice. *bioRxiv*. Available at: http://biorxiv.org/content/early/2017/10/04/198325.abstract.

Yu, Y., Streubel, J., Balzergue, S., Champion, A., Boch, J., Koebnik, R., Feng, J., Verdier, V. and Szurek, B. (2011) Colonization of rice leaf blades by an African strain of *Xanthomonas oryzae* pv. *oryzae* depends on a new TAL effector that induces the rice nodulin-3 *Os11N3* gene. *Mol. Plant-Microbe Interact.* **24**, 1102–1113.

Yuan, M., Chu, Z., Li, X., Xu, C. and Wang, S. (2010) The bacterial pathogen *Xanthomonas oryzae* overcomes rice defenses by regulating host copper redistribution. *Plant Cell*, **22**, 3164–3176.

Yuan, M., Li, X., Xiao, J. and Wang, S. (2011) Molecular and functional analyses of COPT/Ctr-type copper transporter-like gene family in rice. *BMC Plant Biol.* **11**, 69.

Yuan, M., Zhao, J., Huang, R., Li, X., Xiao, J. and Wang, S. (2014) Rice MtN3/saliva/SWEET gene family: evolution, expression profiling, and sugar transport. *J. Integr. Plant Biol.* **56**, 559–570.

Zhou, J., Peng, Z., Long, J. *et al.* (2015) Gene targeting by the TAL effector PthXo2 reveals cryptic resistance gene for bacterial blight of rice. *Plant J. Cell Mol. Biol.* **82**, 632–643.

OUTLOOK

Introduction

Though the work described in this dissertation represents significant progress toward our understanding of sugar transport and phloem loading in maize, these results also point to new questions about leaf development, anatomy, and sucrose transport. Additionally, the single-cell sequencing technology used has only recently been applied to plant tissues, and several types of technical improvements could be made. (I-II) In the scRNA-seq dataset described in Bezrutczyk et al., 2020, only mesophyll and bundle sheath cells and a small number of putative companion cells were recovered. Therefore, modifications to existing methods will be necessary to sequence the transcriptomes of representative cell populations from the vasculature and epidermis if we are to establish a single-cell atlas of the maize leaf. Increasing the overall number of cells would both increase the likelihood of obtaining sufficient numbers of other cell types, and provide more statistical power when describing rare cell populations. I propose modifications to resolve these technical issues. (III-VI) There are unanswered questions regarding how cells of the leaf involved in sugar transport acquire their identity during development, as it appears that the ^{ab}BS and phloem parenchyma may share some characteristics in the rank-2 intermediate veins in maize. It is not clear what benefit abaxial bundle sheath cell localization of sugar transporters confers the maize plant, and it is not known how prevalent this phenomenon is among other species. I propose experiments to address these open questions.

I. Strategies to improve cell type diversity in future maize leaf scRNA-seq datasets

One major limitation to this study is that only mesophyll and bundle sheath cells were recovered in this scRNA-seq dataset, and because of this, we have not been able to characterize the transcriptomes of the cells of the maize vasculature. The first major challenge to accessing the vascular cells is the presence of a suberin-lignin sheath encapsulating the BS and vasculature (Evert et al., 1985, 1996), which prevents efficient protoplast release of these cell types. Because mesophyll cells are protoplasted far more efficiently, they make up the majority of cells in all leaf scRNA-seq datasets that have been produced, unless specifically selected against (Kim et al., 2020; Lopez-Anido et al., 2020). I propose four modifications to the existing protocol to improve the cell diversity in future maize leaf single cell partitioning events. (1) Enzymes which may partially degrade cell walls and improve the release of cells include manganese peroxidase, xylanase, xyloglucanse, and mannanase, as it was shown that

these enzymes were effective for permeabilizing diverse plant tissues for spatial transcriptomic analysis (Giacomello et al., 2017). (2) Pre-partitioning cell selection may allow us to reduce the excess of mesophyll cells released: fluorescence activated cell sorting (FACS) of cells isolated from plants expressing vasculature and bundle sheath-specific fluorescent proteins would allow us to enrich for these cells, and eliminate mesophyll cells. Since such transgenic lines are not available, they first would need to be generated. (3) An alternative method to reduce the number of mesophyll cells in the dataset may be to develop magnetic beads coated with antibodies for a mesophyll-specific cell surface protein. Such a method has been employed in animal cell cultures, using annexin-V coated magnetic beads to remove apoptotic cells from suspensions (Annexin-V Microbead Kit, Miltenyi Biotec, Bergisch-Gladbach, Germany). Though examples of maize mesophyll cell-specific surface proteins are not readily found in literature, a search for transporters or receptor proteins which are common to all mesophyll cells in the maize leaf scRNA-seq dataset may yield several candidate proteins. (4) It is important to note that several attempts at cDNA synthesis after partitioning yielded an extremely low concentration of cDNA; several experiments in which Arabidopsis leaf and SAM tissue, rice leaf, and barley leaf were partitioned also resulted in extremely low cDNA yield (personal correspondence). Low cDNA yield may be the result of sub-optimal viability of protoplasts, which must be rigorously evaluated before partitioning.

II. Strategies to improve the number of cells in scRNA-seq maize leaf datasets

Increasing the number of cells sequenced will make it more likely that more cell types can be obtained, as well as provide more statistical power when comparing populations. The number of cells that can be partitioned in a single 10x Genomics Chromium experiment is limited because the ‘doublet’ rate climbs linearly with an increasing number of cells applied to the chip. For example, it has been shown that if 10,000 cells are applied, up to 7.6% of the resulting GEMs are expected to contain not one but two cells. Doublets can be difficult to differentiate from singlets in the downstream analysis pipeline because existing algorithms rely on the assumption that a doublet will contain twice as much mRNA as a singlet, or are strongly dependent on the quality of clustering (Bach et al., 2017; Dahlin et al., 2018). Therefore, it is preferable to load fewer than 10,000 cells to minimize the occurrence of doublets. Methods that do not involve droplet partitioning such as SPLIT-seq (Rosenberg et al., 2018) rely instead on combinatorial barcoding of split-pools of cells in a series of 96-well plates, and have been used to sequence the individual transcriptomes of hundreds of thousands of cells. This method is limited only by the number of barcoding rounds, as increasing the number of barcoding

rounds or number of wells allows for more cells to be partitioned. However, split-pool combinatorial barcoding has not yet been performed in plant cells, and because this method requires the uptake and ligation of barcodes within intact individual cells, the protocol may need to be optimized for protoplasts.

III. Implications for ^{ab}BS-specific SWEET localization.

It is not clear what advantage ^{ab}BS cell SWEET13a, b, and c localization may confer the maize plant, given that the homologs of SWEET13a, b, and c are found in the phloem parenchyma in Arabidopsis. In rank-1 and major veins, which are mostly involved in long distance transport of photoassimilates rather than loading, SWEETs are predominantly expressed in the phloem parenchyma, as in Arabidopsis. In transmission electron microscopy images in which cell types can be distinguished by cytosolic features, it appears that the ^{ab}BS cells are located directly adjacent to companion cells in many veins (Evert et al., 1978, 1985, 1996). Though this observation has been made based on a very limited number of images, it is possible that the simplest explanation for enrichment of transporter genes in ^{ab}BS is that ^{ab}BS cells are well-positioned to transport sucrose into the apoplasm adjacent to companion cells, rendering phloem parenchyma-mediated transport unnecessary. The fact that Arabidopsis phloem parenchyma display transfer cell invaginations (Arun Chinnappa et al., 2013) suggests that surface area may be a limiting factor for phloem loading in this species. It is possible that to increase the surface area across which sucrose can be transported to the apoplasmic space, maize exports sucrose from ^{ab}BS cells directly, and also from phloem parenchyma in a minority of veins. However, increasing the portion of apoplasmic space across which sucrose is transported raises a potential problem: it is thought that sucrose export via the phloem

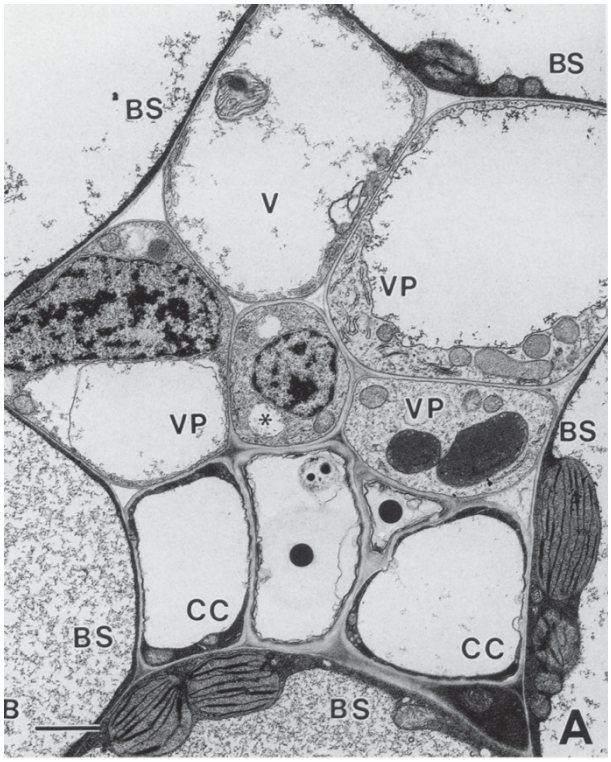

Figure 1. Electronmicrograph of immature rank-2 intermediate vein. Cell wall space shared between bundle sheath (BS) cells and companion cells (CC) is more extensive than between phloem parenchyma (VP) and companion cells. (Evert et al., 1996)

parenchyma serves to maintain extracellular sucrose in a small area adjacent to the companion cell, to prevent sucrose being swept away in the transpiration stream of water flowing out of xylem vessels and xylem parenchyma (Keunecke et al., 2001). However, SUT1 in maize is thought to be involved in sucrose retrieval, and may prevent sucrose loss via the transpiration stream by active uptake into adjacent parenchyma cells (Baker et al., 2016). The transformation of maize with sucrose-responsive FRET sensors could be used to estimate both the concentration and distribution pattern of sucrose in the vascular apoplasmic space, which would allow us to distinguish between these hypotheses. Additionally, because the outer tangential and radial walls of BS cells are suberized, it is likely that transport proteins will show a polarized localization pattern on the vascular-facing side of the BS only, and potentially only directly adjacent to cells to which sugars are exported. Transforming maize plants with a GFP translational fusion driven by the native SWEET13a, b, or c promoter may allow us to determine if SWEETs show a polarized pattern of localization within the BS or phloem parenchyma cells.

V. Do mobile signals in the developing leaf govern vascular cell fate?

Many of the genes encoding transporters which are expressed in the phloem parenchyma of Arabidopsis are expressed in the ^{ab}BS cells of maize rank-2 intermediate veins (Kim et al., 2020), including clade III SWEET sucrose transporters and UmamiT amino acid transporters, suggesting ^{ab}BS cells have acquired aspects of phloem parenchyma identity. In both maize and Arabidopsis, BS and phloem parenchyma cell lineages are thought to diverge relatively early in vein development (Bosabalidis et al., 1994; Dengler et al., 1985; Esau, 1943), making it unlikely that this expression pattern is determined by cell lineage. Instead, positional cues may determine which cells adjacent to the SE-CC express the genes involved in nutrient transport. Mobile signals are known to be critical for patterning of root vasculature in Arabidopsis (De Rybel et al., 2016), and it is possible that positional cues, possibly originating in companion cells, elicit expression of transporters in adjacent cells. Small peptides, receptor kinases, and mobile transcription factors have all been shown to be involved in cell-to-cell signaling during plant development (Van Norman et al., 2011). Specifically, it is possible that a transcription factor which is necessary for the expression of SWEETs and other transporters came under the influence of an abaxial and BS-specific cue; the putative transport transcriptional network may then be expressed in abaxial BS cells. If we are able to obtain single cell transcriptomes for the vascular cells including companion cells, this would facilitate the search for potential mobile

signals and receptors that determine which cells express transcriptional networks necessary for phloem loading.

VI. IS ^{ab}BS-specific localization of SWEETs important for C4 syndrome?

Given that rank-2 intermediate veins are unique to C4 monocots, and that the BS-specific localization of SWEETs was most prevalent in rank-2 intermediate veins, it is possible that this phenomenon may be common to other C4 monocots. In order to determine if this mechanism is generalizable to other C4 monocots, I propose performing in situ hybridization on the homologs of *SWEET13a*, *b*, and *c* on other species with varying evolutionary distance from maize. Of all major crop species, *Sorghum bicolor* is the most closely related to maize, and will be the first target for *in situ* hybridization of the SWEET13 homologs: *SbSWEET8-1*, *8-2*, and *8-3* (Mizuno et al., 2016). Alternatively, it is possible that ^{ab}BS localization of SWEETs in maize arose during the domestication process to facilitate greater sucrose flux from the leaf. To evaluate this alternative hypothesis, we will determine which cell type contains mRNAs for *SWEET13a*, *b*, and *c* in the leaf of *Zea mays* spp. *parviglumis*: the wild ancestor of maize, also known as teosinte.

Understanding the prevalence of this phenomenon will help us determine whether ^{ab}BS-mediated phloem loading is important for C4 photosynthesis. If so, this discovery may have implications for the engineering of Kranz anatomy for C4 photosynthesis in C3 crops such as rice. Because rice likely employs an apoplasmic phloem loading mechanism, it is possible that engineering C4 rice will require modifications to the phloem loading mechanism to accommodate an increased flux of photoassimilates. To determine if it is possible to engineer apoplasmic phloem loading in rice, rice plants could be transformed with ZmSWEET13a, b, and c and ZmSUT1 under their native promoters as an apoplasmic phloem loading cassette, and the phenotype of transformed rice plants assessed with photosynthesis measurements of leaves, evaluation of the plants' gross morphology, and quantification of yield compared to wild-type. Given that ^{ab}BS-mediated phloem loading mechanism is employed by one of the most productive crops in the world, it is possible that engineering similar mechanisms in other crops will increase photoassimilate transport efficiency, thereby increasing yield.

BIBLIOGRAPHY

Arun Chinnappa, K.S., Nguyen, T.T.S., Hou, J., Wu, Y., and McCurdy, D.W. (2013). Phloem parenchyma transfer cells in Arabidopsis - an experimental system to identify transcriptional regulators of wall ingrowth formation. Front. Plant Sci. *4*, 102–102.

Bach, K., Pensa, S., Grzelak, M., Hadfield, J., Adams, D.J., Marioni, J.C., and Khaled, W.T. (2017). Differentiation dynamics of mammary epithelial cells revealed by single-cell RNA sequencing. Nat. Commun. *8*, 2128.

Baker, R.F., Leach, K.A., Boyer, N.R., Swyers, M.J., Benitez-Alfonso, Y., Skopelitis, T., Luo, A., Sylvester, A., Jackson, D., and Braun, D.M. (2016). Sucrose transporter ZmSut1 expression and localization uncover new insights into sucrose phloem loading. Plant Physiol. *172*, 1876–1898.

Bezrutczyk, M., Hartwig, T., Horschman, M., Char, S.N., Yang, J., Yang, B., Frommer, W.B., and Sosso, D. (2018a). Impaired phloem loading in *zmsweet13a,b,c* sucrose transporter triple knock-out mutants in *Zea mays*. New Phytol. *218*, 594–603.

Bezrutczyk, M., Yang, J., Eom, J.-S., Prior, M., Sosso, D., Hartwig, T., Szurek, B., Oliva, R., Vera-Cruz, C., White, F.F., et al. (2018b). Sugar flux and signaling in plant–microbe interactions. Plant J. *93*, 675–685.

Bezrutczyk, M., Zöllner, N.R., Kruse, C.P.S., Hartwig, T., Lautwein, T., Köhrer, K., Frommer, W.B., and Kim, J.-Y. (2020). Phloem loading via the abaxial bundle sheath cells in maize leaves. BioRxiv 2020.09.06.284943.

Bosabalidis, A.M., Evert, R.F., and Russin, W.A. (1994). Ontogeny of the vascular bundles and contiguous tissues in the maize leaf blade. Am. J. Bot. *81*, 745–752.

Botha, C.E.J. (2013). A tale of two neglected systems-structure and function of the thin- and thick-walled sieve tubes in monocotyledonous leaves. Front. Plant Sci. *4*, 297.

Butler, A., Hoffman, P., Smibert, P., Papalexi, E., and Satija, R. (2018). Integrating single-cell transcriptomic data across different conditions, technologies, and species. Nat. Biotechnol. *36*, 411–420.

Candela, H., Johnston, R., Gerhold, A., Foster, T., and Hake, S. (2008). The *milkweed pod1* gene encodes a KANADI protein that is required for abaxial/adaxial patterning in maize leaves. Plant Cell *20*, 2073.

Canny, M.J., and McCully, M.E. (1986). Locating water-soluble vital stains in plant tissues by freeze-substitution and resin-embedding. J. Microsc. *142*, 63–70.

Capeheart, T., Liefert, Olga, Olson, D., and McConnel, M. (2020). Feed Outlook (USDA).

Carraro, N., Forestan, C., Canova, S., Traas, J., and Varotto, S. (2006). *ZmPIN1a* and *ZmPIN1b* encode two novel putative candidates for polar auxin transport and plant architecture determination of maize. Plant Physiol. *142*, 254.

Chang, Y.-M., Liu, W.-Y., Shih, A.C.-C., Shen, M.-N., Lu, C.-H., Lu, M.-Y.J., Yang, H.-W., Wang, T.-Y., Chen, S.C.-C., Chen, S.M., et al. (2012). Characterizing regulatory and functional differentiation between maize mesophyll and bundle sheath cells by transcriptomic analysis. Plant Physiol. *160*, 165.

Chen, L.Q., Hou, B.H., Lalonde, S., Takanaga, H., Hartung, M.L., Qu, X.Q., Guo, W.J., Kim, J.G., Underwood, W., Chaudhuri, B., et al. (2010). Sugar transporters for intercellular exchange and nutrition of pathogens. Nature *468*, 527–532.

Chen, L.Q., Qu, X.Q., Hou, B.H., Sosso, D., Osorio, S., Fernie, A.R., and Frommer, W.B. (2012). Sucrose efflux mediated by SWEET proteins as a key step for phloem transport. Science *335*, 207–211.

Chen, L.-Q., Lin, I.W., Qu, X.-Q., Sosso, D., McFarlane, H.E., Londoño, A., Samuels, A.L., and Frommer, W.B. (2015). A cascade of sequentially expressed sucrose transporters in the seed coat and endosperm provides nutrition for the Arabidopsis embryo. Plant Cell *27*, 607.

Chu, Z., Yuan, M., Yao, J., Ge, X., Yuan, B., Xu, C., Li, X., Fu, B., Li, Z., Bennetzen, J.L., et al. (2006). Promoter mutations of an essential gene for pollen development result in disease resistance in rice. Genes Dev. *20*, 1250–1255.

Dahlin, J.S., Hamey, F.K., Pijuan-Sala, B., Shepherd, M., Lau, W.W.Y., Nestorowa, S., Weinreb, C., Wolock, S., Hannah, R., Diamanti, E., et al. (2018). A single-cell hematopoietic landscape resolves 8 lineage trajectories and defects in Kit mutant mice. Blood *131*, e1–e11.

Danila, F.R., Quick, W.P., White, R.G., Caemmerer, S. von, and Furbank, R.T. (2019). Response of plasmodesmata formation in leaves of C4 grasses to growth irradiance. Plant Cell Environ. *42*, 2482–2494.

De Rybel, B., Mähönen, A.P., Helariutta, Y., and Weijers, D. (2016). Plant vascular development: from early specification to differentiation. Nat. Rev. Mol. Cell Biol. *17*, 30–40.

Dengler, N.G., Dengler, R.E., and Hattersley, P.W. (1985). Differing ontogenetic origins of PCR ("Kranz") sheaths in leaf blades of C4 grasses (Poaceae). Am. J. Bot. *72*, 284–302.

Denton, A.K., Maß, J., Külahoglu, C., Lercher, M.J., Bräutigam, A., and Weber, A.P.M. (2017). Freeze-quenched maize mesophyll and bundle sheath separation uncovers bias in previous tissue-specific RNA-Seq data. J. Exp. Bot. *68*, 147–160.

Denyer, T., Ma, X., Klesen, S., Scacchi, E., Nieselt, K., and Timmermans, M.C.P. (2019). Spatiotemporal developmental trajectories in the Arabidopsis root revealed using high-throughput single-cell RNA sequencing. Dev. Cell *48*, 840-852.e5.

Driscoll, S.P., Prins, A., Olmos, E., Kunert, K.J., and Foyer, C.H. (2005). Specification of adaxial and abaxial stomata, epidermal structure and photosynthesis to CO_2 enrichment in maize leaves. J. Exp. Bot. *57*, 381–390.

Eom, J.-S., Cho, J.-I., Reinders, A., Lee, S.-W., Yoo, Y., Tuan, P.Q., Choi, S.-B., Bang, G., Park, Y.-I., Cho, M.-H., et al. (2011). Impaired function of the tonoplast-localized sucrose transporter in rice, OsSUT2, limits the transport of vacuolar reserve sucrose and affects plant growth. Plant Physiol. *157*, 109–119.

Eom, J.-S., Choi, S.-B., Ward, J.M., and Jeon, J.-S. (2012). The mechanism of phloem loading in rice (Oryza sativa). Mol. Cells *33*, 431–438.

Eom, J.-S., Chen, L.-Q., Sosso, D., Julius, B.T., Lin, I.W., Qu, X.-Q., Braun, D.M., and Frommer, W.B. (2015). SWEETs, transporters for intracellular and intercellular sugar translocation. Curr. Opin. Plant Biol. *25*, 53–62.

Eom, J.-S., Nguyen, C.D., Lee, D.-W., Lee, S.-K., and Jeon, J.-S. (2016). Genetic complementation analysis of rice sucrose transporter genes in Arabidopsis *SUC2* mutant *atsuc2*. J. Plant Biol. *59*, 231–237.

Eom, J.-S., Luo, D., Atienza-Grande, G., Yang, J., Ji, C., Thi Luu, V., Huguet-Tapia, J.C., Char, S.N., Liu, B., Nguyen, H., et al. (2019). Diagnostic kit for rice blight resistance. Nat. Biotechnol. *37*, 1372–1379.

Esau, K. (1943). Ontogeny of the vascular bundle in *Zea mays*. Hilgardia *15*, 325–368.

Evert, R.F., Eschrich, W., and Heyser, W. (1977). Distribution and structure of the plasmodesmata in mesophyll and bundle-sheath cells of *Zea mays* L. Planta *136*, 77–89.

Evert, R.F., Eschrich, W., and Heyser, W. (1978). Leaf structure in relation to solute transport and phloem loading in *Zea mays* L. Planta *138*, 279–294.

Evert, R.F., Botha, C.E.J., and Mierzwa, R.J. (1985). Free-space marker studies on the leaf of *Zea mays* L. Protoplasma *126*, 62–73.

Evert, R.F., Russin, W.A., and Bosabalidis, A.M. (1996). Anatomical and ultrastructural changes associated with sink-to-source transition in developing maize leaves. Int. J. Plant Sci. *157*, 247–261.

Fritz, E., Evert, R.F., and Heyser, W. (1983). Microautoradiographic studies of phloem loading and transport in the leaf of *Zea mays* L. Planta *159*, 193–206.

Fritz, E., Evert, R.F., and Nasse, H. (1989). Loading and transport of assimilates in different maize leaf bundles. Planta *178*, 1–9.

Gebauer, P., Korn, M., Engelsdorf, T., Sonnewald, U., Koch, C., and Voll, L.M. (2017). Sugar accumulation in leaves of Arabidopsis *sweet11/sweet12* double mutants enhances priming of the salicylic acid-mediated defense response. Front. Plant Sci. *8*.

Geiger, D.R., Giaquinta, R.T., Sovonick, S.A., and Fellows, R.J. (1973). Solute distribution in sugar beet leaves in relation to phloem loading and translocation. Plant Physiol. *52*, 585.

Giacomello, S., Salmén, F., Terebieniec, B.K., Vickovic, S., Navarro, J.F., Alexeyenko, A., Reimegård, J., McKee, L.S., Mannapperuma, C., Bulone, V., et al. (2017). Spatially resolved transcriptome profiling in model plant species. Nat. Plants *3*, 17061.

Giaquinta, R. (1976). Evidence for phloem loading from the apoplast. Plant Physiol. *57*, 872.

Giaquinta, R. (1977). Possible role of pH gradient and membrane ATPase in the loading of sucrose into the sieve tubes. Nature *267*, 369–370.

Giaquinta, R.T. (1983). Phloem loading of sucrose. Annu. Rev. Plant Physiol. *34*, 347–387.

Glazebrook, J. (2005). Contrasting mechanisms of defense against biotrophic and necrotrophic pathogens. Annu. Rev. Phytopathol. *43*, 205–227.

Gottwald, J.R., Krysan, P.J., Young, J.C., Evert, R.F., and Sussman, M.R. (2000). Genetic evidence for the in planta role of phloem-specific plasma membrane sucrose transporters. Proc. Natl. Acad. Sci. U. S. A. *97*, 13979–13984.

Hafemeister, C., and Satija, R. (2019). Normalization and variance stabilization of single-cell RNA-seq data using regularized negative binomial regression. Genome Biol. *20*, 296.

Haritatos, E., Keller, F., and Turgeon, R. (1996). Raffinose oligosaccharide concentrations measured in individual cell and tissue types in *Cucumis melo* L. leaves: implications for phloem loading. Planta *198*, 614–622.

Herbers, K., Meuwly, P., Frommer, W.B., Metraux, J.P., and Sonnewald, U. (1996). Systemic acquired resistance mediated by the ectopic expression of invertase: possible hexose sensing in the secretory pathway. Plant Cell *8*, 793–803.

Heyser, W., Heyser, R., Eschrich, W., and Fritz, E. (1977). The influence of externally supplied sucrose on phloem transport in the maize leaf strip. Planta *137*, 145–151.

Heyser, W., Evert, R.F., Fritz, E., and Eschrich, W. (1978). Sucrose in the free space of translocating maize leaf bundles. Plant Physiol. *62*, 491–494.

Hirose, T., Zhang, Z., Miyao, A., Hirochika, H., Ohsugi, R., and Terao, T. (2010). Disruption of a gene for rice sucrose transporter, OsSUT1, impairs pollen function but pollen maturation is unaffected. J. Exp. Bot. *61*, 3639–3646.

Horsfall, J.G., and Dimond, A.E. (1957). lnteractions of tissue sugar, growth substances, and disease susceptibility. Z Pflanzenkr Pflanzenschutz *64*, 415–421.

Juarez, M.T., Twigg, R.W., and Timmermans, M.C.P. (2004). Specification of adaxial cell fate during maize leaf development. Development *131*, 4533.

Julius, B.T., Leach, K.A., Tran, T.M., Mertz, R.A., and Braun, D.M. (2017). Sugar transporters in plants: new insights and discoveries. Plant Cell Physiol. *58*, 1442–1460.

Kanai, R., and Edwards, G.E. (1973). Separation of mesophyll protoplasts and bundle sheath cells from maize leaves for photosynthetic studies. Plant Physiol. *51*, 1133–1137.

Kanno, Y., Oikawa, T., Chiba, Y., Ishimaru, Y., Shimizu, T., Sano, N., Koshiba, T., Kamiya, Y., Ueda, M., and Seo, M. (2016). AtSWEET13 and AtSWEET14 regulate gibberellin-mediated physiological processes. Nat. Commun. *7*, 13245.

Keunecke, M., Lindner, B., Seydel, U., Schulz, A., and Hansen, U.P. (2001). Bundle sheath cells of small veins in maize leaves are the location of uptake from the xylem. J. Exp. Bot. *52*, 709–714.

Kim, J.-Y., Symeonidi, E., Pang, T.Y., Denyer, T., Weidauer, D., Bezrutczyk, M., Miras, M., Zöllner, N., Wudick, M.M., Lercher, M., et al. (2020). Unique and distinct identities and functions of leaf phloem cells revealed by single cell transcriptomics. BioRxiv 2020.09.11.292110.

Knoblauch, M., Knoblauch, J., Mullendore, D.L., Savage, J.A., Babst, B.A., Beecher, S.D., Dodgen, A.C., Jensen, K.H., and Holbrook, N.M. (2016). Testing the Münch hypothesis of long distance phloem transport in plants. ELife *5*, e15341.

Kragler, F., Monzer, J., Shash, K., Xoconostle-Cázares, B., and Lucas, W.J. (1998). Cell-to-cell transport of proteins: requirement for unfolding and characterization of binding to a putative plasmodesmal receptor. Plant J. *15*, 367–381.

Kumar, D., and Kellogg, E.A. (2019). Getting closer: vein density in C4 leaves. New Phytol. *221*, 1260–1267.

Kuwahara, M., Gu, Y., Ishibashi, K., Marumo, F., and Sasaki, S. (1997). Mercury-sensitive residues and pore site in AQP3 water channel. Biochemistry *36*, 13973–13978.

Langdale, J.A., Zelitch, I., Miller, E., and Nelson, T. (1988). Cell position and light influence C4 versus C3 patterns of photosynthetic gene expression in maize. EMBO J. *7*, 3643–3651.

Li, P., Ponnala, L., Gandotra, N., Wang, L., Si, Y., Tausta, S.L., Kebrom, T.H., Provart, N., Patel, R., Myers, C.R., et al. (2010). The developmental dynamics of the maize leaf transcriptome. Nat Genet *42*, 1060–1067.

Liesche, J. (2017). Sucrose transporters and plasmodesmal regulation in passive phloem loading. J. Integr. Plant Biol. *59*, 311–321.

Lin, I.W., Sosso, D., Chen, L.-Q., Gase, K., Kim, S.-G., Kessler, D., Klinkenberg, P.M., Gorder, M.K., Hou, B.-H., Qu, X.-Q., et al. (2014). Nectar secretion requires sucrose phosphate synthases and the sugar transporter SWEET9. Nature *508*, 546–549.

Lopez-Anido, C.B., Vatén, A., Smoot, N.K., Sharma, N., Guo, V., Gong, Y., Anleu Gil, M.X., Weimer, A.K., and Bergmann, D.C. (2020). Single-cell resolution of lineage trajectories in the Arabidopsis stomatal lineage and developing leaf. BioRxiv 2020.09.08.288498.

Macey, R.I. (1984). Transport of water and urea in red blood cells. Am. J. Physiol.-Cell Physiol. *246*, C195–C203.

Mizuno, H., Kasuga, S., and Kawahigashi, H. (2016). The sorghum SWEET gene family: stem sucrose accumulation as revealed through transcriptome profiling. Biotechnol. Biofuels *9*, 127.

Moore, J.W., Herrera-Foessel, S., Lan, C., Schnippenkoetter, W., Ayliffe, M., Huerta-Espino, J., Lillemo, M., Viccars, L., Milne, R., Periyannan, S., et al. (2015). A recently evolved hexose transporter variant confers resistance to multiple pathogens in wheat. Nat. Genet. *47*, 1494–1498.

Münch, E. (1930). Die Stoffbewegungen in Der Pflanze.

O'Connor, D.L., Runions, A., Sluis, A., Bragg, J., Vogel, J.P., Prusinkiewicz, P., and Hake, S. (2014). A division in PIN-mediated auxin patterning during organ initiation in grasses. PLOS Comput. Biol. *10*, e1003447.

Oliva, R., Ji, C., Atienza-Grande, G., Huguet-Tapia, J.C., Pérez-Quintéro, A., Li, T., Eom, J.-S., Li, C., Nguyen, H., Liu, B., et al. (2019). Broad-spectrum resistance to bacterial blight in rice using genome-editing. Nat. Biotechnol. *37*, 1344–1350.

Pengelly, J.J.L., Kwasny, S., Bala, S., Evans, J.R., Voznesenskaya, E.V., Koteyeva, N.K., Edwards, G.E., Furbank, R.T., and von Caemmerer, S. (2011). Functional analysis of corn husk photosynthesis. Plant Physiol. *156*, 503.

Poethig, R.S., and Sussex, I.M. (1985). The cellular parameters of leaf development in tobacco: a clonal analysis. Planta *165*, 170–184.

Riesmeier, J.W., Willmitzer, L., and Frommer, W.B. (1992). Isolation and characterization of a sucrose carrier cDNA from spinach by functional expression in yeast. EMBO J. *11*, 4705–4713.

Riesmeier, J.W., Hirner, B., and Frommer, W.B. (1993). Potato sucrose transporter expression in minor veins indicates a role in phloem loading. Plant Cell *5*, 1591.

Rosenberg, A.B., Roco, C.M., Muscat, R.A., Kuchina, A., Sample, P., Yao, Z., Graybuck, L.T., Peeler, D.J., Mukherjee, S., Chen, W., et al. (2018). Single-cell profiling of the developing mouse brain and spinal cord with split-pool barcoding. Science *360*, 176.

Russell, S.H., and Evert, R.F. (1985). Leaf vasculature in *Zea mays* L. Planta *164*, 448–458.

Ryu, K.H., Huang, L., Kang, H.M., and Schiefelbein, J. (2019). Single-cell RNA sequencing resolves molecular relationships among individual plant cells. Plant Physiol. *179*, 1444–1456.

Sauer, N., and Stolz, J. (1994). SUC1 and SUC2: two sucrose transporters from *Arabidopsis thaliana*; expression and characterization in baker's yeast and identification of the histidine-tagged protein. Plant J. *6*, 67–77.

Sedelnikova, O.V., Hughes, T.E., and Langdale, J.A. (2018). Understanding the genetic basis of C4 Kranz anatomy with a view to engineering C3 crops. Annu. Rev. Genet. *52*, 249–270.

Sharman, B.C. (1942). Developmental anatomy of the shoot of *Zea mays* L. Ann. Bot. *6*, 245–282.

Shulse, C.N., Cole, B.J., Ciobanu, D., Lin, J., Yoshinaga, Y., Gouran, M., Turco, G.M., Zhu, Y., O'Malley, R.C., Brady, S.M., et al. (2019). High-throughput single-cell transcriptome profiling of plant cell types. Cell Rep. *27*, 2241-2247.e4.

Slewinski, T.L., Meeley, R., and Braun, D.M. (2009). Sucrose transporter1 functions in phloem loading in maize leaves. J. Exp. Bot. *60*, 881–892.

Sosso, D., Luo, D., Li, Q.-B., Sasse, J., Yang, J., Gendrot, G., Suzuki, M., Koch, K.E., McCarty, D.R., Chourey, P.S., et al. (2015). Seed filling in domesticated maize and rice depends on SWEET-mediated hexose transport. Nat. Genet. *47*, 1489–1493.

Sosso, D., van der Linde, K., Bezrutczyk, M., Schuler, D., Schneider, K., Kämper, J., and Walbot, V. (2019). Sugar partitioning between *Ustilago maydis* and Its host *Zea mays* L. during infection. Plant Physiol. *179*, 1373.

Srivastava, A.C., Ganesan, S., Ismail, I.O., and Ayre, B.G. (2008). Functional characterization of the Arabidopsis AtSUC2 sucrose/H^+ symporter by tissue-specific complementation reveals an essential role in phloem loading but not in long-distance transport. Plant Physiol. *148*, 200.

Srivastava, A.C., Dasgupta, K., Ajieren, E., Costilla, G., McGarry, R.C., and Ayre, B.G. (2009). Arabidopsis plants harbouring a mutation in AtSUC2, encoding the predominant sucrose/proton symporter necessary for efficient phloem transport, are able to complete their life cycle and produce viable seed. Ann. Bot. *104*, 1121–1128.

Stadler, R., and Sauer, N. (1996). The Arabidopsis thaliana *AtSUC2* gene is specifically expressed in companion cells. Bot. Acta *109*, 299–306.

Sun, M.-X., Huang, X.-Y., Yang, J., Guan, Y.-F., and Yang, Z.-N. (2013). Arabidopsis RPG1 is important for primexine deposition and functions redundantly with RPG2 for plant fertility at the late reproductive stage. Plant Reprod. *26*, 83–91.

Tausta, S.L., Li, P., Si, Y., Gandotra, N., Liu, P., Sun, Q., Brutnell, T.P., and Nelson, T. (2014). Developmental dynamics of Kranz cell transcriptional specificity in maize leaf reveals early onset of C4-related processes. J. Exp. Bot. *65*, 3543–3555.

Timmermans, M.C., Schultes, N.P., Jankovsky, J.P., and Nelson, T. (1998). Leafbladeless1 is required for dorsoventrality of lateral organs in maize. Dev. Camb. Engl. *125*, 2813–2823.

Trifinopoulos, J., Nguyen, L.-T., von Haeseler, A., and Minh, B.Q. (2016). W-IQ-TREE: a fast online phylogenetic tool for maximum likelihood analysis. Nucleic Acids Res. *44*, W232–W235.

Truernit, E., and Sauer, N. (1995). The promoter of the Arabidopsis thaliana *SUC2* sucrose-H^+ symporter gene directs expression of β-glucuronidase to the phloem: Evidence for phloem loading and unloading by SUC2. Planta *196*, 564–570.

Turgeon, R. (2010). The role of phloem loading reconsidered. Plant Physiol. *152*, 1817.

Van Norman, J.M., Breakfield, N.W., and Benfey, P.N. (2011). Intercellular communication during plant development. Plant Cell *23*, 855–864.

Wang, H., Yan, S., Xin, H., Huang, W., Zhang, H., Teng, S., Yu, Y.-C., Fernie, A.R., Lu, X., Li, P., et al. (2019). A subsidiary cell-localized glucose transporter promotes stomatal conductance and photosynthesis. Plant Cell *31*, 1328.

Wang, Y., Huan, Q., Chu, X., Li, K., and Qian, W. (2020). Single-cell transcriptome analyses recapitulate the cellular and developmental responses to abiotic stresses in rice. BioRxiv 2020.01.30.926329.

Williams, M.L., Farrar, J.F., and Pollock, C.J. (1989). Cell specialization within the parenchymatous bundle sheath of barley. Plant Cell Environ. *12*, 909–918.

Yang, B., Sugio, A., and White, F.F. (2006). *Os8N3* is a host disease-susceptibility gene for bacterial blight of rice. Proc. Natl. Acad. Sci. USA *103*, 10503–10508.

Zaka, A., Grande, G., Coronejo, T., Quibod, I.L., Chen, C.-W., Chang, S.-J., Szurek, B., Arif, M., Cruz, C.V., and Oliva, R. (2018). Natural variations in the promoter of OsSWEET13 and OsSWEET14 expand the range of resistance against Xanthomonas oryzae pv. oryzae. PLOS ONE *13*, e0203711.

Zhang, C., and Turgeon, R. (2009). Downregulating the sucrose transporter *VpSUT1* in *Verbascum phoeniceum* does not inhibit phloem loading. Proc. Natl. Acad. Sci. *106*, 18849.